SAHC

Rafael Ramírez Álvarez de Lara Structural analysis of the church of the Monastery of São Miguel de Refojos

Portugal | 2016

ADVANCED MASTERS IN STRUCTURAL ANALYSIS
OF MONUMENTS AND HISTORICAL CONSTRUCTIONS

Master's Thesis

Rafael Ramírez Álvarez de Lara

Structural analysis of the church of the Monastery of São Miguel de Refojos

University of Minho

Czech university of Prague

Education and Culture

Erasmus Mundus

ADVANCED MASTERS IN STRUCTURAL ANALYSIS
OF MONUMENTS AND HISTORICAL CONSTRUCTIONS

Master's Thesis

Rafael Ramírez Álvarez de Lara

Structural analysis of the church of the Monastery of São Miguel de Refojos

This Masters Course has been funded with support from the European Commission. This publication reflects the views only of the author, and the Commission cannot be held responsible for any use which may be made of the information contained therein.

Portugal | 2016

DECLARATION

Name:	Rafael Ramírez Álvarez de Lara
Email:	rafael.alvarezdelara@gmail.com
Title of the Msc Dissertation:	Structural analysis of the church of the Monastery of São Miguel de Refojos
Supervisor(s):	Paulo B. Lourenço, Nuno Mendes
Year:	2016

I hereby declare that all information in this document has been obtained and presented in accordance with academic rules and ethical conduct. I also declare that, as required by these rules and conduct, I have fully cited and referenced all material and results that are not original to this work.

I hereby declare that the MSc Consortium responsible for the Advanced Masters in Structural Analysis of Monuments and Historical Constructions is allowed to store and make available electronically the present MSc Dissertation.

University:	University of Minho
Date:	01 / 09 / 2016
Signature:	Rafael Ramírez Álvarez de Lara

To those who gave me life.

ACKNOWLEDGEMENTS

First of all, I would like to thank my supervisors, Professor Paulo B. Lourenço and Professor Nuno Mendes, for their dedication, guidance, and support throughout this process. My most sincere gratitude to Dr. Mendes, for his patience and for being always there to help me.

I acknowledge the SAHC Consortium for granting me the opportunity to attend this Master and providing financial support.

I would also like to express my appreciation to all the SAHC lecturers, for their teaching and assistance.

Thanks to Giorgos Karanikoloudis, Maria Pia Ciocci, Alberto Barontini, and Federica Greco, who shared their wisdom and contributed to this work.

To my SAHC colleagues, for making these months become a life-changing experience.

My eternal gratitude to my family, for their unconditional support and encouragement.

A special recognition to all my teachers and professors, who guided me to get here.

Thanks to my friends, for the laughter.

ABSTRACT

Contemporary approaches for the conservation of historical constructions imply criteria of minimum intervention with maximum efficiency, durability and reliability. Together with historical research, in situ inspections and laboratory testing, the analysis of the structural behaviour is one of the most important tools currently available to determine the most appropriate techniques for preserving or strengthening ancient constructions and monuments. In this sense, numerical modelling is a fundamental tool to evaluate the overall behaviour of historical buildings, since it can be used to reproduce the real behaviour of their structures and simulate different scenarios, assess safety levels, and evaluate and compare the efficiency of different strengthening techniques.

This thesis addresses the study of the conservation status and structural stability of the church of the Monastery of São Miguel de Refojos, located in Cabeceiras de Basto (Portugal). The church and the sacristy of the ancient Benedictine monastery are classified as Public Interest Building since 1993. The church corresponds to a monumental building in Baroque and Rococo style, and it presents low to moderate structural damage, as well as several non-structural problems mostly related to the high presence of water. The research process is divided into three main phases, namely state-of-the-art and diagnosis, creation and calibration of a 3D numerical model based on the Finite Element Method, and finally, structural analyses to identify the cause of the existing damage of the structure, as well as to assess its safety. In the last step of the works, the non-linear behaviour of the structure is evaluated for vertical loading and the pushover analysis is applied to assess the seismic performance. The interaction soil-structure is also addressed, including the soil effect through the application of springs at the base of the walls. The results of the analyses are studied in terms of the capacity curves, deformation, structural damage patterns and collapse mechanisms.

The results allowed to evaluate the structural behaviour of the church, as well as to identify the most vulnerable elements of the structure. According to the analyses, the building has a considerable safety level in terms of vertical loading, as well as a good overall seismic performance. Although the model is proven useful to assess the global behaviour of the structure and validate the assumptions, additional works are recommended in order to improve the current conclusions on the structural behaviour of the church.

RESUMO

Análise estrutural da igreja do Mosteiro de São Miguel de Refojos

Abordagens contemporâneas para a conservação das construções históricas implicam critérios de intervenção mínima com a máxima eficiência, durabilidade e confiabilidade. Juntamente com a pesquisa histórica, as inspeções no local e os ensaios em laboratório, a análise do comportamento estrutural é uma das ferramentas disponíveis atualmente mais importantes para determinar as técnicas mais adequadas para a preservação e reforço de construções antigas e de monumentos. Nesse sentido, a modelação numérica é uma ferramenta fundamental para avaliar o comportamento global dos edifícios históricos, uma vez que pode ser utilizada para simular o comportamento real das estruturas e simular diferentes cenários, avaliar os níveis de segurança, e avaliar e comparar a eficiência de diferentes técnicas de reforço.

Esta tese aborda o estudo do estado de conservação e a estabilidade estrutural da igreja do Mosteiro de São Miguel de Refojos, localizado em Cabeceiras de Basto (Portugal). A igreja e a sacristia do antigo mosteiro beneditino estão classificados como Imóvel de Interesse Público desde 1993. A igreja corresponde a um edifício monumental, em estilo barroco e rococó, e apresenta danos estruturais com severidade baixa a moderada, bem como várias anomalias não-estruturais associadas sobretudo à elevada presença de água. Os trabalhos de pesquisa estão dividido em três fases principais, nomeadamente, na revisão do estado da arte e diagnóstico, na criação e calibração de um modelo numérico 3D baseado no Método dos Elementos Finitos e, por último, nas análises estruturais para identificar a causa do dano existente da estrutura, bem como para avaliar a sua segurança. Na última fase dos trabalhos foi avaliado o comportamento não-linear da estrutura para as cargas verticais e foi efetuada a análise não linear estática para avaliação do comportamento sísmico. A interação solo-estrutura foi também é efetuada, incluindo o efeito do solo através da aplicação de elementos de mola na base da estrutura. Os resultados das análises foram avaliados através das curvas de capacidade, da deformação da estrutura, dos padrões de dano e dos mecanismos de colapso.

Os resultados permitiram concluir sobre o comportamento da igreja, bem como identificar os elementos mais vulneráveis da estrutura. Os resultados demonstram que a igreja apresenta um nível de segurança considerável para as cargas verticais do peso próprio, assim como um comportamento sísmico adequado. Embora o modelo se tenha mostrando útil para avaliar o comportamento global da estrutura e validar alguns das considerações, recomenda-se efetuar trabalhos adicionais que permitam reforçar as conclusões sobre o comportamento estrutural da igreja.

RESUMEN

Análisis estructural de la iglesia del Monasterio de San Miguel de Refojos

Los planteamientos contemporáneos sobre la conservación de construcciones históricas implican criterios de mínima intervención con la máxima eficacia, durabilidad y fiabilidad. Junto con la investigación histórica, las inspecciones in situ y los ensayos de laboratorio, el análisis del comportamiento estructural es una de las herramientas más importantes disponibles actualmente para determinar las técnicas más adecuadas para la preservación y el refuerzo de construcciones antiguas y monumentos. En ese sentido, el modelado numérico es una herramienta fundamental para evaluar el comportamiento global de edificios históricos, ya que puede ser utilizado para reproducir el comportamiento real de las estructuras y simular diferentes escenarios, validar los niveles de seguridad, y evaluar y comparar la eficacia de diferentes técnicas de refuerzo.

Esta tesis aborda el estudio del estado de conservación y la estabilidad estructural de la iglesia del Monasterio de São Miguel de Refojos, localizado en Cabeceiras de Basto (Portugal). La iglesia y la sacristía del antiguo monasterio benedictino están clasificados de Interés Público desde 1993. La iglesia constituye un edificio monumental en estilo barroco y rococó, y presenta daños estructurales de severidad baja a moderada, así como varias anomalías no estructurales asociadas principalmente a la elevada presencia de agua. El proceso de investigación se divide en tres fases principales, a saber, el estado de la cuestión y diagnosis, la creación y calibración de un modelo numérico 3D basado en el Método de Elementos Finitos, y, por último, los análisis estructurales para identificar la causa del daño existente en la estructura, así como para evaluar su seguridad. En la última etapa de los trabajos, el comportamiento no-lineal de la estructura se evalúa en condiciones de carga vertical y el análisis estático no-lineal se aplica para evaluar el comportamiento sísmico. La interacción suelo-estructura también se analiza, incluyendo el efecto del suelo mediante la aplicación de muelles en la base de los muros. Los resultados de los análisis se estudian a través de curvas de capacidad, deformaciones, patrones de daño estructural y mecanismos de colapso.

Los resultados permitieron evaluar el comportamiento estructural de la iglesia, así como identificar los elementos más vulnerables de la estructura. Atendiendo a los análisis, el edificio presenta un nivel de seguridad considerable en términos de carga vertical, así como un adecuado comportamiento sísmico. Aunque se ha demostrado la utilidad del modelo para analizar el comportamiento global de la estructura y validar las hipótesis iniciales, se recomiendan trabajos adicionales con el fin de profundizar en las conclusiones sobre el comportamiento estructural de la iglesia.

TABLE OF CONTENTS

LIST OF FIGURES

LIST OF TABLES

1. INTRODUCTION

1.1 Context and motivation

Masonry is one of the oldest construction materials and it has been widely used for centuries by different cultures and civilizations. Nowadays, masonry constructions represent a significant portion of the existing building stock in the world, especially relevant when considering historical structures and monuments. Therefore, the study and conservation of masonry buildings becomes of interest due to their intrinsic historical, cultural, social, economic and aesthetic values.

Despite the advanced research and considerable examples in the masonry conservation field, a thorough understanding of the structural behaviour of this kind of structures is still challenging. On one hand, there is a great variety of masonry building typologies and a general lack of information about the construction techniques and historical changes to the structures, making each case a unique example to evaluate. Moreover, most historical constructions presents damage and deterioration caused by ageing, environmental exposure or natural hazards. Furthermore, these buildings may have suffered alterations caused by humans and their architectural and structural properties do not remain equal to their original configuration. On the other hand, the heterogeneous nature of masonry at a material level involves peculiarities and difficulties not present in other materials. Thus, an accurate simulation of their mechanical behaviour requires more complex constitutive models, which must be able to take into account its current conservation status.

In order to preserve the monuments and assure their safety, it is essential to understand the overall behaviour of their structures. Together with historical investigation, in situ inspections and laboratory testing, the analysis of the structural behaviour is one of the most important tools currently available to determine the most appropriate techniques for preserving or retrofitting historical constructions and monuments.

Prior to any intervention, the identification of structural properties and possible damage sources has a significant importance. First, the sources of structural damage should be detected and corrected, or otherwise any intervention would be ineffective or even counterproductive. Then, the necessary intervention should be proposed according to an effective conservation approach, with special focus on achieving the minimum impact with maximum efficiency, durability, reliability, and, when possible, reversibility.

Destructive tests are normally avoided when dealing with protected heritage buildings. However, non-destructive or minor-destructive testing can provide important information about the structural properties. Nevertheless, some estimations or assumptions regarding the structural parameters are necessary in many cases and then the characterisation of the mechanical properties becomes an engineering judgment task.

Numerical modelling is a fundamental tool for the assessment and strengthening of historical constructions, since it can be used to simulate the global behaviour of the structure based on its physical properties, even if there are always some uncertainties intrinsically linked to the model. The parameters of the numerical models can be calibrated with respect to the results obtained from experimental tests. Thus, the numerical model is able to reproduce the real behaviour of the structure and it can be used to simulate different scenarios, assess safety levels, and evaluate and compare the efficiency of different intervention proposals.

1.2 Objectives of the work

The general objective of this dissertation is to evaluate the structural behaviour of the church of the Monastery of São Miguel de Refojos, namely to identify the main causes of the existing structural damage and to evaluate the seismic performance of the church.

The particular objectives of this work are:

(a) Collect and evaluate the information resulting from previous works and in situ testing, in order to prepare a 3D numerical model.

(b) Prepare a finite element model considering the main geometrical features of the building.

(c) Calibrate the numerical model with respect to the experimental results.

(d) Identify the main cause of the existing damage for the gravitational loading, including the study of the soil-structure interaction.

(e) Evaluate the seismic behaviour of the church based on pushover analysis.

1.3 Methodology and scope of the study

In order to accomplish the objectives of the work, a state-of-the-art is first carried out including a brief description of the church and its history, followed by a record of the previous main conservation works. Then, the current condition of the structure is assessed based on the in situ inspection and the main structural parameters are estimated according to the experimental tests.

Subsequently, the numerical modelling is carried out. Considering the geometric and material data previously collected, a three-dimensional finite element model of the church is prepared. First, an eigenvalue analysis is performed and the dynamic properties are compared with the experimental results of the dynamic identification tests in order to assess the quality of the model. A calibration of the numerical model is then carried out. Afterwards, non-linear structural analyses are carried out for both gravity and lateral seismic loading. Two different analyses are performed, namely the nonlinear static analysis for the vertical loading, aiming at evaluating the existing damage and assessing the stability of the structure, and the pushover analysis to study the seismic performance of the church. The pushover analysis is carried out using a one-directional uniform loading pattern based on lateral forces proportional to mass. The interaction soil-structure is also studied, including the soil effect through the application of springs with properties obtained from geotechnical tests.

Finally, the results of the aforementioned analyses are discussed and compared to justify the observed damage and present condition of the structure, as well as to assess its safety. The conclusions are drawn and some recommendations for further works are proposed.

1.4 Thesis outline

This thesis is organised in seven chapters. Chapter 1 explains briefly the motivation of the work, the main objectives of the thesis, the adopted methodology and the overall organisation of the document.

Chapter 2 presents a review on the state-of-the-art, including a short history of the Monastery of São Miguel de Refojos and an architectural description of the building with special focus on its church. Moreover, the conservation works carried out in the church and the cloister since the 19th century are presented.

Chapter 3 summarizes the inspection works carried out in the church of São Miguel de Refojos, namely visual inspection and damage identification, temperature and humidity monitoring, dynamic identification tests, georadar tests, geotechnical survey and water table assessment. The structural properties and the current condition of the building are discussed in light of these works.

Chapter 4 introduces the main geometrical and material features of the church that were used for the construction of the finite element model. In addition, preliminary linear static and eigenvalue analyses are presented. Finally, the model is calibrated by comparing the results of the numerical modal analysis with the experimental results obtained from the dynamic identification tests. The calibration is done by updating of the different moduli of elasticity. The MAC values are also used to evaluate the calibration in terms of mode shapes.

Chapter 5 presents the initial non-linear analyses of the church for vertical loading including different soil configurations to simulate the real condition of the structure. The results collected from the inspection works are used to set up a series of possible foundation scenarios and the results of the

different analyses are compared with the current damage in order to validate the assumptions. First, the analysis considering self-weight and other vertical loading is presented and discussed. Finally, a vertical overloading capacity analysis is presented.

Chapter 6 contains the non-linear structural analyses of the church for horizontal loading. The seismic structural response based on pushover analysis is calculated for both the transversal and longitudinal directions of the building. For each case, the results are presented and discussed, including the capacity curves of the structure and the observed numerical damage pattern.

Chapter 7 presents the final conclusions. Additionally, difficulties faced during the work, discussion of results and recommendations for further studies are stated

2. THE MONASTERY OF SÃO MIGUEL DE REFOJOS

2.1 Historical background

The population of Cabeceiras de Basto in the north of Portugal was born together with the construction of the old Monastery of São Miguel de Refojos from which the village developed. The exact date of the construction of the original monastery is not known, however, a letter by D. Afonso Henriques in 1131 mentions the order of St. Benedict and proves the existence of the monastery at least since that year (DGPC 2015).

During the early years, the monastery experienced a growing period and became one of the richest of the Minho region and inside the Benedictine Order. Subsequently, it held the ruinous administration of the commendatory abbots (1428-1537), who squandered many convent goods and incomes. This phase resulted in a dark period for the monastery and was only overcome after 1570 with the integration of Refojos in the English Benedictine Congregation and the change in its governance system. With a new implemented triennial abbots regime the monastery began its process of economic and architectural recovery (Lemos et al., 2013) (Sequeira 2006).

Although there were some attempts to promote and carry out different interventions, the main works for the renovation of the monastery of Refojos did not begin until the first half of the seventeenth century. Those works would include the construction of a new church with two towers. The old religious temple was then completely demolished and rebuilt according to the principles already established for another case: the Benedictine monastery of São Martinho de Tibães, in Braga. André Soares, main architect of Tibães, worked extensively in the northern regions of Portugal and became very influential during the Baroque period. One of his disciples, Frei José de Sto. António Vilaça, was responsible of the renovation works in Refojos de Basto. Following the same canon used for Tibães, the architectural renovation of the old monastery in Cabeceiras was carried out by the synthesis of Mannerist reminiscences and an overall Baroque organisation (Pereira 1992). The gate of the monastery shows an inscription with the year 1690, which probably corresponds to the year when the works were concluded. The cloister was also built during the seventeenth century and served as the secondary access to the church, as well as a place of prayer, meeting and burial of the monks (DGPC 2015).

The Baroque-style interventions initiated in the seventeenth century lasted until the following century. The main interventions in the church, which resulted in its current aspect, began in 1675 and were

completed in 1766. This building represents one of the most monumental works left by the Benedictine Order in Portugal, the only temple of this order with a dome. The church also stands out for its large dimensions, the exuberant Baroque-Rococo style, the rich gilded decoration, the granitic ornaments and the monumentality of the gables. The documents available and the dates written in some parts of the church allow to define the progress of the construction. The portal dates from 1763 (carved on the top of the main façade indicating the date of its construction), and the dome and towers were built between 1761 and 1764 (DGPC 2015) (Lemos, et al. 2013).

The extinction of the Religious Orders in 1834 resulted into many vicissitudes for the monastery, such as partial abandonment and sale at auction by the State. Fortunately, the building could overcame that neglecting phase that extended until the first third of the twentieth century. After that period the building was subjected again to different restoration and repair works. Nowadays, the monastery is used as part of the Cabeceiras de Basto Town Hall and the Externato of São Miguel de Refojos (DGPC 2015).

2.2 Description of the church

The Monastery of S. Miguel de Refojos is located in Cabeceiras de Basto, in the northern district of Braga (Portugal). Its church, sacristy and the ceiling of one of the rooms in the former Benedictine monastery are classified as Public Interest Property since 1933. The location of the Monastery meets the classical criteria typically used for the organisation of this type of religious buildings, particularly linked to the topography, soil characteristics and the presence of water. Thus, the Monastery of Refojos is surrounded by hills in the north and east sides, and it is placed near a small watercourse. The presence of water is essential in a convent since it is a necessary element for the rituals and the daily tasks of the monks. In the case of Refojos the water of the river was diverted to the interior through stone channels (PAUTA 2000). Currently, the river is located entirely outside the building, running through the south and east of the monastery (Figure 1).

The church of S. Miguel de Refojos appears as a monumental building in Baroque-Rococo style, adjacent to the south part of the monastery (Sequeira 2006). The church has a Latin cross plan, comprising the nave, transept and chancel, and it is orientated in a classical east-west disposition (Figure 2 to Figure 15). The external volume of the church is about 60 m long and 24 m width in the transept. The interior height of the church equals 18 m in the nave and 16 m in the chancel. In the centre of the transept, the crossing is covered by a dome with an oval-shaped plan standing over pendentives. The body of the dome is made up by a drum, a cupola and a lantern on top. The maximum height of the church is located in this central dome with approximately 35 m. The walls are made of stone masonry, namely granite, and have variable thickness ranging from 0.85 m to 2.20 m.

Figure 1. Location and views of the Monastery of S. Miguel de Refojos

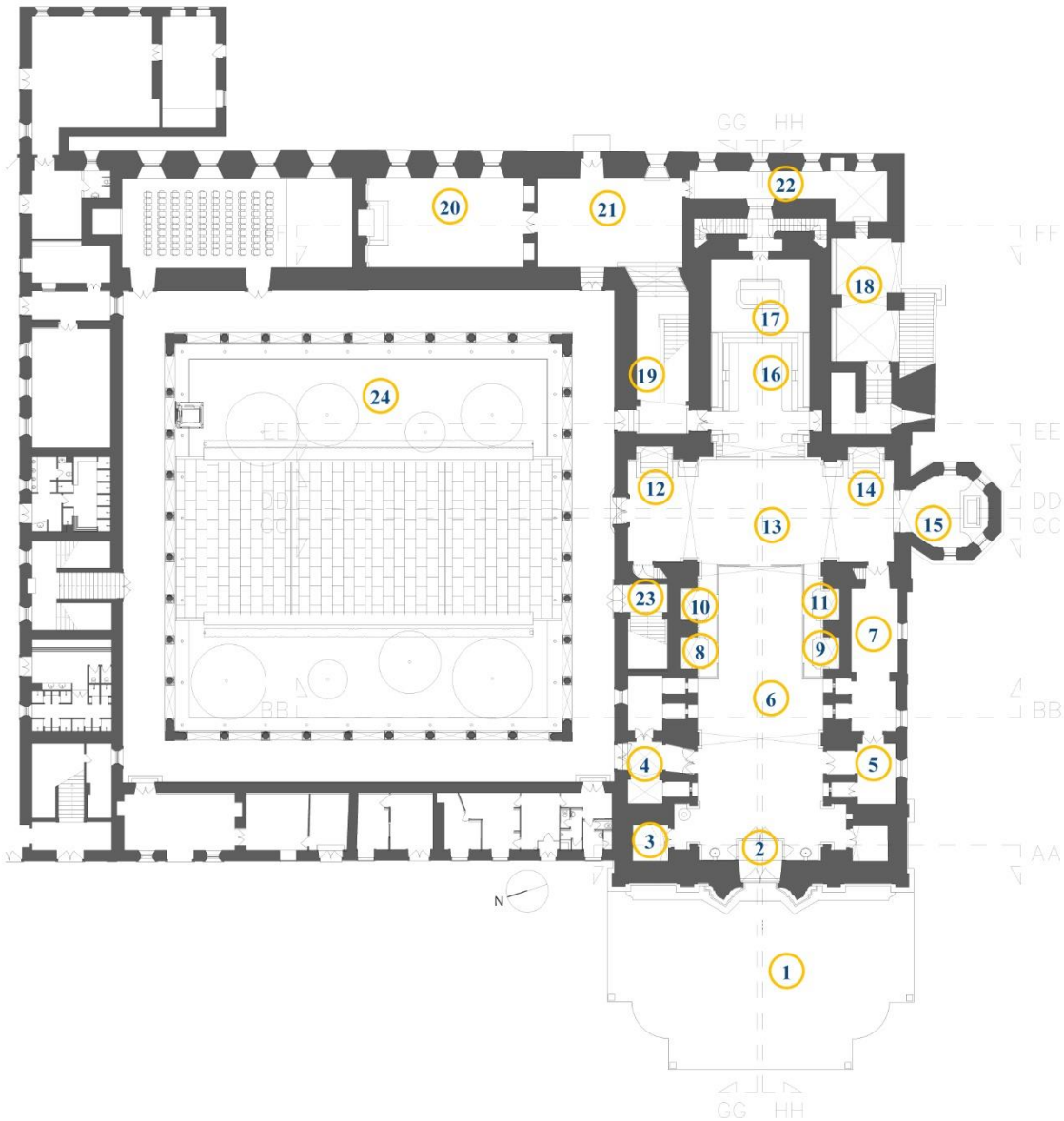

1 - Church front yard
2 - Church entrance
3 - Baptistery
4 - Area for support of ecclesiastical activities
5 - Access to secondary sacristy
6 - Nave
7 - Sacristy
8 - Altar Our Lady of the Immaculate Conception
9 - Altar Sta. Ana
10 - Altar Sta. Quitéria
11 - Altar Our Lady of Sorrows
12 - Altar Our Lady of the Rosary
13 - Crossing covered by the dome
14 - Altar Sacred Heart of Jesus
15 - Chapel of the Blessed Sacrament
16 - Presbytery
17 - High altar
18 - Mortuary chapel
19 - Atrium of the Museum of Sacred Art
20 - Old sacristy
21 - Former ante-sacristy
22 - Store of the Museum of Sacred Art
23 - Vertical access
24 - Cloister

Figure 2. Ground floor plan

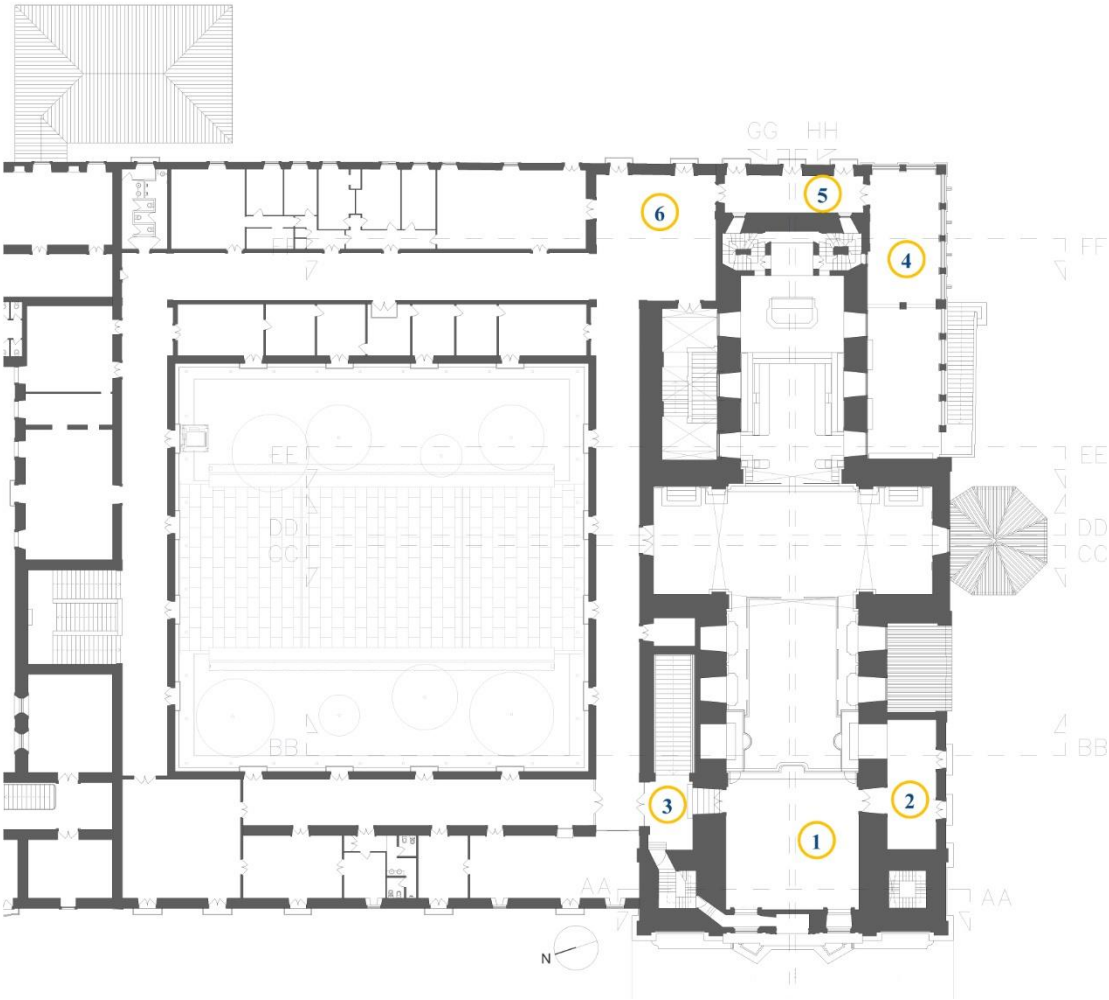

1 - Choir loft
2 - Bellows room
3 - Vertical access
4 - Solarium balcony and porch
5 - South entrance
6 - Abbey auditing room

Figure 3. First floor plan

The west façade of the church (Figure 5) dates from 1763 as it is shown over the main entrance in carved granite. Above the entrance there is a balcony, a niche with the statue of S. Miguel and two large windows. The top of the façade is made up by a central opening and a gable. The façade has two adjacent bell towers with quadrangular plan and about 40 meters high. The towers have two niches with the statues of S. Bento (north tower) and Sta. Escolástica (south tower) (Sequeira 2006). The north tower also has a clock and four bells, whereas the tower on the south corner is only decorative, showing no clock or bells.

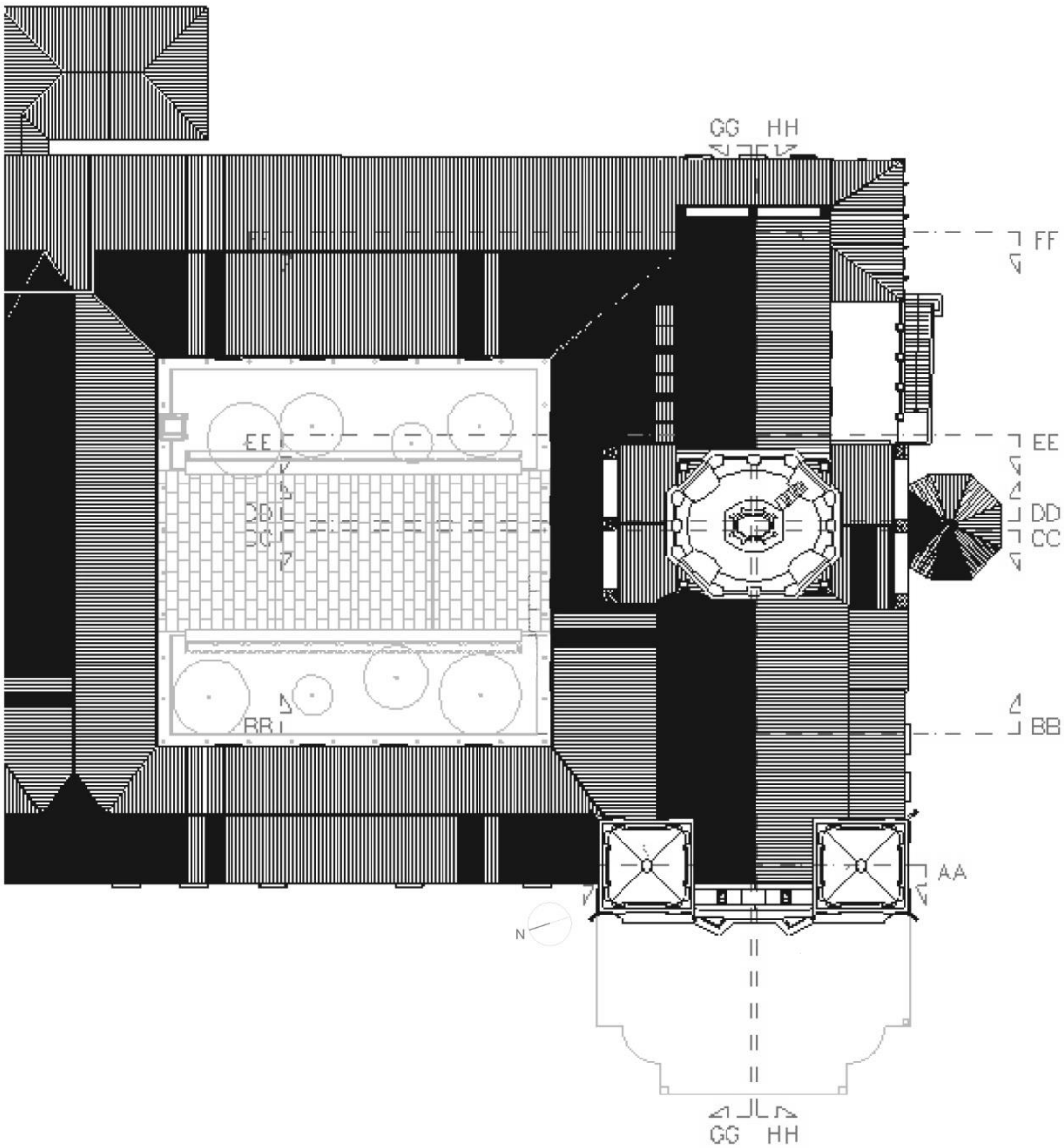

Figure 4. Roof plan

Inside the church, above the main entrance, the choir loft is supported by a ribbed vault with coffers in granite and a segmental arch profile (Figure 8). The adjacent lateral bodies of the nave are occupied by the baptistery, the areas for support of the church activities, the secondary access to the sacristy and the sacristy (Figure 2). The nave has two altars and a pipe organ on each lateral wall (Figure 3). The organ on the right side (south wall) is operational, while the one on the left (north wall) is mute, thus only decorative. The bellows of the operating organ are located in a room behind the instrument at the choir level. The ceiling of the nave is made up by a barrel vault (Figure 8 and Figure 9).

The transept was built in Renaissance style and it shows lateral altars with baroque altarpieces and large windows at the top (Figure 2 and Figure 3). In the crossing, four arches in granite support the drum, cupola and lantern (Figure 10 and Figure 11). The transept also gives access to the Chapel of the Blessed Sacrament located in the south and outside the main body of the church. This chapel has octagonal plan and it is about 8.50 m high. The detached position of this volume might indicate that the chapel was built in a later period (Sequeira 2006).

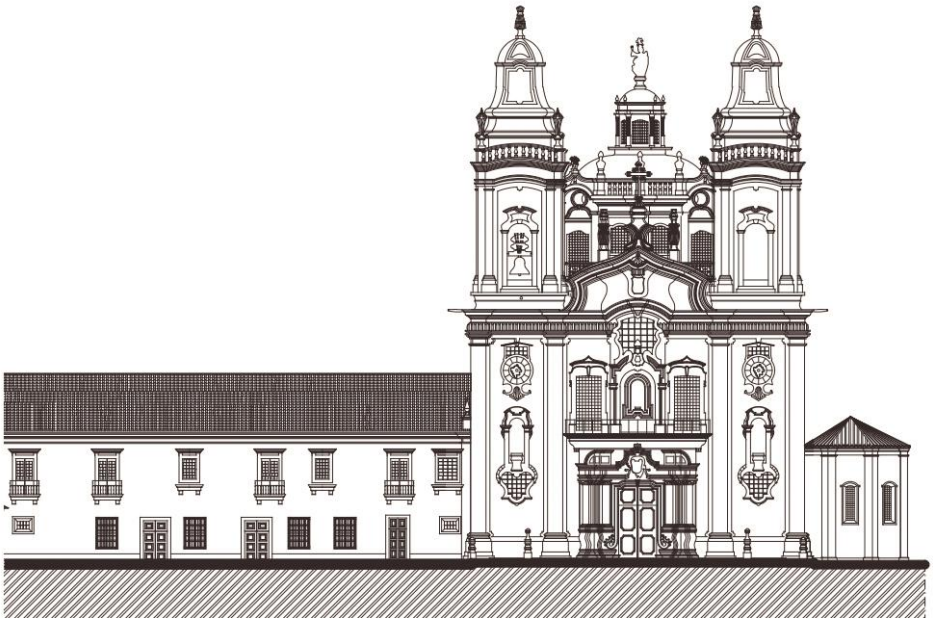

Figure 5. Main façade of the church (west façade)

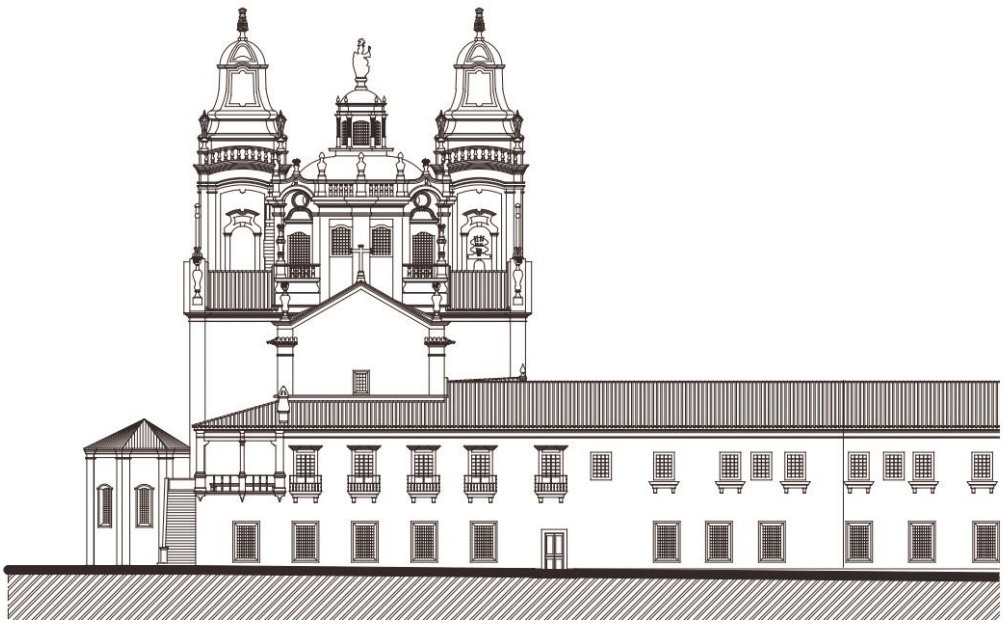

Figure 6. East façade of the church

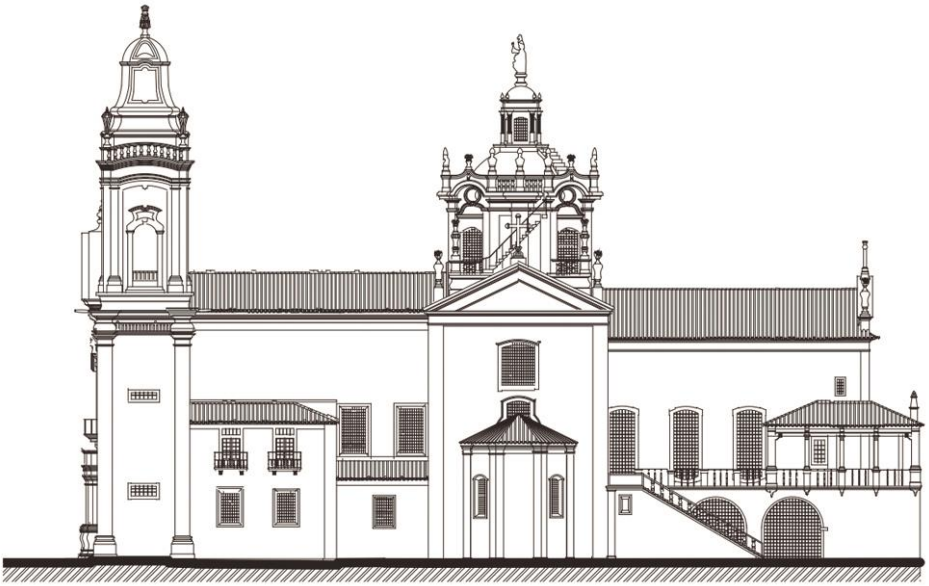

Figure 7. South façade of the church

The chancel of the church, which comprises the presbytery and the main altar, has three large windows in each lateral wall and a barrel vault at the top (Figure 3 and Figure 12). Outside and in the south side, a flight of granite stairs gives access to the solarium terrace (Figure 7). The solarium has a porch with stone columns and the southern entrance to the monastery (Figure 3). On the other hand, the space under the terrace is used as a mortuary chapel (Figure 2).

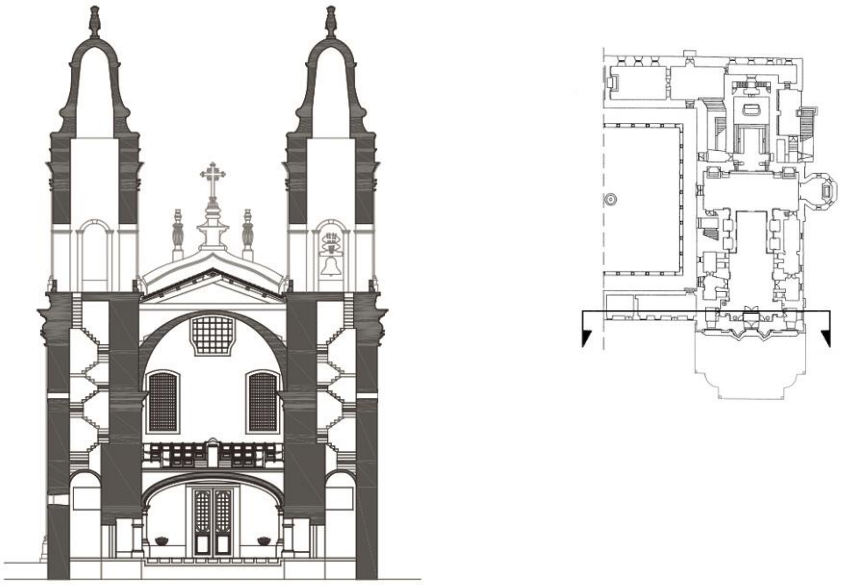

Figure 8. Transversal cross-section AA

The interior of the monastery to the north of the high altar is occupied by the atrium of the Museum of Sacred Art and the former ante-sacristy (Figure 2). The old ante-sacristy connects with the old sacristy and the store for the museum. These three spaces are found at a lower level in relation to the floor of the church or the cloister (Figure 14 and Figure 15).

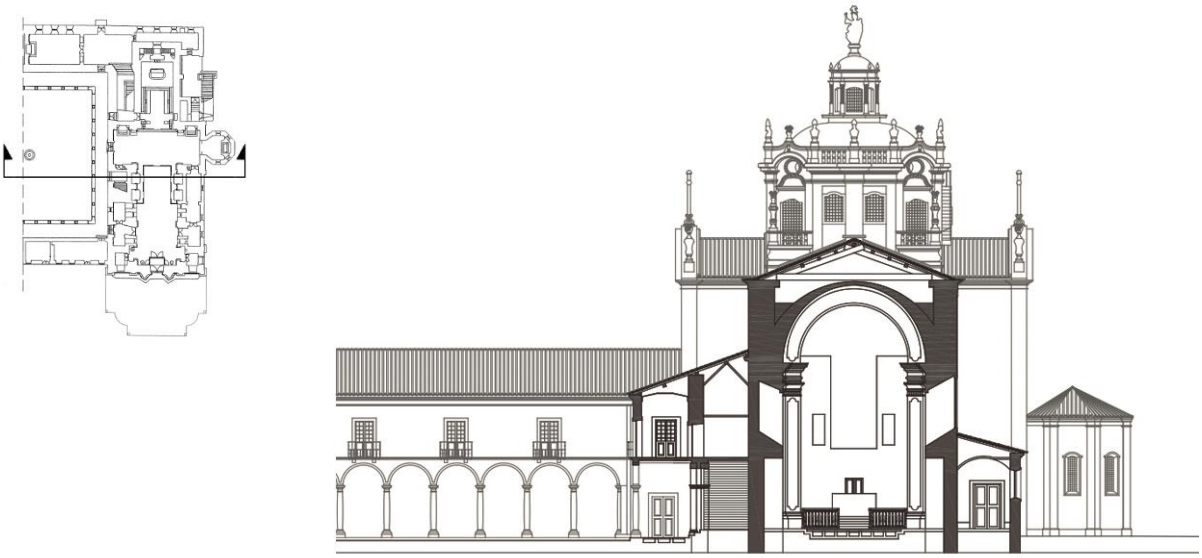

Figure 9. Transversal cross-section BB

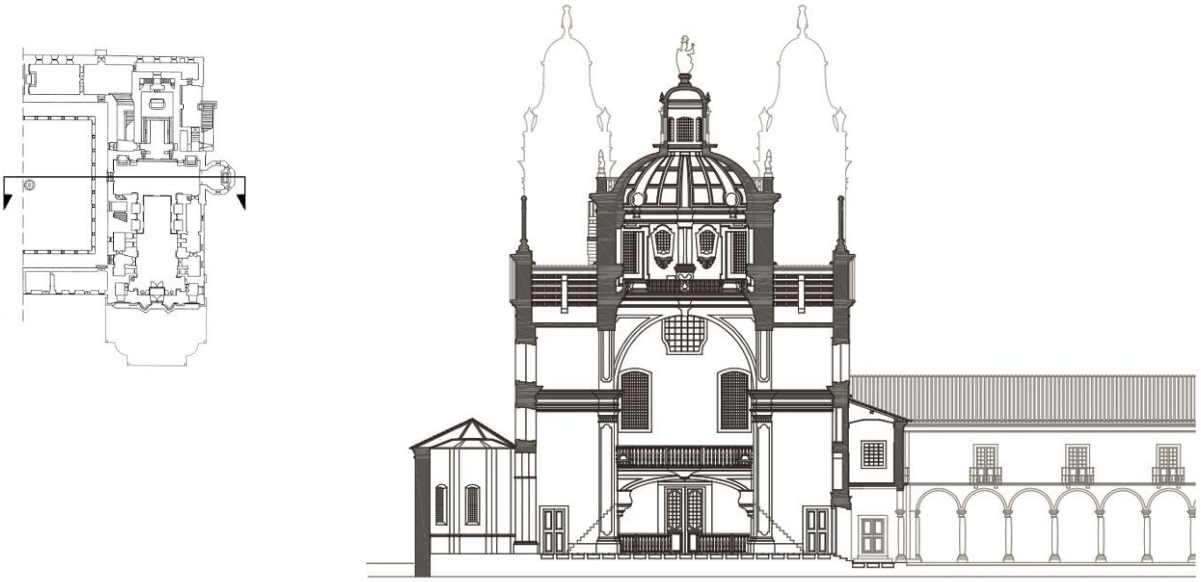

Figure 10. Transversal cross-section CC

The cloister is located in the centre of the monastery and it is the only remaining element from the interventions made during the first half of the seventeenth century. The main entrance to the monastery connects directly with this central courtyard and it shows a carved 1690 above the door, which may correspond to the final date of construction of the cloister (Lemos, et al. 2013). The cloister has a quadrangular plan, about 40x40 m^2, and four perimeter galleries with nine arches each (Figure 2, Figure 9, Figure 11 and Figure 12).

Figure 11. Transversal cross-section DD

Figure 12. Transversal cross-section EE

The nave, chancel and transept are covered by gable roofs. These roofs are supported by a timber structure oriented in the shortest direction and with ceramic tiles finish. On the other hand, the solarium porch and the Chapel of the Blessed Sacrament are covered by hipped roofs with similar supporting structure and finish. (Figure 4).

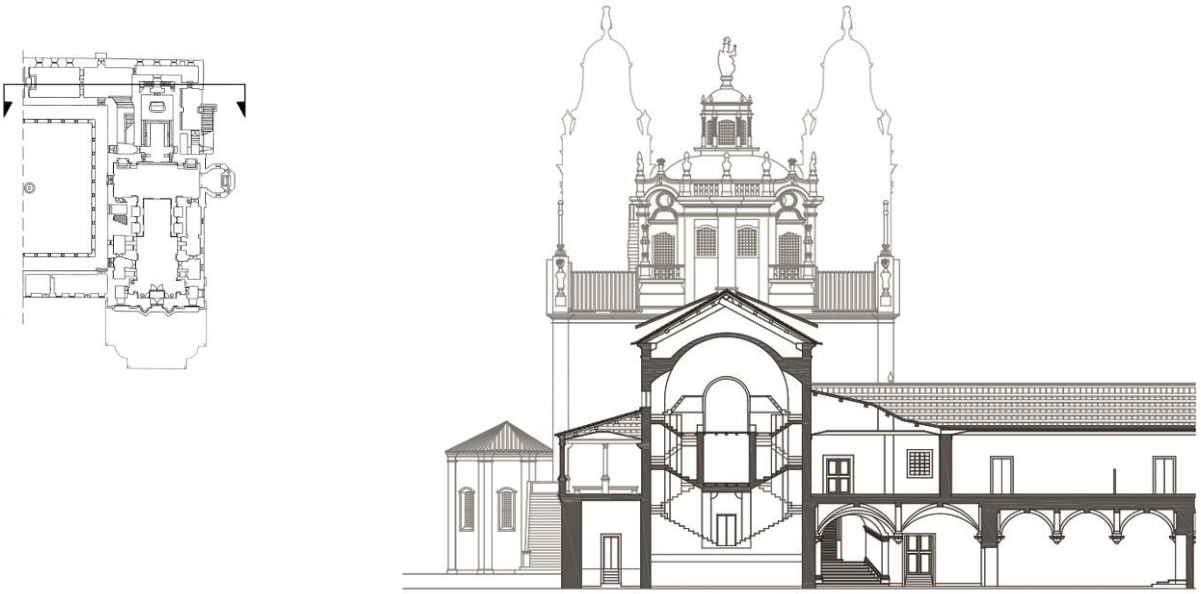

Figure 13. Transversal cross-section FF

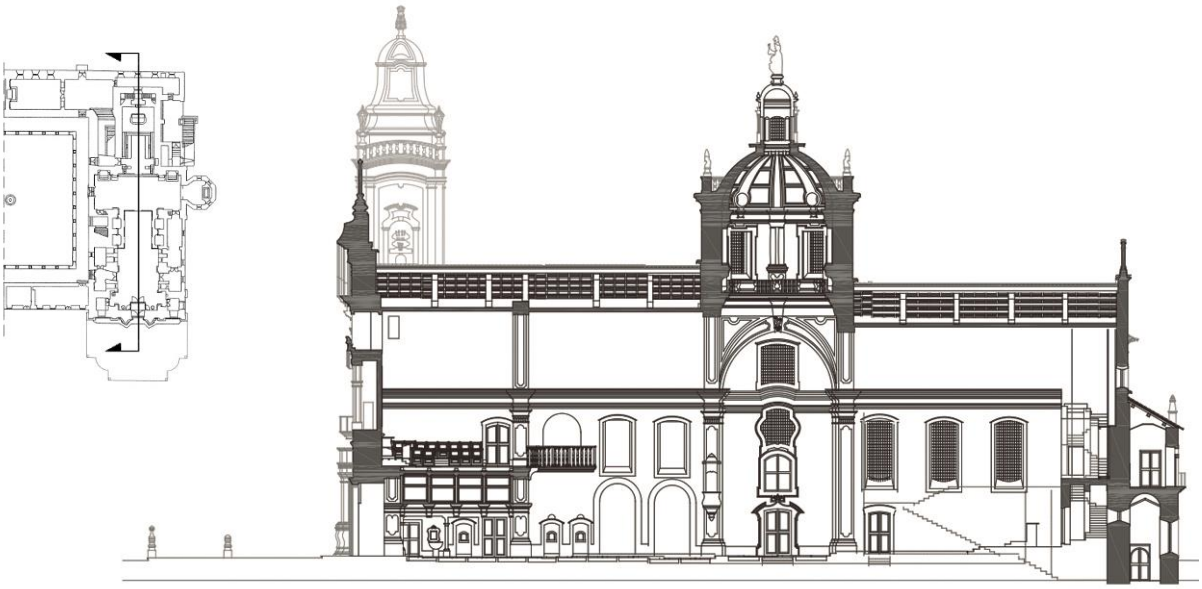

Figure 14. Longitudinal cross-section GG

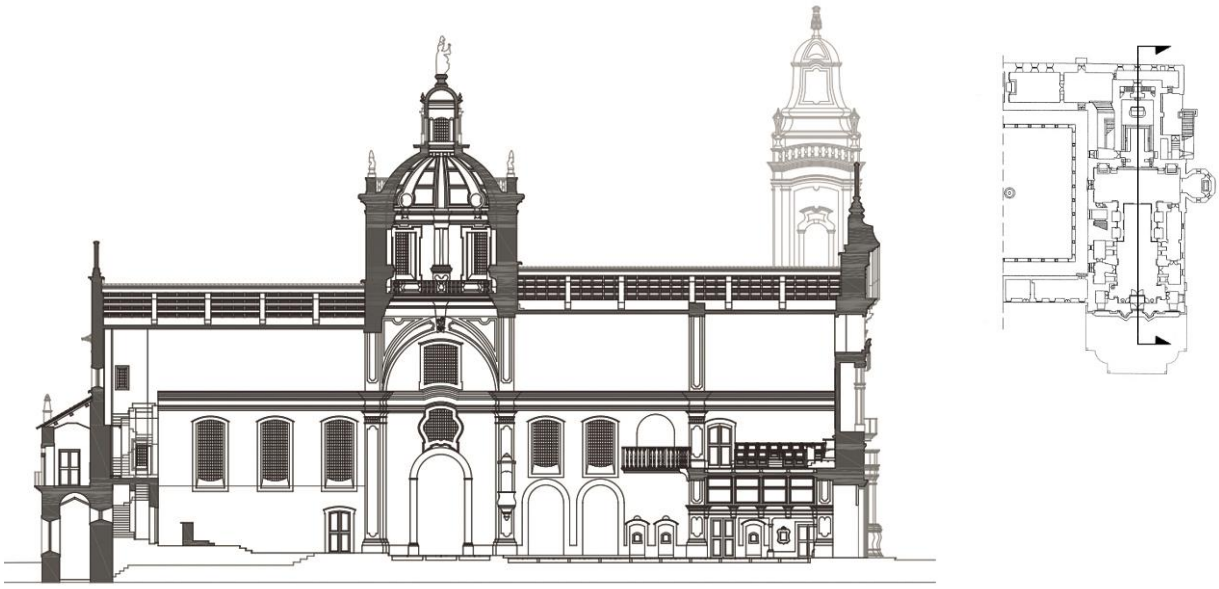

Figure 15. Longitudinal cross-section HH

The structure of the roof above the choir loft and nave is accessible from the north tower and it consists of trusses with approximately 10.75 m span (Figure 16). The spacing between trusses is 3.90 m on average with the exception of the ones located at one and the other side of the central arch, where a formerly existing truss may have been removed (Figure 16). Several vertical uprights are currently placed over the arch to sustain the secondary timber beams in this area. The cross section of the bottom and top chords is approximately 0.45x0.45 m^2 and 0.16x0.30 m^2, respectively. The trusses also have four struts with cross-section of approximately 0.08x0.13 m^2 (Figure 17 and Figure 18).

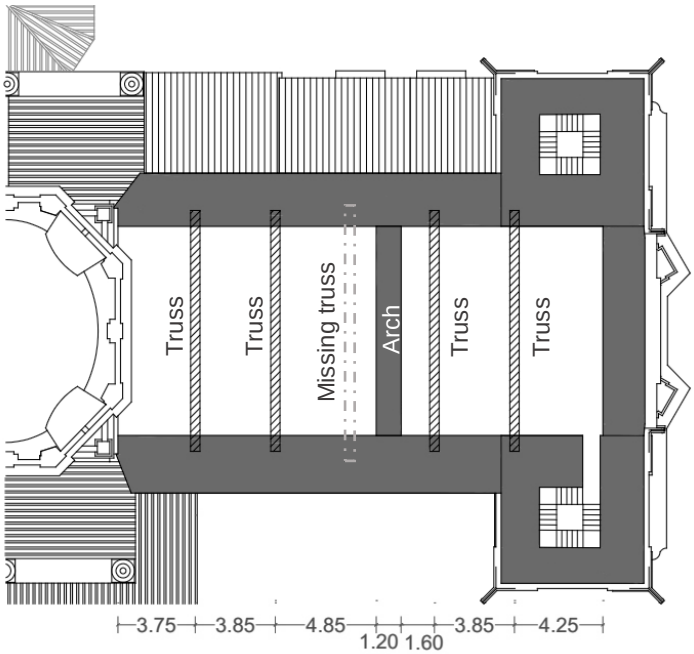

Figure 16. Plan of the roof above the choir loft and nave (dimensions in m)

The filling material on the vault extrados has different dimensions, whereby the height of the infill is not constant at one and the other side of the arch. The distance between the top of the wall and the infill is equal to 1.50 m and 1.20 m in the vault of the nave and that above the choir, respectively (Figure 17 and Figure 18). The vault of the nave was also evaluated using GPR testing (see Section 3.4). The extrados of the vault and the roof structure of the chancel and transept could not be inspected due to access limitations.

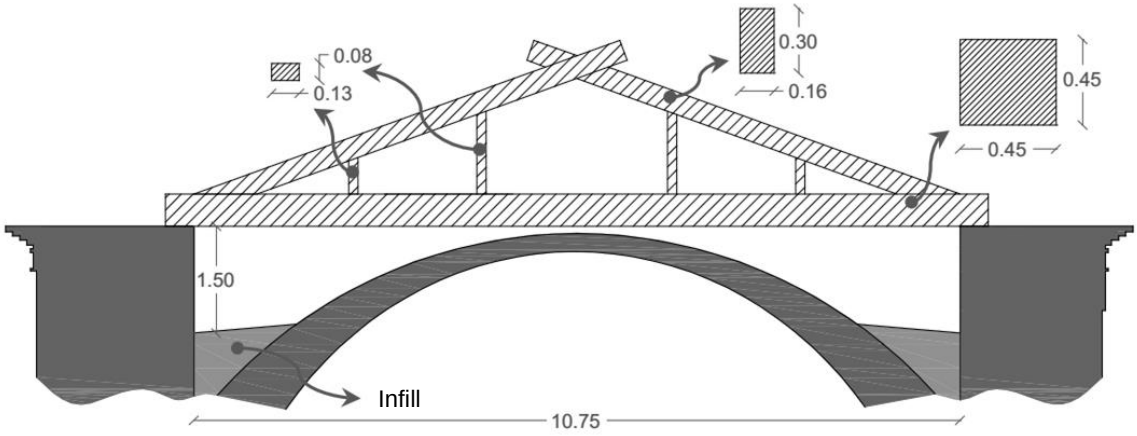

Figure 17. Transversal cross-section of the roof above the choir (dimensions in m)

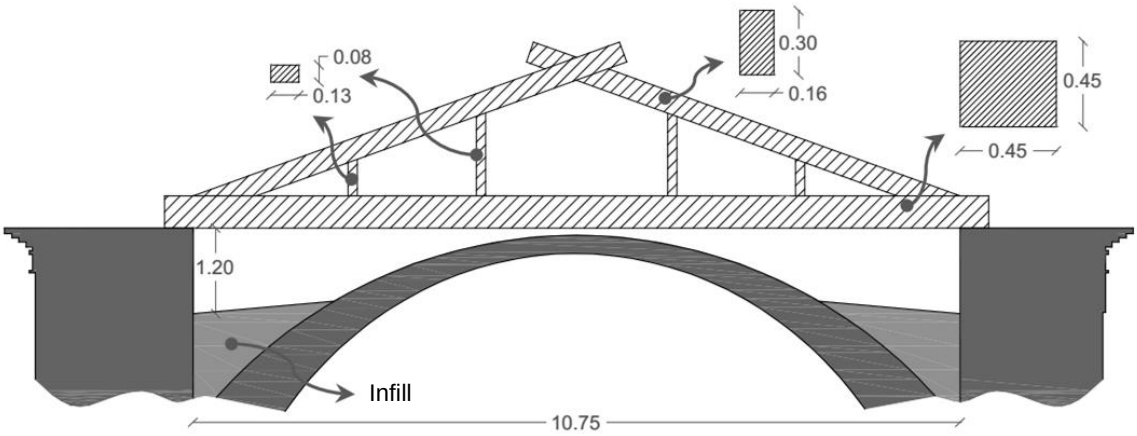

Figure 18. Transversal cross-section of the roof above the nave (dimensions in m)

2.3 Past interventions in the church and cloister

The Monastery of São Miguel underwent several structural and non-structural interventions over the years. Most of the works were focused on the restoration and repair of the church and the cloister. A summary of the interventions is presented in Appendix A.1, including a brief description of the works carried out in the church and the cloister between 1829 and 2013.

The documentary records show that the main façade of the church and the bell towers were subjected to several interventions, such as crack repair, granite cleaning, and treatment of plaster and painted surfaces. The façades underwent reparation works in 1966, 1972-1974, 1981-1982, 1998, 2000 e 2010. On the other hand, the interventions on the towers were made in 1829, 2000-2001 and 2010. The repair performed in 1829 on the south bell tower must be highlighted, since that tower is the one that currently shows the most severe damage.

The excessive moisture content in floors and walls due to the presence of water was a main concern over the years. It is shown by the external drainage works and the construction of a collector for drainage of the sacristy, cloister and other facilities, done in 1949. Another example would be the drainage works of the transept ground floor between 1985 and 1990.

The roofs were also target of several interventions, including cleaning, repairs, reconstructions and tiles replacement. The conservation works carried out in the dome in 1999 and 2000 are especially noteworthy; they involved the implementation of lead sheets over the cupola and the lantern.

Among the structural interventions, it must be noticed the work carried out in 2009 to restore the pipe organs. The works included structural reinforcement of the arches behind the organs by application of a steel bar and anchors at the level of the cornice.

Finally, the cloister suffered several interventions in recent years, such as: (a) Re-pavement of the galleries (1944); (b) Construction of a drainage collector (1949); (c) Restoration and landscaping works (1965); (d) General painting; (e) False ceiling installation (2001). In 2103, the cloister was remodelled.

3. DIAGNOSIS OF THE CHURCH

A diagnosis of the church of the Monastery of Cabeceiras de Basto was carried out, aiming at evaluating the damage and the conservation state of the building. The works started in December 2014 and were developed by a team of the University of Minho (Lourenço, et al. 2016). This chapter presents the main results obtained from the aforementioned works.

3.1 Damage survey

The identification and description of the damage involved a comprehensive analysis of the different constructive and structural elements, both from the outside and from the inside of the building. During the inspection, different structural and non-structural damage were evaluated. Considering the scope of the dissertation, only the structural-related damages are presented here.

3.1.1 External inspection of the church

The inspection of the church exterior aimed to identify the damage in walls, towers and dome, including the crack patterns. Moreover, the inspection from the outside allowed to identify the composition of the roofs and assess their condition. Due to the dimensions of the church, the inspection was performed with the help of an articulated aerial platform with a maximum lift height of 40 m. Note that the inspection of the north side of the church was limited by the inability to operate the lift platform inside the cloister.

A general assessment of the structural condition of the walls and towers shows that the church presents low to moderate damage (see Appendices A.2.1 to A.2.4). A possible movement of the south bell tower has caused moderate structural damage, which is visible in the connection between the tower and the main façade, and between the tower and the south wall of the nave (Appx. A.2.1 and A.2.2). In addition to the in-plane deformation, the top of the south wall presents also out-of-plane movement. The damage on the top of the transept walls is also noticeable, mainly near the connection between orthogonal walls (Appx. A.2.3 and A.2.4).

The damage of the towers affects mainly the stone cornices and mouldings (Appx. A.2.1 and A.2.2). These elements show minor cracks with reduced width and consequently scarce importance for the structural behaviour. The most severe damage appears in the connection between the south tower and the main façade (Figure 19). This connection shows a vertical crack with a maximum width of about 4 cm. The crack was filled with mortar in a past intervention. However, its current condition presents an

increase of the crack width, indicating that after the repairing works some movements occurred in this part of the structure (Appx. A.2.1 and Figure 19).

Figure 19. Crack in the connection between the main façade and the south tower

Regarding the south wall of the nave, the most severe structural damage is located in the cornice near the south tower. The stone moulding shows reopening of a crack that was previously repaired with mortar. The cornice has a maximum in-plane deformation of about 3 mm (Figure 20a). Furthermore, it shows out-of-plane movement as well, with maximum total displacement of about 35 mm (Figure 20b). Finally, the cornice also shows horizontal cracks near the south transept (Figure 21). The east walls of the transepts present reopening of old cracks in the stone cornices and new cracks affecting the plaster (Appx. A.2.4 and Figure 22).

(a) (b)

Figure 20. Deformation of the cornice in the south wall of the nave near the south tower:
(a) deformation in the wall plane; (b) deformation out-of-plane.

Figure 21. Horizontal crack and deformation in the cornice of the south wall of the nave.

(a) (b)

Figure 22. Damage in the walls of the south transept: (a) cracking and missing tiles near the corner with the south wall; (b) cracks near the south wall of the chancel.

The south wall of the chancel shows minor damage located in the windows and cornice (Appx. A.2.2). the east façade also presents minor cracking affecting the cornice (Appx. A.2.4).

A general cleaning of the external surfaces of the church was performed after the external inspection, involving the places accessible from the lifting platform (towers, main façade and south façade). The cleaning included removal of vegetation, cleaning of drain boxes and downpipes and painting of the plastered surfaces of the main façade.

3.1.2 Internal inspection of the church

The internal inspection of the church aimed to identify structural damage as well as other non-structural damage, such as infiltration of rainwater and the presence of moisture.

The lintel of the main entrance of the church shows transversal cracks with reduced width (Figure 23a). The flat arch of the south wall, below the south tower, has a crack along the vertical joint near the spring. This fissure reveals relative deformation between the granite units in the direction of the joint and shows also slight damage in the stone (Figure 23b).

The vault of the choir loft presents three cracks at the joints of the ribs near the centre of the vault (Figure 24). The arch of the choir has repaired cracks near the connection with the south wall of the nave and a crack in the centre of the arch (Figure 25). The cracks in the connection with the north wall of the nave were also filled with mortar, but they reopened due to new movements. The gap near the south wall showed some movement and in 2009 was monitored by application of a crack-meter on top of the arch (choir loft level). The monitoring indicates that the crack has not had any further significant movement, and the current opening of the slit is less than 1 mm.

(a) (b)

Figure 23. Damage near the main façade: (a) view of the bottom surface of the lintel of the main entrance; (b) crack in the flat arch below the south tower.

Figure 24. Cracks in the intrados of the choir vault.

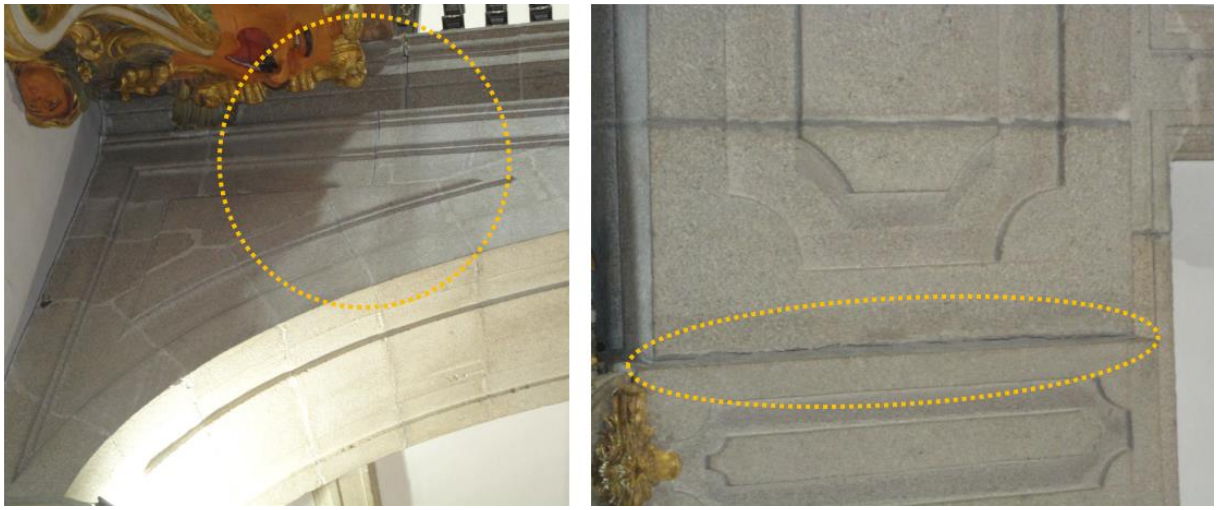

(a) (b)

Figure 25. Cracks in the arch of the choir loft: (a) crack near the connection with the south wall of the nave; (b) crack at mid-span.

The nave walls (main façade, north and south walls) show non-structural damage concentrated near the base and related to the presence of water: rising damp, efflorescence, fungi, and stone deterioration. The intrados of the nave vault shows moisture stains near the dome and under the infill material, which indicate a possible infiltration of rainwater through the roof. In addition, the bottom surface of the vault has two diagonal cracks with reduced width visible in the plaster (Figure 26).

Figure 26. Moisture stains and cracks in the in the nave vault.

In general, the damage in the transept is concentrated at the top of the walls and is related to the visible damage identified during the exterior inspection (Appx. A.2.2 and A.2.3). The ceiling of the north transept is affected by non-structural damage related with the infiltration of water (Figure 27a). In addition, it has a longitudinal crack in the connection between the arch and the dome (Figure 27b). On the other hand, the south transept also shows damage related to water infiltration, moisture stains and deterioration of plaster and paint. The south transept shows two cracks, namely a vertical crack in the cornice near the connection with the chancel wall (Figure 28a) and a longitudinal crack along the connection between the arch and the vault (Figure 28b).

(a) (b)

Figure 27. North transept: (a) water infiltration; (b) crack along the connection with wall.

(a) (b)

Figure 28. South transept: (a) crack on the cornice near the chancel wall; (b) crack and rainwater infiltration on top of the arch

The Chapel of the Blessed Sacrament shows significant settlements of the soil foundation. The deformation is visible in the decorative wooden elements that cover the masonry walls, with a maximum displacement of 5.50 cm (Figure 29).

(a) (b)

Figure 29. Damage in the Chapel of the Blessed Sacrament: (a) wood deterioration and soil settlement; (b) maximum displacement equal to 5.50 cm.

The arch of the dome in front of the chancel has a crack near the keystone and shows joints with loss of mortar (Figure 30). Several repairs carried out in past interventions can be identified in the other arches of the crossing.

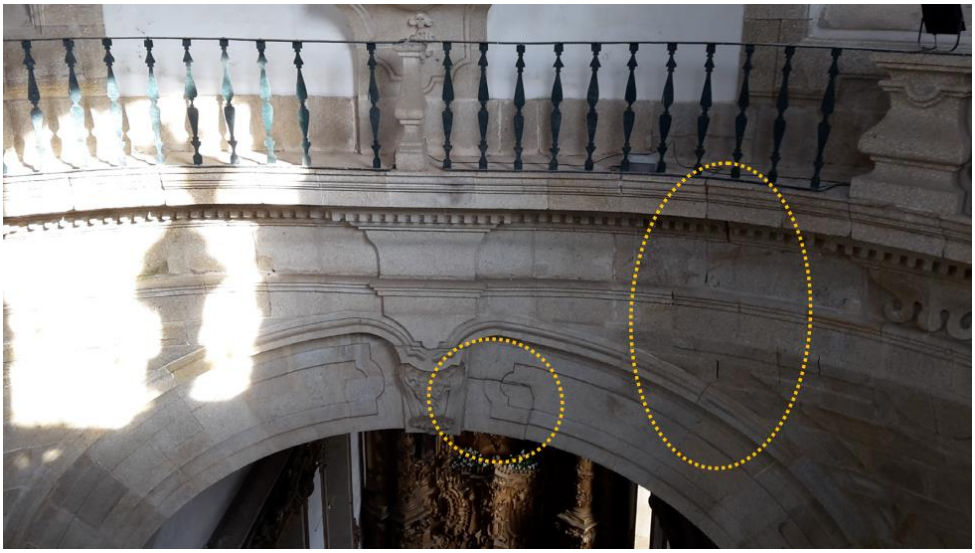

Figure 30. Arch below the dome between the crossing and the chancel: crack near the keystone and joints without mortar.

The lintel of one window and the lintel of the door located in the north wall of the chancel show an old crack repaired with mortar (Figure 31a and b). The cornice presents damage near the altar (Figure 31c). The south wall of the chancel has also cracks around the openings and in the cornice near the altar (Figure 32a and b). The intrados of the chancel vault shows damp patches and cracks with reduced width in the transversal direction (Figure 33). Finally, the ground floor of the chancel presents significant settlements near the altar (Figure 34a). The maximum deformation of the floor occurs along the south wall of the chancel and is equal to 13.50 cm (Figure 34b).

(a) (b) (c)

Figure 31. North wall of the chancel: (a) repaired crack with no signs of movement; (b) repaired crack on the door lintel; (c) crack with out-of-plane movement on the cornice next to the altar.

(a) (b) (c)

Figure 32. South wall of the chancel: (a) crack with downward displacement on the top of the opening; (b) crack on the cornice near the altar; (c) moisture stains and deterioration of plaster.

The walls of the stairs located near the south façade behind the high altar have several cracks (Figure 35), mainly along the connection between orthogonal walls, openings and floors. On the contrary, the walls of the stairs near the north façade show no significant damage.

The annex bodies to the south of the nave shows significant deterioration related to the presence of water, namely moisture stains on the walls and ceiling, efflorescence and fungi. The vault of the secondary access to the sacristy (Figure 36) has minor diagonal cracks. In the sacristy, the vault shows a crack with reduced width (Figure 37a). Also in the sacristy, the arch has a crack near the south wall and in between the stone units (Figure 37b). The wall of the stairs of the pulpit on the south side of the nave has a vertical crack with reduced opening (Figure 37c).

The adjacent bodies located to the north of the nave and chancel show minor or none structural damage. On the other hand, these annexed parts present significant non-structural damage due to the presence of water, namely moisture stains, deterioration of plaster and painted surfaces, rising damp and fungi. In the back part of the church, behind the altar, the ceiling of the museum store shows cracks with reduced opening, particularly near the entrance and the central arch (Figure 38).

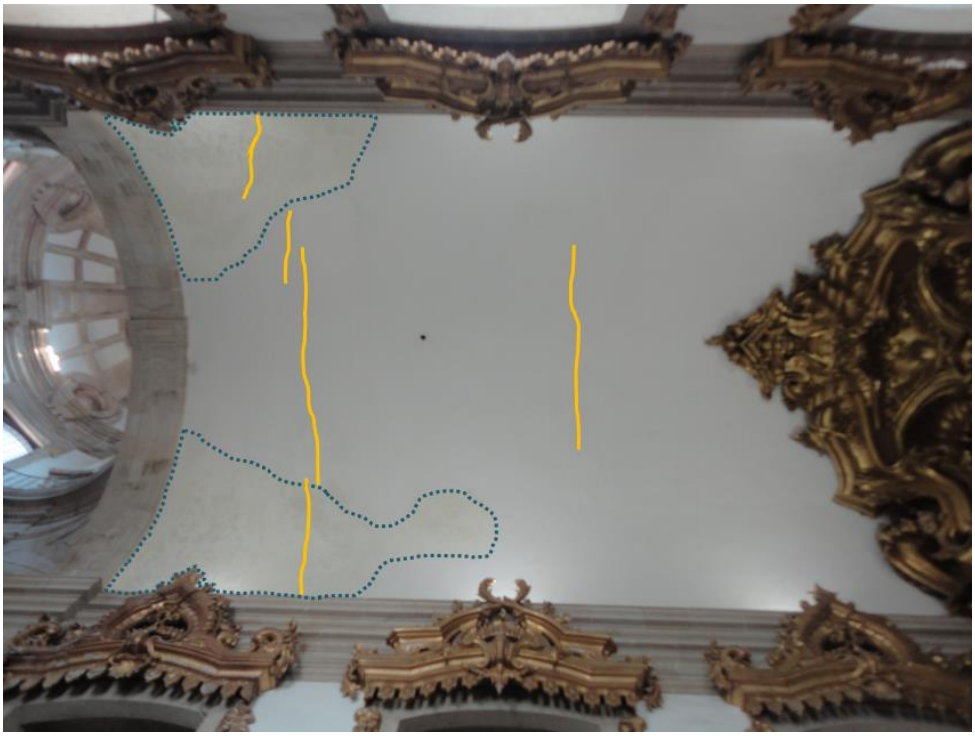

Figure 33. Moisture stains and cracks in the plaster of the chancel vault.

(a)

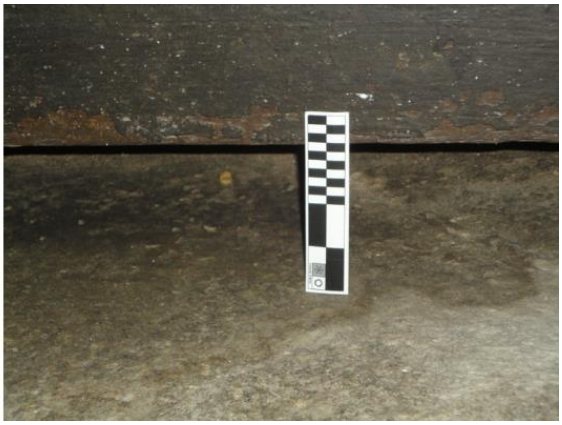

(b)

Figure 34. Deformation of the high altar floor: (a) floor settlement near the south wall of the chancel; (b) maximum deformation equal to 13.50 cm.

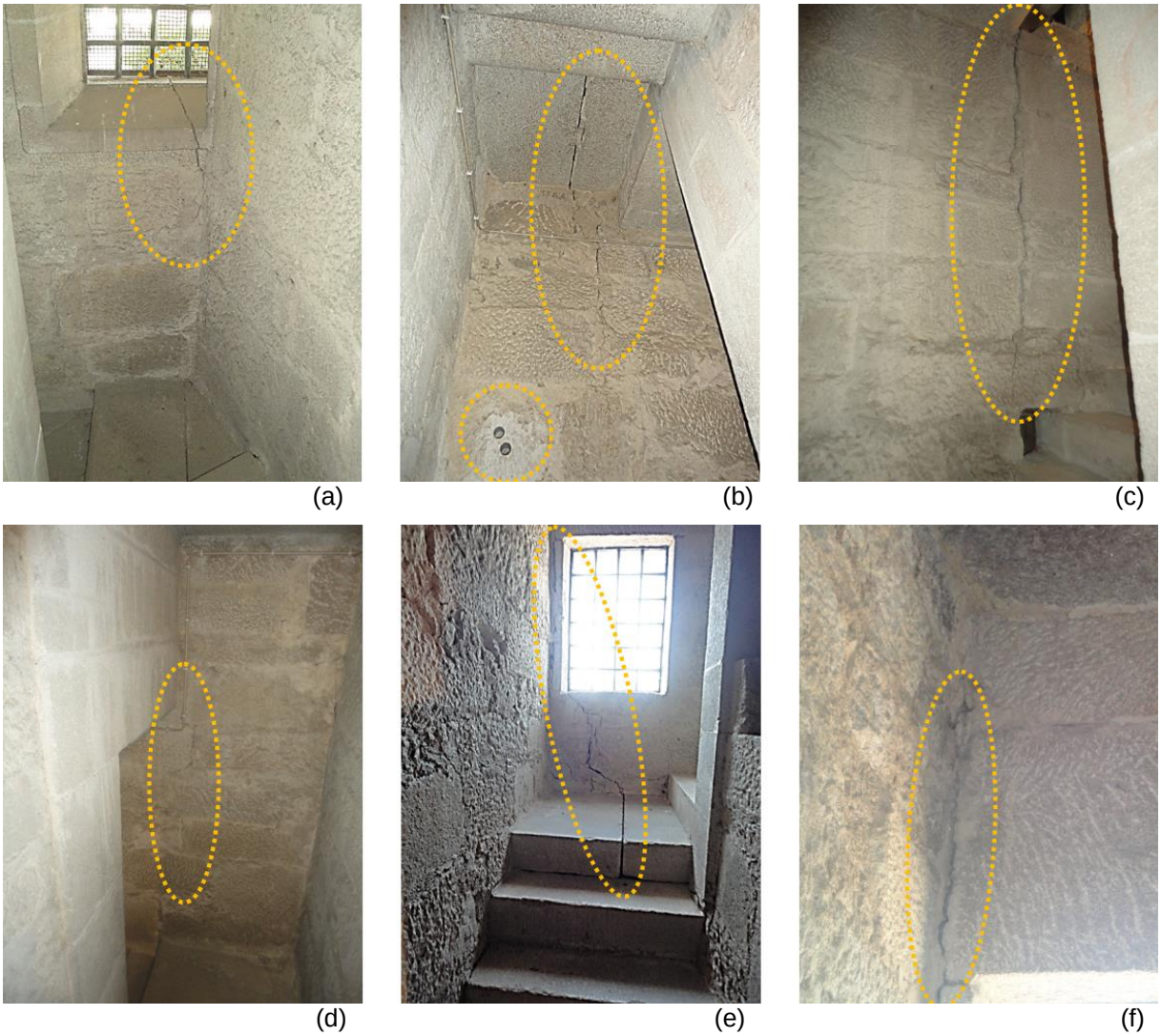

Figure 35. Cracks on the walls of the staircase behind the altar: (a) crack near the lower opening of the south wall; (b) crack in a horizontal stone joint extending to the wall; (c) crack in the angle between the south wall of the chancel and the orthogonal wall; (d) crack between orthogonal walls near the first flight of the stairs; (e) crack near the higher opening of the south wall; (f) detail of the crack on top of the opening of the south wall.

Figure 36. Cracks and moisture stains on the vault of the secondary access to the sacristy.

(a)

(b)

(c)

Figure 37. Sacristy: (a) diagonal crack on the vault extending to the lunette; (b) crack in the arch between stone blocks; (c) vertical crack on the wall of the staircase to access to the south pulpit

(a)

(b)

Figure 38. Damage in the store of the Museum of Sacred Art: (a) cracks on the ceiling near the entrance; (b) crack in the cross vault extending from the arch.

In the first floor, non-structural damage due to the rainwater penetration is observed. The ceiling above the choir presents moisture stains along the edges of the vault and the main façade (Figure 39b). The walls present other non-structural damage associated to the infiltration of rainwater through the existing crack in the connection between the main façade and the south tower. Minor structural damages can be found as well. The external wall of the bellows room (Figure 39a) shows a crack near a doorjamb. The arch of the access to the choir loft presents a crack following a joint near the keystone (Figure 40).

(a) (b)

Figure 39. Damage in the first floor: (a) moisture stains in the vault above the choir loft; (b) crack and moisture stains on a wall in the bellows room.

(a) (b)

Figure 40. Damage in the arch of the entrance to the choir loft: (a) general overview; (b) crack detail.

On the other side of the church, behind the altar, a general good state of conservation was observed. In the abbey auditing room there is a repaired vertical crack near the doorjamb of the south access (Figure 41). The access room in the south does not show other significant damage.

The north tower, which is the one fully accessible, shows no significant internal damage, highlighting only the existence of parts repaired with mortar, electric light mains on the walls and some metal elements with corrosion (Figure 42).

(a) (b)

Figure 41. Damage in the abbey auditing room: (a) repaired crack near the south entrance; (b) detail of the crack near the top of the wall.

(a) (b)

Figure 42. Interior of the north tower: (a) general overview; (b) metallic element with corrosion.

The top parts of the nave walls show several cracks, namely in the connection between the façades and the towers (Figure 43). Moreover, the extrados of the nave vault has deposits of materials near the masonry walls (Figure 43e and f). As previously stated, a formerly existing truss was removed. The visible reduction of the cross-section in the secondary beams of the roof corroborates this hypothesis (Figure 44a). The timber beams are bonded with the walls through metallic elements that currently show corrosion (Figure 44b). Similar damage appears in connections between wooden elements joined by nails (Figure 44c). In general, the timber elements show cracks in the longitudinal direction (Figure 44d).

Figure 43. Top part of the walls over the nave vault (extrados): (a) general overview; (b) crack in the connection between the main façade and the south tower; (c) crack in the main façade; (d) crack near the access from the north tower; (e) and (f) material deposit and debris.

Figure 44. Roof above the nave: (a) visible cut of the cross-section of a secondary beam, indicating the removal of a former truss; (b) detail of the connection between a truss and the top of the wall; (c) damage in the connection of the top chords; (d) fissure along the top chord.

3.2 Temperature and relative humidity monitoring

Relative humidity and air temperature are important aspects associated to the damage and comfort. The temperature (T), dew point (PO) and the relative humidity (HR) were monitored inside the church in four locations: (a) The high altar (S1); (b) Chapel of the Blessed Sacrament (S2); (c) Pulpit in the southern wall of the nave (S3); (d) Organ at the north of the choir loft (S4). Measurements were recorded during the time period between December 18, 2014 and February 4, 2016, covering a complete year (see Appendix. A.3). The sampling period of the measurements is equal to one hour.

The four chosen points present similar records for the three monitored parameters (Appendix A.3). The average minimum temperature occurred in winter (9 °C), increased in spring (17 °C) and reached the maximum in summer (22 °C). The average relative humidity followed an opposite trend, reaching a maximum in winter (74%), decreasing in spring (65%) and meeting the minimum in summer (62%).

Considering the entire monitoring period for the four locations, the values for the average total, maximum and minimum temperature within the church are equal to 15 °C, 27 °C and 4 °C, respectively. The dew point for the average total, maximum and minimum is equal to 9 °C, 20 °C and -6 °C, respectively.

Finally, regarding the relative humidity, the overall average and average maximum and minimum inside the church are equal to 71%, 97% and 35%, respectively.

The Portuguese code RCCTE (RCCTE 2006) defines the requirements to ensure thermal comfort without excessive energy necessities in new buildings and major refurbishments. According to this document, the reference comfort conditions are air temperature equal to 20 °C for the heating season (winter) and air temperature of 25 °C and 50% relative humidity for the cooling season (summer). Although the modern codes, such as the RSECE (RSECE 2006), are not applicable to the church in study, it is worth noticing that the average temperature and relative humidity recorded in the summer (22 °C, 62%) are more favourable than the regulatory limits. However, the average minimum winter temperature (9 °C) is significantly lower than the comfort temperature recommended for the same period (20 °C) and the maximum relative humidity is excessively high.

3.3 Dynamic identification tests

The dynamic identification tests were carried out in order to estimate the dynamic properties of the church (natural frequencies and mode shapes), which can be used to validate advanced numerical models as well. The accelerations of the structure caused by ambient vibration (wind action, traffic, etc.) were recorded using piezoelectric accelerometers with 10 V/g sensitivity (± 0.5 g pk), acquisition boards with 24-bit resolution and a USB chassis connected to a computer. The acceleration time series were acquired with a sampling frequency equal to 200 Hz. The total duration of the signals is equal to 30 min.

The planning for the dynamic identification test included five setups, in which the vibrations were measured at the top of the walls of the nave, in the dome and in the chancel, in both transversal (X) and longitudinal (Y) directions of the church (Figure 45). The setups were correlated using a reference accelerometer (REF) placed on the balcony of the dome in the transversal direction of the church. The setups 1 and 2 were performed using ten accelerometers placed on the top of the walls of the nave, including the main façade and the balcony of the dome. The setups 3 and 4 included the reference accelerometer and two accelerometers placed on the cornice of the chancel. Finally, the setup 5 included the reference accelerometer and four accelerometers placed near the high altar corners.

The signs of the dynamic identification tests were processed in ARTeMIS Modal software (SVS 2009), by using two different methods, namely: (a) Enhanced Frequency Domain Decomposition (EFDD); (b) Stochastic Subspace Identification based on Unweighted Principal Component (SSI-UPC). Both methods allowed estimating six modes, with frequencies ranging from 1.79 Hz to 5.14 Hz. The results allow highlighting two peaks with high amplitude, namely the frequency peaks associated with the second (2.75 Hz) and third (3.72 Hz, 3.73 Hz) modes.

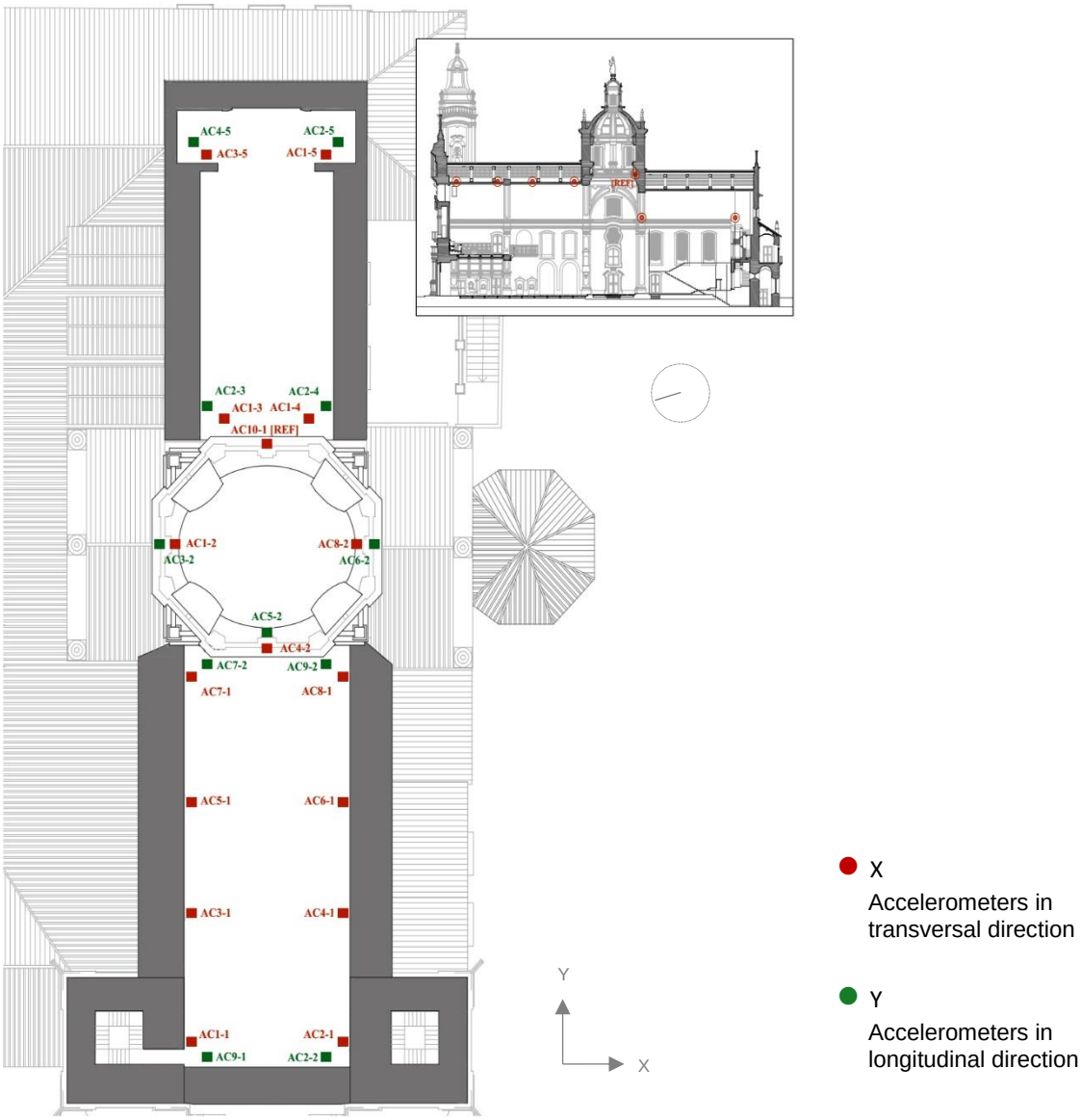

Figure 45. Location of the accelerometers for the dynamic identification tests.

The six estimated modes are associated with local and global modes mainly in the transversal direction of the church (Figure 46). Only one mode is detected in the longitudinal direction. The transversal direction of the church corresponds to the direction in which the structure is more flexible and thus is associated with the modes with lower frequencies, which are more easily detected by the dynamic identification tests.

The first mode of vibration (1.79 Hz) is associated with a local mode of the nave, possibly related to the vibration of the towers in the transversal direction. The second mode (2.75 Hz) is the first global mode, with simple curvature in the transversal direction of the church. The third vibration mode (3.72 Hz) has double curvature, corresponding to a global translation of the church in the transversal direction. The fourth mode of vibration (4.07 Hz) is the first one in the longitudinal direction, emphasizing the local

behaviour of the southwest corner, which may be associated with the existing damage in this part (Figure 79). The fifth mode (4.78 Hz) corresponds to a global mode of the church in the transversal direction where the dome moves in the opposite direction regarding the nave and chancel (triple curvature). Finally, the sixth mode of vibration (5.14 Hz) corresponds to a combined mode with a greater contribution in the transversal direction of the church and rotation of the dome.

The vibration modes for the two methods were compared using the MAC (Model Assurance Criterion) (Ewins 2000). The MAC of the first three modes of vibration show values between 0.89 and 0.99 (0.93 average), indicating that the results obtained by the two methods are very similar (Table 1). The remaining three modes of vibration associated with the higher frequencies have low MAC values, with an average equal to 0.56.

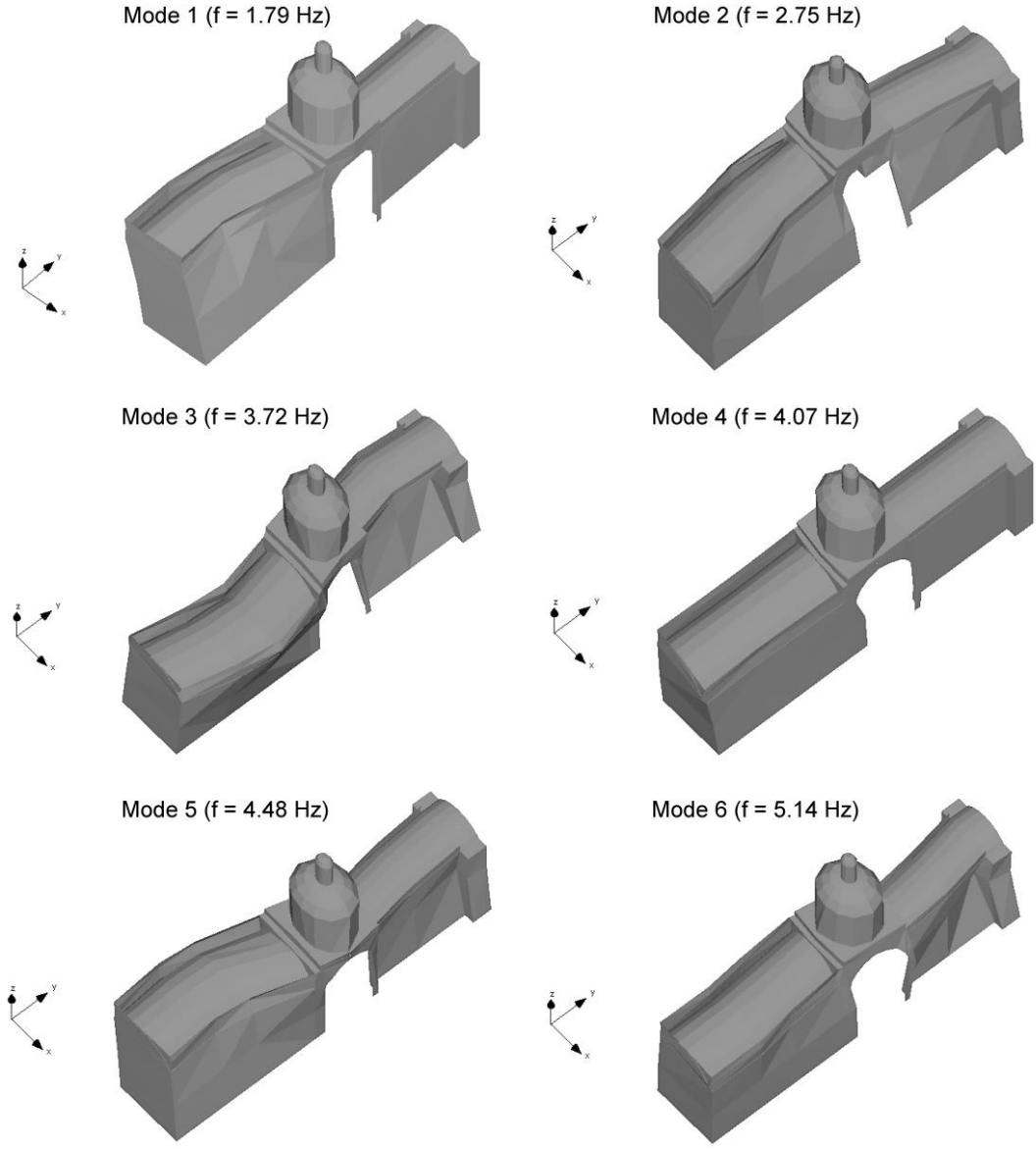

Figure 46. Modes estimated by SSI-UPC method.

Table 1. MAC values for the modes estimated through the EFFD and SSI-UPC methods.

		SSI-UPC					
		Mode 1 (1.79 Hz)	**Mode 2** (2.75 Hz)	**Mode 3** (3.72 Hz)	**Mode 4** (4.07 Hz)	**Mode 5** (4.48 Hz)	**Mode 6** (5.14 Hz)
EFFD	**Mode 1** (1.79 Hz)	**0.89**	0.08	0.43	0.00	0.27	0.11
	Mode 2 (2.75 Hz)	0.07	**0.99**	0.11	0.00	0.28	0.00
	Mode 3 (3.73 Hz)	0.46	0.04	**0.90**	0.02	0.04	0.02
	Mode 4 (4.19 Hz)	0.01	0.04	0.03	**0.53**	0.07	0.14
	Mode 5 (4.56 Hz)	0.58	0.05	0.13	0.01	**0.56**	0.03
	Mode 6 (5.06 Hz)	0.16	0.00	0.00	0.09	0.00	**0.60**

3.4 Georadar tests

GPR tests were performed in different parts of the monastery using an equipment with 500, 800 and 1600 MHz antennas. The georadar tests had several objectives. On one hand, the scope was to verify the existence of underground channels or water pipes. On the other hand, the tests conducted on the surfaces of walls and ceilings aimed to identify the unseen constructive elements and characterise the structure. Taking into account the scope of this thesis, only a brief description of the GPR tests is presented.

3.4.1 Tests on the walls of the church

GPR readings were carried out in various locations of the walls, namely in the main façade, the longitudinal walls of the nave, the walls of the transept and the walls of the Blessed Sacrament Chapel.

On the inner surface of the main façade two test were performed, aiming at detecting the inner leaf and assess its dimension. The thickness of this layer was estimated equal to 60 cm. However, it was also found that the thickness of the inner layer is not constant along the height of the wall, varying from 50 to 65 cm (wider in the base). Smaller values of about 48 cm thick were also detected.

On the other hand, readings on the outer surface of the main façade were made to obtain information about the exterior leaf of the wall. An external layer of about 52-58 cm was identified. Values up to 73 cm were also observed. The internal core could be identified, with thickness varying from 25 to 40 cm. A signal distant 1.70 m was also detected, which would correspond to the inner surface of the inner leaf.

Other sets of walls were also analysed, namely in the nave, transept, Chapel of the Blessed Sacrament, bellows room, stairs behind the altar and north tower. The results make evident that the internal walls of the nave are made up by three leaves with a thickness of 33-34 cm in the outer layer and an inner leaf of approximately 50-55 cm thick. In the transept, the exterior wall is not homogeneous in height. The results show a thickness ranging from 1.00 to 1.20 m (thicker below), with exterior masonry leaves between 30 and 45 cm. The same was observed in the lateral walls of the choir loft. The walls in the lateral altars of the nave show a composite structure with three layers and irregular inner core, stones with thicknesses ranging from 36 to 55 cm and overall thickness of the wall between 1.15-1.20 m.

The walls of the Chapel of the Blessed Sacrament corresponds to a composite wall as well, showing a total breadth between 77 and 80 cm, an inner leaf of about 48 cm and an outer layer of about 32 cm. In the bellows room the outer south wall was evaluated. As in the previous cases, the test showed a composite wall, with inner leaf about 30 cm thick and a total width of 70 cm. On the walls behind the altar several horizontal and vertical readings were performed. The results show that the walls are composed by irregular leaves, with stones 53-55 cm thick on the inner side and 32-37 cm on the outside. The walls of the north tower were also evaluated. The radargrams identified a wall with a total thickness about 1.00 to 1.25 m. The constitutive structure of the towers also correspond to a composite wall, wherein the inner leaf is about 35 to 46 cm thick.

3.4.2 Tests on the vaults of the nave and choir

Georadar was also used to identify the constitution of the vaults of the nave and choir loft. Regarding the tests performed in the choir, none of the obtained results could be used to determine the thickness of the vault. It was only possible to estimate the thickness of the vault ribs (about 52-55 cm).

The vault of the nave shows a thickness of about 16 cm. An additional measurement was made in an attempt to assess the infill near the vault springers. The reading showed that from the central longitudinal axis until about 3 m there is no infill (thickness about 16 cm), and from that distance an irregular layer of dust, gravel and waste about 15-30 cm thick is detected. Since no other interface was identified, it was estimated that the springer of the vault is made of masonry, as a massive element or "backing".

3.5 Geotechnical survey

The geotechnical prospection plan consisted of three Standard Penetration Tests (SPT) outside the church and four Light Dynamic Penetrometer tests (DPL) inside the church (Figure 47). This type of tests inside the building were chosen taking into account the deformation of the ground floor and the accessibility conditions. The location of the SPT tests was defined according to the main damage, namely the damage at the connection between the south tower and the main façade and the damage at the south wall.

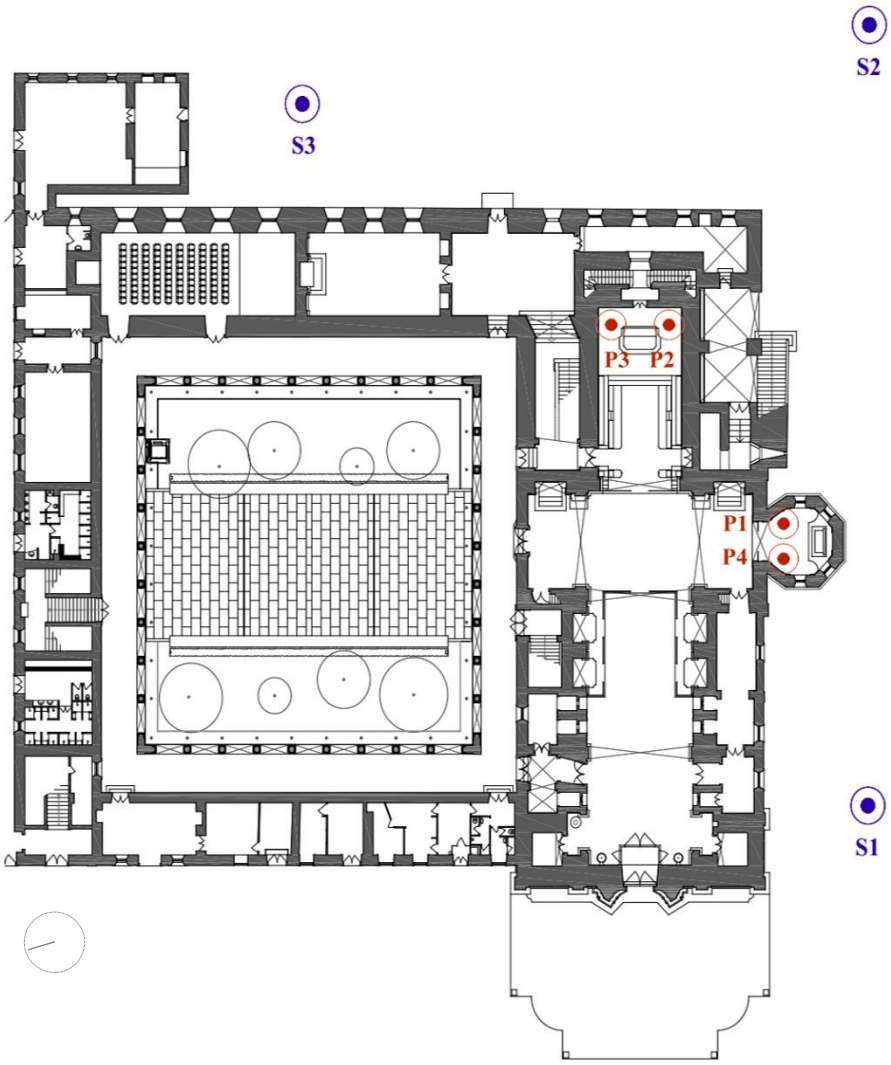

Figure 47. Location of the geotechnical tests: Standard Penetration Tests, SPT (S1, S2, S3); Light Dynamic Penetrometer tests, DPL (P1, P2, P3, P4)

3.5.1 Standard Penetration Tests (SPT)

Three mechanical drillings outside the church were made with hollow augers (Figure 47). Through the interior of the drilling holes Standard Penetration Tests (SPT) were carried out approximately every 1.50 m in order to characterise the mechanical properties of the soil. Several piezometers for groundwater level control were also installed in the bore holes.

The main observations obtained from the drilling surveys are presented below and in Figure 48:

a) Drilling S1

- 0.00 m to 2.50 m: Muddy clay with sand. It contains small scattered rock fragments, with angular, pebble size. Dark brown mouldable material.

- 2.50 m to 4.20 m: Gravelly sand layer consisting of coarse sand and abundant angular rock pieces with dispersed pebble size. Grey colour.
- 4.20 m to 10.50 m: Clayey silty sediments finely decomposed (high alteration degree - W5) with gneissic aspect. Well preserved texture showing various metamorphic deformation cycles. Rust appearance and brownish colour.

b) Drilling S2

- 0 m to 4.00 m: Muddy clay with sand. It contains small scattered rock fragments, with angular, pebble size. Dark brown mouldable material.
- 4.00 m to 5.50 m: Gravelly sand layer consisting of poorly calibrated coarse sand containing intercalated clay levels as well as abundant angular rock pieces with dispersed pebble size. Brown colour.
- 5.50 m to 9.00 m: Clayey silty sediments finely decomposed (high alteration degree - W5) with gneissic aspect. Well preserved texture showing various metamorphic deformation cycles. Rust appearance at 6.00 m and turning greyish in depth.

c) Drilling S3

- 0 m to 2.00 m: Silty to muddy clay with sand. At the depth of 0.80 m it contains a coarse gravelly level. Dark brown mouldable material.
- 2.00 m to 4.00 m: Muddy clay with sand. At 2.50 m depth it contains a coarse gravelly level.. Dark brown mouldable material.
- 4.00 m to 5.30 m: Gravelly sand layer consisting of coarse sand and abundant angular rock pieces with dispersed pebble size. Brownish colour.
- 5.30 m to 6.10 m: Sediments with high to medium alteration level and gneissic aspect. Significant textural deformation. Joints predominantly at 60º/70º with smooth surfaces, coated with iron oxides. Very fractured. Brown beige colour.

The geologic profile is characterized by a superficial layer of soft clay, which extends until approximately 4.00 m deep. Then there is a gravelly sand transition layer and finally a modified and highly fractured rock layer. This rock starts at depths between 4.20 and 5.50 m. Regarding the mechanical characteristics, the superficial layer of clay is very little resistant and deformable, presenting SPT values lower than 10. The resistance gradually increases in depth until the altered and fractured rock. The water level is extremely shallow (about 1.00 m below the surface). This aspect is according to the expected, due to the existence of the stream nearby.

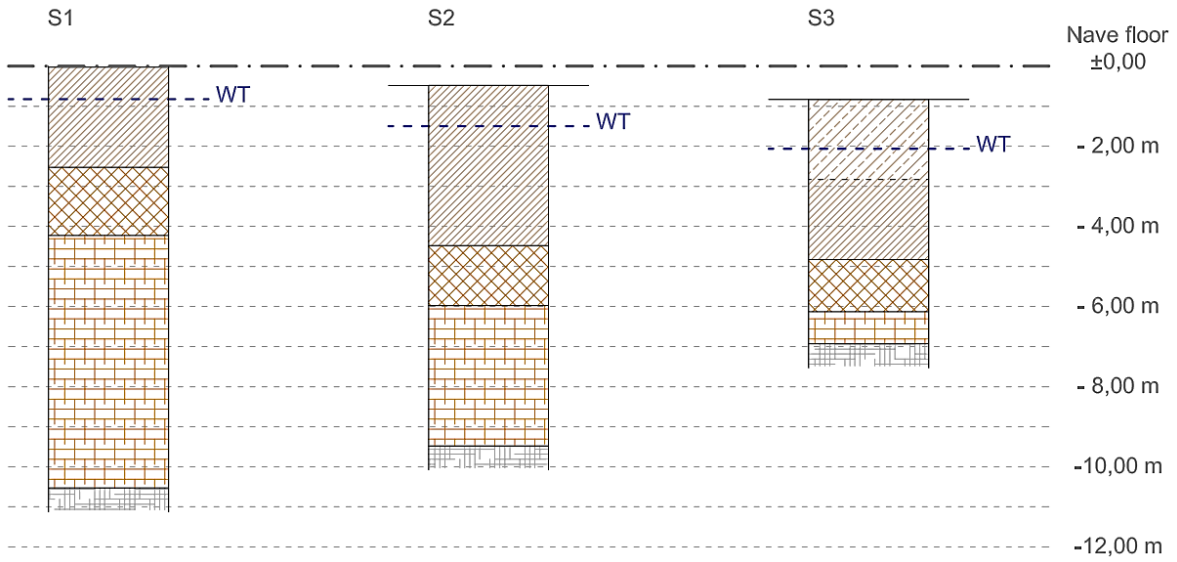

Figure 48. Standard soil profiles obtained from the mechanical tests with indication of the water table level (see Section 3.7 Water table assessment).

3.5.2 Light Dynamic Penetrometer (DPL)

Regarding the Light Dynamic Penetrometer tests (Figure 47), DPL 4 is discarded as not representative since it was stopped about 1.00 m deep. The remaining tests corroborate the results observed in the SPT tests. The two tests performed on the main altar (DPL 2 and 3) show very similar results, with a very soft material up to about 3.00 m, after which the resistance is gradually increasing until a very resistant material at a depth of 4.00 m. The test number 1 shows very similar results, in this case with a soft layer that develops up to about 4.00 m deep.

In conclusion, there is a superficial clayey layer with low resistance and high deformability that extends to depths between 3.50 to 4.00 m approximately. Below this layer, there is a gravelly sand layer with greatly improved features. Finally, a layer of altered rock can be found. The existence of the surface layer with poor geotechnical characteristics might have caused the settlements detected on the ground floor. Some damage observed in the structure could also be the results from settlements of the foundations.

3.6 Inspection trenches

The damage observed in the building, namely the existing crack in the main façade and the deformations of the ground floor in the altar and the Chapel of the Blessed Sacrament, may be associated with insufficient strength capacity of the foundations. Thus, three inspection trenches were opened outside, next to the front, east and south façades (Figure 49). The trenches were carried out taking into account several purposes, namely the identification of the foundation level, the corroboration of the type of soil

with respect to the results of the geotechnical survey, the evaluation of the type of masonry of the walls basement, and the detection and evaluation of the existence of a draining system.

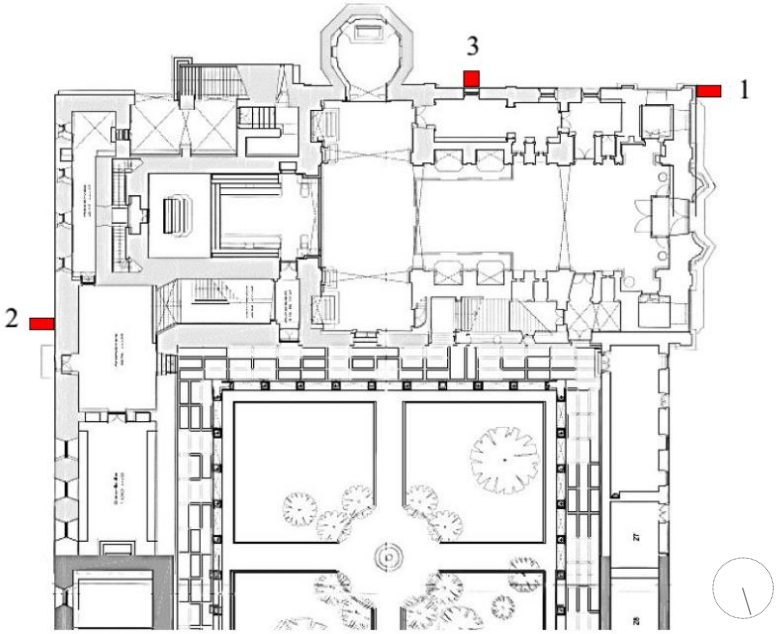

Figure 49. Location of the excavation trenches outside the church.

The excavation 1 was located in the southwest corner near the tower and was 2 m long and 1 m wide (Appx. A.2.5). The excavation was aborted at about 1.45 m depth due to the fast rise of the water level. Thus, it was impossible to identify the depth of the foundation below the tower, which may be located several meters deep. Nevertheless, it was possible to confirm the composition of the tower walls, made of irregular large granite units.

The excavation 2 was performed along the east façade of the monastery and had 2 m in the direction perpendicular to the wall and 1 m wide (Appx. A.2.6). The water level stabilized at about 1.30 m from the floor level. Due to the presence of a drain tube and the high water level, the excavation of the second inspection trench was finalised.

A third inspection trench was excavated near the south façade of the church, with 1.65 m in the direction perpendicular to the wall and 1.50 m wide (Appx. A.2.7). The water level stabilized at about 1.10 m deep with respect to the height of the top surface at the hole. Once more, due to the presence of the drain and the high water level the excavation was concluded.

Due to the technical hitches regarding the excavation, the trenches outside the church did not allow to identify the dimension of the foundations. However, they made possible to identify the presence of drains along the façades and also allowed to check that the water level can be found very close to the ground floor of the church, even in summer.

3.7 Water table assessment

The presence of water in the soil near foundations and floors is usually associated with the existence of rising damp, moisture stains on the walls and stone floors, material deterioration, presence of fungi at the base of the walls and overall discomfort inside the building. Since the church of the Monastery of S. Miguel de Refojos presents all these aspects, the water level surrounding the church was evaluated using the installed piezometers in the boreholes of the geotechnical survey and the inspection trenches near the exterior walls.

Appendices A.2.8 and A.2.9 show the profile of the maximum and minimum height of the water level in the alignment of piezometers S1 and S2 and the alignment of piezometers S2 and S3, respectively. Six measurements were made during the spring and summer seasons, and the values were related to the height of the church floor. The maximum water table level measured in S1 and S2 was about 0.77 m below the nave floor and 0.55 m above the level of the store floor in the Museum of Sacred Art (Appx. A.2.8). The maximum height of the water table measured in S3 was about 0.45 m below the floor of the old ante-sacristy (Appx. A.2.9). Assuming a linear variation of the water level between piezometers, the water level in the two analysed profiles is very close to the church floor and it even appears above the height of the floors in the Museum of Sacred art, former ante-sacristy and old sacristy. The flow of water in the soil occurs in the west-east direction as expected, with an average gradient of 0.8% (measured between S1 and S2).

The inspection tranches were left opened for about two weeks, aiming to check the water level along the church walls. During that time, the water level rose relatively to the groundwater level checked immediately after the completion of the excavations. For the soil in the front yard the water level stabilized at about 0.93 m below the nave floor (Figure 50a). The water level also increased in the second trench (next to the east façade), stabilizing at about 0.65 m below the floor of the old ante-sacristy (Figure 50c). Note that this value is lower than the minimum value of the water level profile in piezometers S2 and S3 (about 0.55 m), indicating that the volumes of the church under the ground act as a barrier to the flow of water in the soil. Finally, the water level at the trench number 3 (south façade) stabilized at about 1.10 m below the nave floor (Figure 50d).

A new evaluation of the water table level was performed in May 2016, during the development of this dissertation. The measurements were carried out in the holes of the geotechnical survey and the results revealed little variation with respect to the previous data:

- S1: Water level detected at -0.86 m from the surface (-0.89 m below the nave ground floor).
- S2: Water level at -0.90 m from the surface (-1.38 m measured from the nave floor and -0.06 m below the floor of the Museum of Sacred Art store).
- S3: Water level at -1.20 m from the surface (-2.09 m from the nave ground floor and -1.22 m below the old ante-sacristy floor).

(a) (b)

(c) (d)

Figure 50. Water table visible in the inspection trenches days after the excavation (summer period). (a) Excavation 1: water level at -0.93 m below the nave floor; (b) Excavation 2 right after the conclusion of the excavation works; (c) Excavation 2: water level at -0.65 m deep with respect to the floor of the old ante-sacristy; (d) Excavation 3: water table at -1.10 m measured from floor of the nave.

4. PREPARATION AND CALIBRATION OF THE NUMERICAL MODEL

The numerical model of the church of the Monastery of São Miguel de Refojos was prepared using the software DIANA (DIsplacement ANAlyser) (TNO DIANA BV 2014). A preliminary 3D model was defined in AutoCAD and then imported to Midas FX+ pre/post processor, where the numerical model was prepared based on the Finite Element Method (FEM).

4.1 Units

The input for DIANA is free from units, therefore a consistent system of units must be chosen and all data must be introduced with respect to that system (TNO DIANA BV 2014). By doing so, the software will give the output in the appropriate units chosen. Table 2 presents the system of units adopted for the preparation of the numerical model.

Table 2. System of units used in the definition of the model (TNO DIANA BV 2014)

Unit:	Length	Mass	Time	Temperature	Velocity	Acceleration	Force	Stress
Derivation:	l	m	t	T	$l \cdot t^{-1}$	$l \cdot t^{-2}$	$m \cdot l \cdot t^{-2}$	$m \cdot l^{-1} \cdot t^{-2}$
m - t - kN	m	t	s	ºK	m/s	m/s^2	kN	kPa

4.2 Geometry

According to the scope of the study, the main volume of the church was modelled, as well as the annexed parts located at one and the other side of the nave and chancel (Figure 51). The stiffness of the remaining parts of the monastery adjacent to the studied volume was considered and modelled using springs. In the geometrical definition, the architectural details were simplified and only the main structural solid parts were modelled. The roof structure above the transept and chancel was hypothesised since the access to those parts for visual inspection was not possible.

Considering the different parts of the building, the level of the floor varies considerably from one space to the others, with a maximum level of +1.50 m in the rear part of the altar (reference level 0.00 m at the ground floor of the nave) and a minimum level at -1.58 m measured in the store of the Museum of Sacred Art, right behind the altar. In the model, an overall base level was assumed for all the walls and it is located at -2.08 m below the nave floor level (0.50 m lower than the floor of the Museum store).

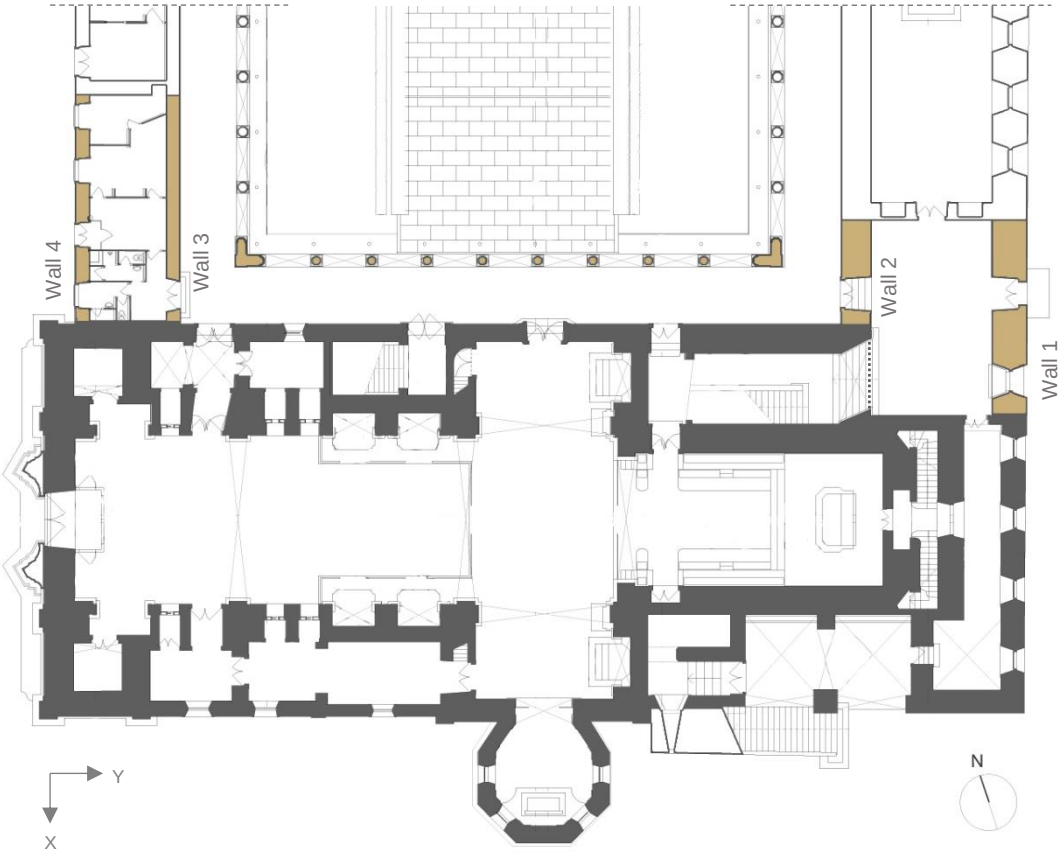

Figure 51. Parts of the building considered for the model (dark hatch) and adjacent parts included as springs (lighter hatch). Axes: X (transversal direction), Y (longitudinal direction)

4.3 Type of elements

The first numerical model of the building was prepared with a mesh consisting only of solid elements. However, due to computational difficulties some simplifications were needed. Finally, two different types of elements were used: solid elements for the massive parts of the church, namely walls, arches and columns, and shell elements for the thinner structural components, i.e. the vaults covering the church and lateral annexes. Beam elements were also used for simulating the timber trusses.

In total, the numerical model comprehends 376,955 nodes and 1,630,699 elements. The greatest portion of the model, more than 96%, correspond to the massive solid part and it is built with four-node isoparametric tetrahedron elements TE12L (Figure 52a). Three-node triangular isoparametric curved shell elements T15SH (Figure 52b) and six-node triangular isoparametric curved shell elements CT30S (Figure 52c) were employed for meshing the vaults. On the other hand, three-node three-dimensional class-III beam elements CL18B were used for the trusses of the roof. Finally, SP1TR elements are employed for the definition of one-node translation springs (stiffness of the adjacent buildings).

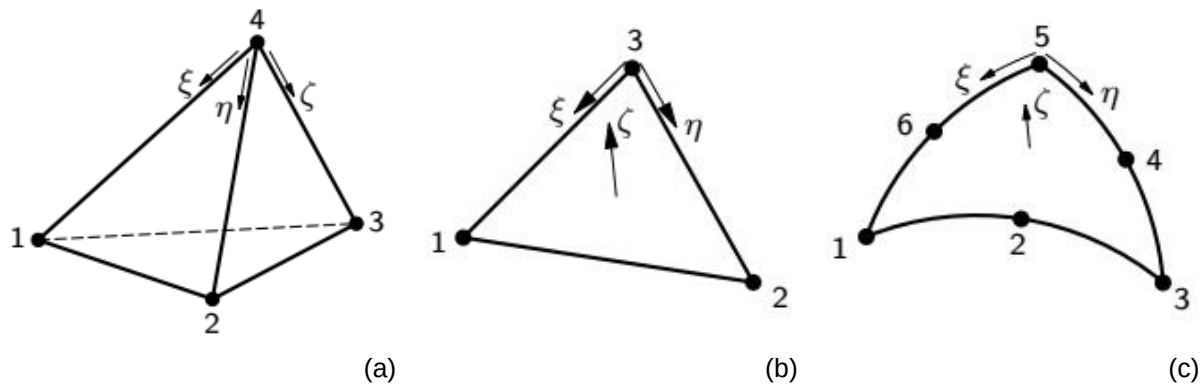

Figure 52. Main elements used in the model: (a) TE12L, 4-node tetrahedron element; (b) T15SH, 3-node curved shell element; (c) CT30S, 6-node curved shell element. (TNO DIANA BV 2014)

4.4 Materials

Different materials were identified taking into account the results of the GPR tests and the visual inspection of the church, namely brick masonry (vaults), good quality ashlar masonry (thin walls in the chancel, arches, ornamental top of towers and dome), and three-leaf masonry walls (main thick walls and the rest of the elements). Inside the masonry group, an auxiliary granite stone is applied for the lintels. Finally, the beam elements of the roof structure were characterised as timber (Figure 53).

Due to the lack of quantitative information regarding the physical and mechanical properties of the materials, for the first trial model typical values are adopted based on literature, according to the qualitative information from the inspection tests.

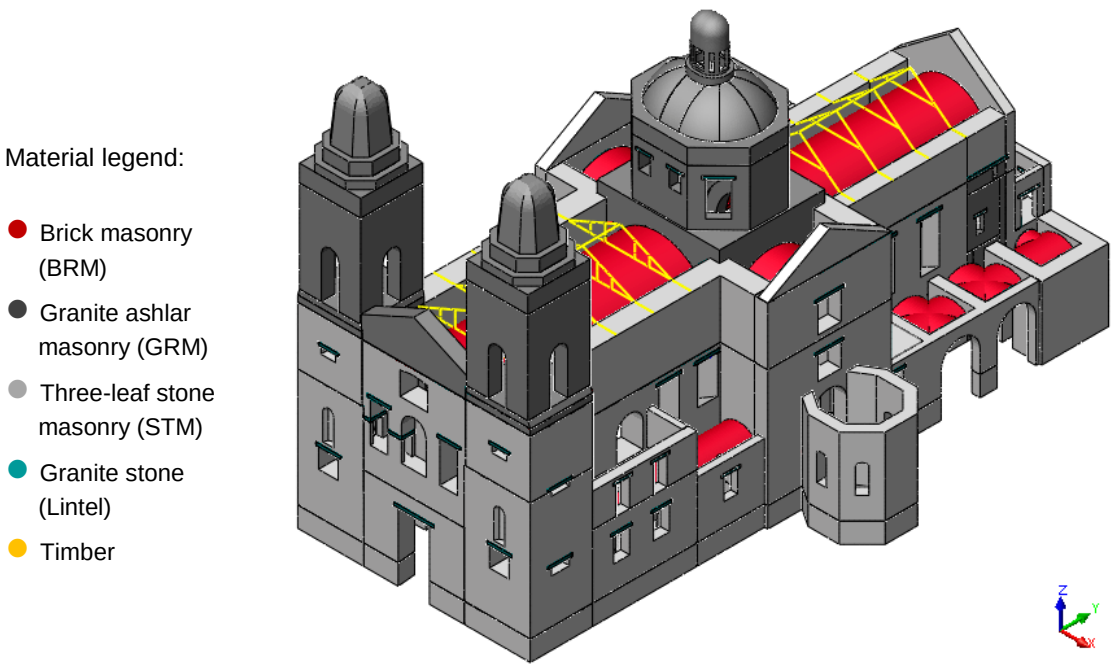

Figure 53. Axonometric view of the model with identification of the different materials

For the main group of masonry materials, the Modulus of elasticity E was initially estimated based on the Italian code NTC-08 (NTC 2008). An average value from the range proposed in the code was selected for each typology of masonry, as presented in Table 3.

Table 3. Linear-elastic properties of masonry (NTC 2008)

Brick masonry (BRM)

Material property	Symbol	Value	Unit
Density	ρ	1800	kg/m^3
Modulus of elasticity	E	1500	MPa
Poisson's ratio	ν	0.20	--

Three-leaf stone masonry (STM)

Material property	Symbol	Value	Unit
Density	ρ	2000	kg/m^3
Modulus of elasticity	E	1250	MPa
Poisson's ratio	ν	0.20	--

Granite ashlar masonry (GRM)

Material property	Symbol	Value	Unit
Density	ρ	2100	kg/m^3
Modulus of elasticity	E	1750	MPa
Poisson's ratio	ν	0.20	--

A specific granite material was created in order to define the lintel elements. The properties of the granitic stone (Table 4) were estimated as the average values of a set of experimental tests (Vasconcelos 2005). Note that the Modulus of elasticity defined through the experiments is quite high. That assumption can be incorrect when considering old stone blocks extracted from upper parts of the quarry. However, within the context of a material definition of the numerical model, this assumption seems appropriate since the ultimate goal is to define a stiff material applicable to the lintels and limited damage is expected on these elements of the church.

Table 4. Linear-elastic properties of granite lintels (Vasconcelos 2005)

Granite

Material property	Symbol	Value	Unit
Density	ρ	2500	kg/m^3
Modulus of elasticity	E	30000	MPa
Poisson's ratio	ν	0.20	--

Finally, the material properties for timber elements were obtained from experimental tests and the probabilistic model code, as proposed by (Poletti 2013). The values used for the wooden linear elements are shown in Table 5.

Table 5. Linear-elastic properties of timber (Poletti 2013)

Pine wood

Material property	**Symbol**	**Value**	**Unit**
Density	ρ	600	kg/m^3
Modulus of elasticity (parallel to fibres)	E_0	13000	MPa
Poisson's ratio	ν	0.30	--

4.5 Loads

For the scope of this work, only vertical gravitational loads and the seismic horizontal loads were considered in the numerical analysis.

4.5.1 Self-weight

The gravitational loads of the structure were considered automatically by DIANA according to the density of the material and the geometric properties of the elements (Table 6).

Table 6. Self-weight of the modelled elements organised by material

Material	Elements	Density [t/m^3]	Volume [m^3]	Mass [t]	Weight [kN]
Timber	Roof trusses	0.60	22.60	13.56	133.01
Brick masonry	Vaults	1.80	187.93	338.28	3,318.54
Three-leaf stone masonry	Thick walls	2.00	6,613.24	13,226.48	129,751.77
Granite ashlar masonry	Thin walls	2.10	1,719.73	3,611.43	35,428.16
Granite stone	Lintels	2.50	129.91	324.76	3,185.92
				TOTAL	171,817.40

4.5.2 Roof load

The self-weight of the roof (tiles, battens, rafters and purlins) was assumed equal to 1 kN/m^2 and applied as a linear distributed load to the timber trusses according to the roof area supported by each element (Table 7). The lateral end of each part of the roof is supported directly by the walls and, therefore, the load was applied directly on the solid elements. The possibility of modelling the loads as concentrated nodal masses was rejected since the roof loads are of little influence in the global weight of the structure.

Table 7. Weight of the roof considered as a load

Location	Element	Roof load [kN/m^2]	$L_{transversal}$ [m]	Distributed load, q_{roof} [kN/m]
Nave roof	Trusses	1.00	3.85	3.85
	End walls	1.00	1.95	1.95
Chancel roof	Trusses	1.00	3.80	3.80
	End walls	1.00	1.90	1.90
North transept roof	End walls	1.00	2.25	2.25
South transept roof	End walls	1.00	2.50	2.50

4.5.3 Infill load

The infill material above the vaults usually provides some stiffness to the rest of the structure according to its cohesion and strength. Since no information was collected regarding the properties of the infill, the stiffness of this part was not taken into account and a more conservative approach was adopted. As in the previous case, the possibility of defining the loads as a concentrated nodal mass was also rejected due to the low relevance of these parts when comparing them with the global weight of the structure. Hence, the infill material above the smaller vaults of the annexes was not considered. On the other hand, the filling material above the main vaults was modelled as a distributed superficial load. The value of the infill load represents the weight of the material, which was assumed 12 kN/m^3, and it increases with the depth assuming a triangular simplification (Table 8). Note that the height of the infill on the vaults of the transepts and the chancel had to be hypothesised.

Table 8. Weight of the vaults infill material applied as a load

Location	Maximum depth of infill, h [m]	h/2 [m]	Infill load [kN/m^3]	Distributed load, q_{infill} [kN/m^2]
Choir vault	3.20	1.60	12.00	19.20
Nave vault	3.50	1.75	12.00	21.00
Chancel vault	2.30	1.15	12.00	13.80
North transept vault	2.40	1.20	12.00	14.40
South transept vault	2.40	1.20	12.00	14.40

4.5.4 Seismic load

In the seismic analysis, a pushover analysis with horizontal load pattern proportional to the mass of the structure was adopted, which corresponds to the first distribution of lateral forces defined by Eurocode 8 (EN 1998-1 2004)).

4.6 Boundary conditions

For the initial phases of the structural analysis, all degrees of freedom of the nodes at the base level are restricted, i.e. pinned, providing a clamped boundary condition for the walls. Subsequently, the soil-structure interaction and the boundary conditions at the base was also evaluated using interface elements (see Chapter 5).

Regarding the connection between different elements of the structure, the joint between the timber trusses and the top part of the walls was considered to be simply supported, as detected during the visual inspection (Figure 44b). Furthermore, the supporting portion of the truss extends all the way into the wall in order to avoid possible concentration of stresses.

The parts of the monastery adjacent to the modelled volume are defined as springs with a certain stiffness in the normal direction of the wall (Figure 51). For each element the stiffness is calculated considering the type of material, the contact area and the length of the wall, as well as a correction factor that takes into account the existence of openings and therefore the effective mass:

$$k_n = \frac{E \cdot A}{L} \cdot CF \quad [kN/m] \tag{1}$$

The resultant stiffness is then divided by the number of nodes in the connection area and the final value is introduced in DIANA as a new material and property (Table 9).

Table 9. Normal stiffness provided by the adjacent perpendicular walls

Element	**E** [kN/m^2]	**A** [m^2]	**L** [m]	**k_n** [kN/m]	**C.F.** [%]	**$k_{n\text{-}c}$** [kN/m]	**No. nodes**	**$k_{n\text{-}c\text{-}nodes}$** [kN/m]
Wall_1a	1.25E+06	14.30	11.90	2.13E+08	65%	1.38E+08	232	5.96E+05
Wall_1b	1.25E+06	3.42	8.96	3.83E+07	65%	2.49E+07	56	4.45E+05
Wall_2	1.25E+06	3.68	6.30	2.90E+07	70%	2.03E+07	192	1.06E+05
Wall_3a	1.25E+06	6.38	13.90	1.11E+08	85%	9.42E+07	123	7.66E+05
Wall_3b	1.25E+06	6.10	13.90	1.06E+08	55%	5.83E+07	108	5.40E+05
Wall_4a	1.25E+06	6.45	13.90	1.12E+08	55%	6.16E+07	104	5.93E+05
Wall_4b	1.25E+06	3.54	13.90	6.15E+07	70%	4.31E+07	52	8.28E+05

On the other hand, the influence of the cloister was calculated as the sum of the lateral stiffness of each column, assumed to be pinned, plus the corresponding solid part of the arch on top of them:

$$k_n = No.elements \cdot \left(\frac{3 \cdot E \cdot I_{column}}{h_{column}^3} + \frac{3 \cdot E \cdot I_{eq.rec}}{h_{eq.rec}^3} \right) \quad [kN/m] \tag{2}$$

where $I_{eq.rec}$ and $h_{eq.rec}$ correspond to the massive part on top of the columns, assumed to be pinned as well and simplified as a rectangle with equivalent area.

The stiffer effect of the corners in the cloister was taken into account by virtually increasing the number of elements in the equation. As done for the walls, the resultant stiffness is divided by the number of nodes and applied in DIANA as a new material and property (Table 10).

Table 10. Normal stiffness provided by the cloister

Element	**E** [kN/m^2]	**A** [m^2]	**L** [m]	**k_n** [kN/m]	**C.F.** [%]	**$k_{n\text{-}c}$** [kN/m]	**No. nodes**	**$k_{n\text{-}c\text{-}nodes}$** [kN/m]
Cloister	1.25E+06	--	--	2.66E+05	100%	2.66E+05	267	9.96E+02

4.7 Linear static analysis

A first analysis was performed taking into account only the gravitational loads, i.e. self-weight of the elements plus the loads defined as to substitute the roof and the infill material (Table 11). This analysis was carried out aiming at checking that there were no irregularities in the model, such as geometric, material or loading inconsistencies.

Table 11. Total vertical reaction (FBZ(V))

	Load cases	Expected result [kN]	Result from analysis [kN]
Independent cases	Load case 1: Self-weight of elements	171,817.40	171,810.17
	Load case 2: Roof load	385.71	385.76
	Load case 3: Infill load	4,201.93	4,197.61
Final global case	Load case 4: Global weight	177,705.52	176,393.54

The first control is presented in Table 11 and it consists in the comparison between the total vertical reaction obtained through the analysis and the same resultant value estimated by simple calculation. As expected, the range of the results is according to the expected and the total error is less than 1%.

Other possible verification is the control of displacements. According to the analysis, the maximum vertical displacement of the structure subjected to its self-weight is equal to 9 mm (Figure 54). The range and distribution of maximum and minimum displacements is according to the expected. Finally, the stress at the base of the walls was also verified. The results show the expected distribution of stresses, with maximum compression between 1.00 and 1.50 MPa located at the base of the walls under the dome and towers (Figure 55).

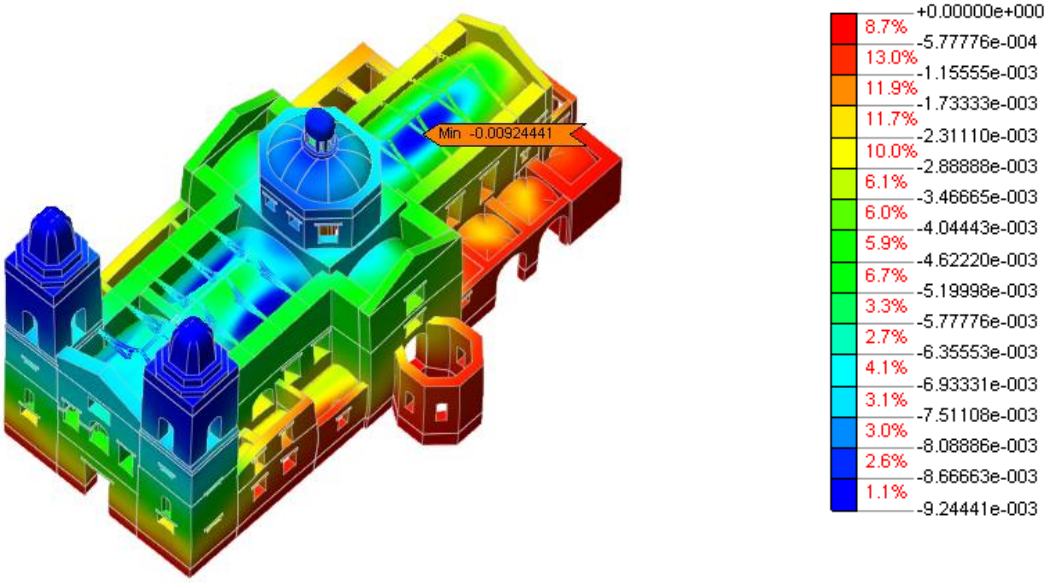

Figure 54. Linear static analysis for gravitational loads: Vertical displacement DtZ(V), LC4. (Units: m)

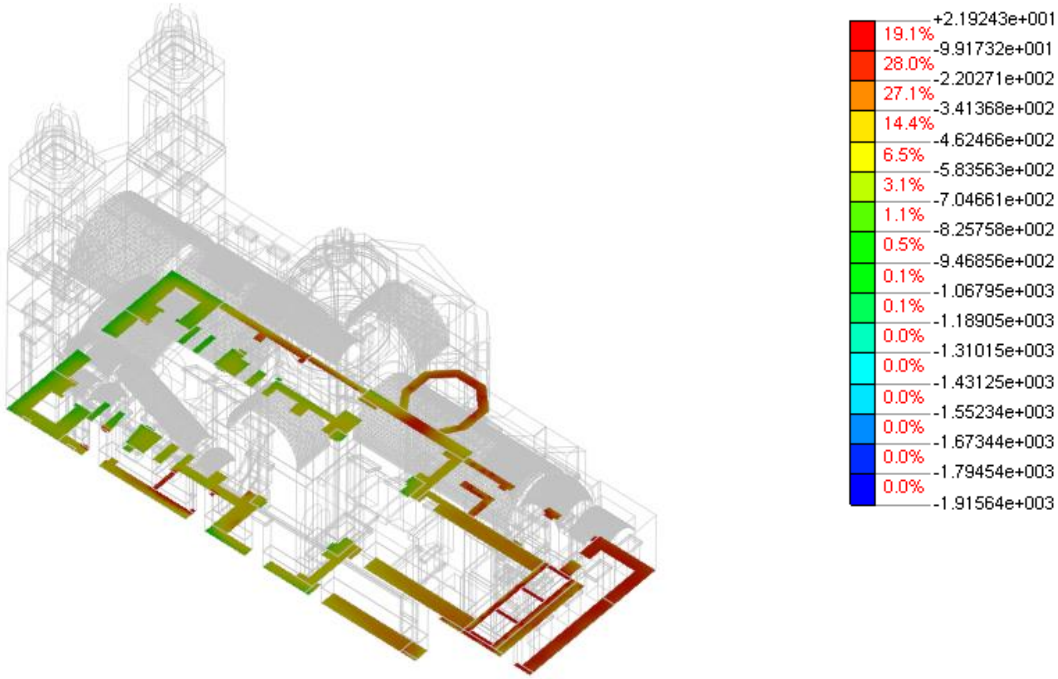

Figure 55. Structural linear static: Maximum compressive principal stress at the base of the walls, LC4. (Units: kPa)

4.8 Eigenvalue analysis

The eigenvalue analysis aims at identifying the natural frequencies and mode shapes of a structure.

The Eurocode 8 (EN 1998-1 2004) states that, for a modal response analysis of structures with box-behaviour, the response of all modes of vibration contributing significantly to the global response shall be taken into account based on two requirements: (a) the sum of the effective modal masses should be at least 90% of the total mass of the structure; and (b) all modes with effective modal masses greater than 5% of the total mass must be considered. However, historical masonry buildings do not fit into the scope of the Eurocode 8 criteria. In this type of constructions, usually the first few modes already provide sufficient information as to accurately characterise the structural response.

For the current case, only the first three modes of vibration obtained experimentally were considered to be of relevance since the last three present low MAC values (see Section 3.3). In order to evaluate the numerical model, an initial eigenvalue analysis was carried out using the linear mechanical properties previously defined. From the results, three modes are picked out according to their similar modal shape with respect to the experimental ones (Figure 56). The first mode of vibration (f_{num} = 1.64 Hz) is associated to a local mode of the nave and related to the vibration of the towers in an opposed diagonal direction. The second one (f_{num} = 2.43 Hz) is a global mode with simple curvature in the transversal direction of the church. It must be noticed that this second mode is actually the fifth one given by the numerical analysis. The third vibration mode (f_{num} = 3.44 Hz) corresponds to a global translation of the

church with double curvature in the transversal direction. Similar to the previous case, this last mode appears as the seventh mode in the numerical analysis.

Mode 1

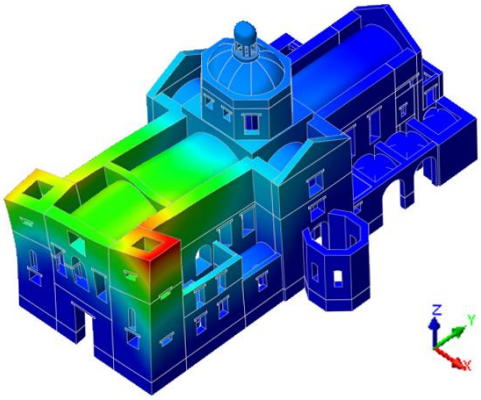

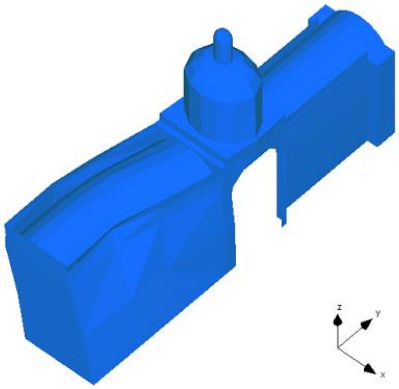

Numerical: 1.64 Hz Experimental: 1.79 Hz

Mode 2

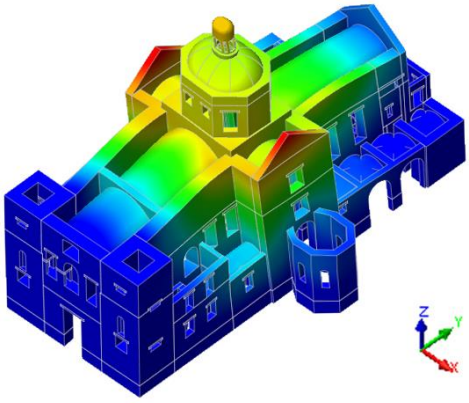

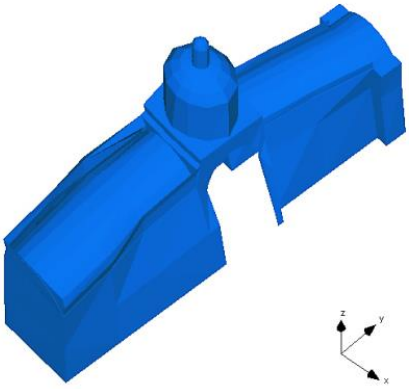

Numerical: 2.43 Hz Experimental: 2.75 Hz

Mode 3

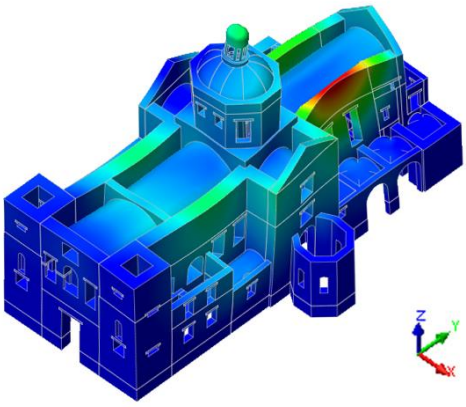

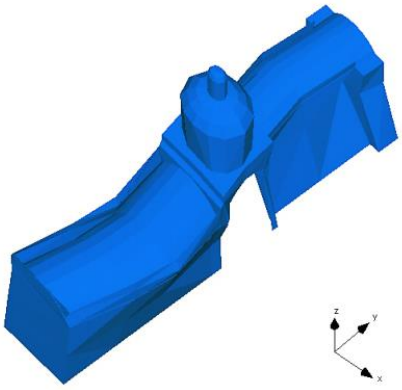

Numerical: 3.44 Hz Experimental: 3.72 Hz

Figure 56. Comparison of numerical and experimental mode shape configurations

Table 12 shows the results of the identified numerical modes with indication of the frequency of each mode and the mass participation in the global X and Y directions.

Table 12. Results of the numerical modal analysis

Mode	f_{num} [Hz]	Mass part. in X [%]	Mass part. in Y [%]
Mode 1	1.64	15.45	0.63
Mode 2	2.43	32.22	0.06
Mode 3	3.44	0.07	6.33

From Figure 56, a qualitative comparison of the numerical and experimental mode shape configurations can be done. It can be observed that the deflected shapes of the structure are alike for these three modes.

Subsequently, a comparison between the numerical and experimental frequencies is presented. Table 13 presents the percentage of error of the estimated numerical frequencies with respect to the experimental ones according to the following expression:

$$Error = \frac{\left|f_{num,i} - f_{exp,i}\right|}{f_{exp,i}} \cdot 100 \quad [\%] \tag{3}$$

Table 13. Comparison of experimental and numerical frequencies

Mode	f_{exp} [Hz]	f_{num} [Hz]	Error [%]
Mode 1	1.79	1.64	8.4
Mode 2	2.75	2.43	11.5
Mode 3	3.72	3.44	7.5

From the previous results it is possible to conclude that there is a considerable variation between the experimental and numerical results with an average error equal to 9%. In general, the frequencies obtained with the numerical analysis are lower than the experimental ones. That means that the model is not sufficiently stiff and therefore some properties or parameters should be modified in order to obtain more accurate results.

4.9 Calibration of the dynamic properties

Once the dynamic properties of the structure have been identified, the correlation between the experimental and the numerical modal responses should be examined. The numerical model was calibrated by an updating process so that the model would achieve a higher reliability, closely simulating the real behaviour of the structure. As explained in (Mendes 2012), the updating is based on an optimization process that minimizes the difference between the experimental and mathematical responses. Particularly, the frequencies of the numerical model were calibrated assuming the Young's modulus of the materials as the variables to calibrate. Note that the mode shapes are not included in the calibration process but a later verification is performed using the Model Assurance Criterion (MAC).

The calibration of the numerical frequencies is performed following the Douglas-Reid method (Douglas and Reid 1982) that proposes the following expression depending on the natural frequencies:

$$f_i^N(X_1, X_2, \dots, X_n) = C_i + \sum_{k=1}^{n} [A_{ik} X_k + B_{ik} (X_k)^2] \tag{4}$$

where f_i^N represents the frequencies of the numerical model, $X_k (k = 1,2, \dots, n)$ are the variables to calibrate and A_{ik}, B_{ik} and C_i are constants. To satisfy the expression, $(2n + 1)$ constants must be calculated:

$$\begin{cases} f_i^N({X^B}_1, {X^B}_2, \dots, {X^B}_n) = C_i + \sum_{k=1}^{n} [A_{ik} {X^B}_k + B_{ik} ({X^B}_k)^2] \\ f_i^N({X^L}_1, {X^B}_2, \dots, {X^B}_n) = C_i + \sum_{k=1}^{n} [A_{ik} {X^L}_k + B_{ik} ({X^B}_k)^2] \\ f_i^N({X^U}_1, {X^B}_2, \dots, {X^B}_n) = C_i + \sum_{k=1}^{n} [A_{ik} {X^U}_k + B_{ik} ({X^B}_k)^2] \\ \dots \\ f_i^N({X^B}_1, {X^B}_2, \dots, {X^L}_n) = C_i + \sum_{k=1}^{n} [A_{ik} {X^L}_k + B_{ik} ({X^L}_k)^2] \\ f_i^N({X^B}_1, {X^B}_2, \dots, {X^U}_n) = C_i + \sum_{k=1}^{n} [A_{ik} {X^U}_k + B_{ik} ({X^U}_k)^2] \end{cases} \tag{5}$$

where ${X^B}_k$ are the reference values of the variable to calibrate (initial or base values), and ${X^L}_k$ and ${X^U}_k$ are the respective lower limit and upper limit values. The choice of this set of values must be done with judgment since the results will depend on that selection.

Once the constants are defined, a least square minimization of the difference between the numerical frequencies f_i^N and the experimental frequencies f_i^E is used:

$$\pi = \sum_{i=1}^{m} w_i {\varepsilon_i}^2 \tag{6}$$

$$\varepsilon_i = \sum_{i=1}^{m} f_i^E - f_i^N(X_1, X_2, \dots, X_n) \tag{7}$$

where π is the objective function, ε is the residual function, w is the weight constants and m is the number of frequencies considered in the updating.

For the current case study the calibration was performed assuming the modulus of elasticity of the different materials as the variable to calibrate. Only the main constitutive materials are considered for the updating, i.e. the brick masonry present in the vaults, and the granite ashlar masonry and three-leaf stone masonry that make up the walls, arches and dome. The timber material of the roof structures and the granite stone used in lintels were considered less relevant for the global behaviour and therefore they are not used in the calibration.

The reference value for the modulus of elasticity of the different materials was initially estimated from the Italian code NTC-08 (NTC 2008) (see Section 4.4). The upper and lower limits are equally selected from that range, assuming the highest and lowest values associated to the same type of materials. The final variables used in the updating process are presented in Table 14.

Table 14. Reference, upper and lower values of the variables used for calibration

Material type	**Reference values**		**Upper and lower limit values**	
	Variable:	E [MPa]	Variable:	E [MPa]
Brick masonry (BRM):	$V_{1,REF}$ =	1500	$V_{1,UP}$ =	2000
			$V_{1,LOW}$ =	1200
Granite ashlar masonry (GRM):	$V_{2,REF}$ =	1750	$V_{2,UP}$ =	2800
			$V_{2,LOW}$ =	1250
Three-leaf stone masonry (STM):	$V_{3,REF}$ =	1250	$V_{3,UP}$ =	1750
			$V_{3,LOW}$ =	1020

Once the different values for the variables have been established, different eigenvalue analyses were performed changing just one of the properties each time. By doing this, a set of frequencies is obtained for the selected modes for each case. The calibration and optimisation algorithms were used following the Douglas-Reid method previously detailed and a final set of updated frequencies is obtained together with the recalculated values for the initial variables (Table 15 and Table 16).

Table 15. Frequencies obtained for the different combinations of variables and updated frequencies

		Mode 1 f_1 [Hz]	**Mode 2** f_2 [Hz]	**Mode 3** f_3 [Hz]
	EXPERIMENTAL	1.79	2.75	3.72
REF	$V_{1,REF}$, $V_{2,REF}$, $V_{3,REF}$	1.64	2.44	3.44
V1	$V_{1,UP}$, $V_{2,REF}$, $V_{3,REF}$	1.65	2.46	3.48
BRM	$V_{1,LOW}$, $V_{2,REF}$, $V_{3,REF}$	1.64	2.42	3.41
V2	$V_{1,REF}$, $V_{2,UP}$, $V_{3,REF}$	1.76	2.55	3.61
GRM	$V_{1,REF}$, $V_{2,LOW}$, $V_{3,REF}$	1.54	2.35	3.32
V3	$V_{1,REF}$, $V_{2,REF}$, $V_{3,UP}$	1.82	2.74	3.85
STM	$V_{1,REF}$, $V_{2,REF}$, $V_{3,LOW}$	1.54	2.27	3.21
	UPDATED	**1.80**	**2.68**	**3.77**
	Error [%]	0.6	2.6	1.3

Table 16. Updated values for the moduli of elasticity used as variables

Material type:	**Brick masonry**	**Granite ashlar masonry**	**Three-leaf stone masonry**
Updated variable: *E* [MPa]	1360	1900	1620

The updated frequencies differ from the experimental results with an average error less than 2%. On the other hand, the values of the Young's moduli for the different materials are within the expected range, showing a more flexible brick masonry than the one initially considered and, on the contrary, stiffer granite and stone masonries. Hence, the calibration of the frequencies is successfully accomplished and the model is tuned for further analyses. Note that the second mode presents the larger error, which is only around 2.6%.

In the first step of the calibration of the numerical model, the updating process was only focused on the frequencies of three modes. No mention was made to the mode shapes, which is an important aspect to take into account as well. However, considering the similarities of the mode shapes between the numerical and the experimental results (Figure 56), a simpler approach could be adopted, leaving the mode shapes control as a later verification.

The Modal Assurance Criterion (MAC) provides a measure of the consistency (linearity) between the estimated modal vectors (Allemang 2003):

$$MAC_{u,d} = \frac{\left|\{\varphi_i^u\}^T\{\varphi_i^d\}\right|^2}{\{\varphi_i^u\}^T\{\varphi_i^u\}\{\varphi_i^d\}^T\{\varphi_i^d\}} \tag{8}$$

where φ^u and φ^d are the mode shape vector of two different models. The MAC value ranges from 0 to 1, where 1 indicates 100% match of both mode shape vectors. The modal assurance criterion can be used for validation of experimental results, as well as for evaluation of the correlation between experimental and numerical models.

The current work addresses the latter case, where the reliability of the numerical model was assessed with respect to the experimental results. Thus, the nodes of the model that correspond to the location of the accelerometers (Figure 45) are picked out and analysed. First, the displacements registered in the transversal and longitudinal directions by the accelerometers are normalised. A parallel process is performed for the chosen numerical nodes in the equivalent directions. Then, the values of the normalised shape vectors are put into the equation (8) and the MAC value is obtained.

In Figure 57 a graphical comparison between experimental and numerical frequencies and MAC values is plotted. In the graph, the distance of the dots from the 45º line indicates the frequency difference while the size of the dots indicates the ratio of MAC values for each mode. Thus, when the dots are exactly on the 45º line, the error between numerical and experimental frequencies is zero.

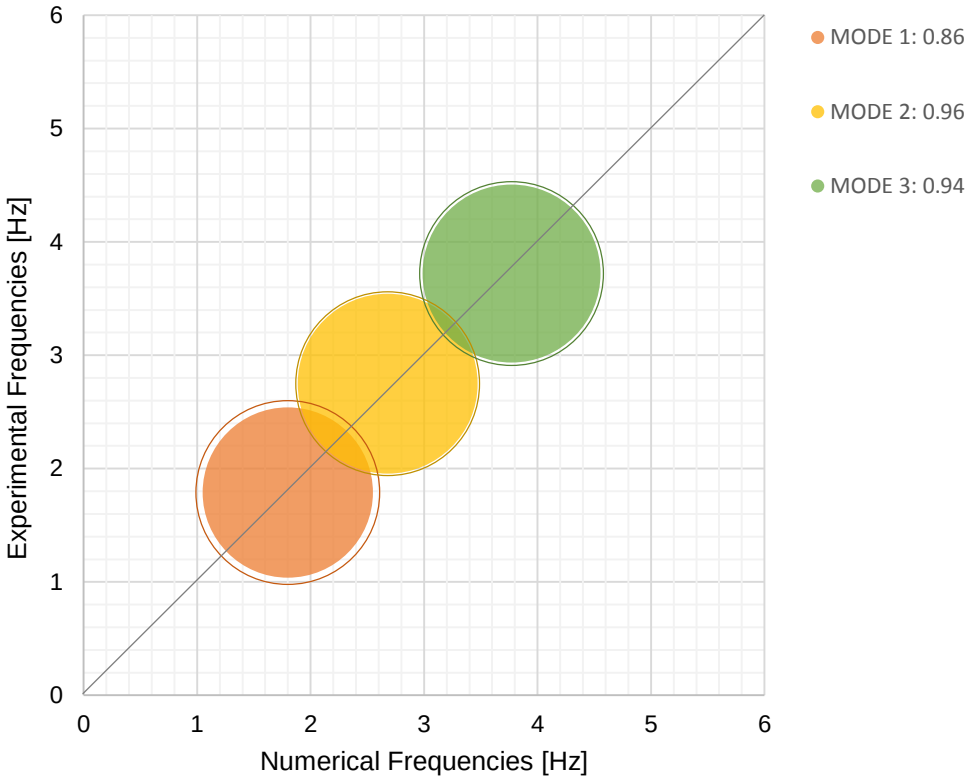

Figure 57. Graph with scaled-MAC values and frequency comparison for the calibrated modes

According to the results, the MAC values obtained for the three modes of vibration are consistent with the frequency calibration and the initial shape configuration, in which the average MAC is equal to 0.92. Since the updated numerical model presents dynamic properties (frequencies and mode shapes) close to the experimental dynamic properties estimated from the dynamic identification tests, it is assumed that the numerical model is successfully calibrated and can be used for the numerical analysis.

5. ANALYSIS OF THE SOIL-STRUCTURE INTERACTION

Once the model has been generated and calibrated, the following section of the thesis deals with the analysis to evaluate the existing damage in the church. Since the damage pattern can be associated to the properties of the foundation soil, several hypotheses for the soil-structure interaction were evaluated through the non-linear static analysis for gravitational loads. Thus, the hysteretic behaviour and the non-linear parameters of the materials were defined. The response of the structure was discussed based on the capacity curves, deformation and crack patterns.

5.1 Constitutive material law and material properties

The non-linear behaviour of masonry was modelled using the Total Strain Crack Model (TSCM) in DIANA (TNO DIANA BV 2014). The TSCM describes the tensile and compressive behaviour of a material with a stress-strain relationship. In particular, a Rotating Crack model was adopted. Within this approach, the stress-strain relationship is evaluated in the principal directions of the strain vector, which, at the same time, define the direction of the crack opening (TNO DIANA BV 2014).

The input for the Total Strain Crack models comprises two parts: (1) the definition of the basic linear-elastic parameters, such as material density, modulus of elasticity and Poisson's ratio; and (2) the definition of the behaviour in tension and compression with the corresponding non-linear material properties. For the Rotating Crack model it is not necessary to define the shear behaviour. In this model a unique shear term is evaluated and updated, based on the current damage, during the analysis. The Rotating Crack model prevents the shear stress locking problem, which can occurs in the Fixed Crack model.

Regarding the basic linear-elastic parameters, the set of materials and properties defined in the previous section were used (see Chapter 4). In particular, the updated Young's modulus values of the masonry materials obtained after the calibration were adopted. With respect to the tensile and compressive behaviour of masonry, codes and values proposed in literature were used in order to define the necessary properties for the non-linear range. The final parameters defined for the different masonry groups are shown in Table 17.

The compression behaviour was represented by a non-linear parabolic function (Figure 58a). This curve is defined from the relation between fracture energy in compression and crack bandwidth of the mesh elements. The crack bandwidth value is automatically considered by DIANA according to the area ($h =$

$\sqrt{2A}$ and $h = \sqrt{A}$ for linear and quadratic curved shells, respectively) or the volume ($h = \sqrt[3]{V}$ for the solid tetrahedra) of the elements (TNO DIANA BV 2014).

In order to define the compressive strength of the different masonry groups, a relation $E = \alpha \cdot f_c$ was adopted. According to (Tomazevic 1999), the parameter α for masonry may vary from 200 to 1000. A mid-range value $\alpha = 600$ of the interval was used ($f_c = E/600$). The ductility index for the compressive fracture energy was assumed equal to 1.6 mm, as recommended value for a compressive strength lower than 12 MPa (CEB-FIB 1993). The ductility index in compression is given by the ratio between the fracture energy and the compressive strength of the material ($d_{u,c} = G_c/f_c$).

Table 17. Updated linear-elastic and non-linear properties of masonry

Brick masonry (BRM)

Material property	Symbol	Value	Unit
Density	ρ	1800	kg/m^3
Modulus of elasticity	E	1360	MPa
Poisson's ratio	ν	0.20	--
Masonry compressive strength	f_c	2.26	MPa
Compressive fracture energy	G_c	3620	N/m
Masonry tensile strength	f_t	0.15	MPa
Tensile fracture energy	G_f^I	50	N/m

Three-leaf stone masonry (STM)

Material property	Symbol	Value	Unit
Density	ρ	2000	kg/m^3
Modulus of elasticity	E	1620	MPa
Poisson's ratio	ν	0.20	--
Masonry compressive strength	f_c	2.70	MPa
Compressive fracture energy	G_c	4320	N/m
Masonry tensile strength	f_t	0.15	MPa
Tensile fracture energy	G_f^I	50	N/m

Granite ashlar masonry (GRM)

Material property	Symbol	Value	Unit
Density	ρ	2100	kg/m^3
Modulus of elasticity	E	1900	MPa
Poisson's ratio	ν	0.20	--
Masonry compressive strength	f_c	3.16	MPa
Compressive fracture energy	G_c	5050	N/m
Masonry tensile strength	f_t	0.15	MPa
Tensile fracture energy	G_f^I	50	N/m

The tensile behaviour was defined by an exponential softening curve (Figure 58b). This curve is based on the definition of the tensile fracture energy, the crack bandwidth of the elements and the tensile strength of the material. The value of the fracture energy associated with the Mode-I was assumed equal to 50 N/m (Lourenço 2010). On the other hand, for the tensile strength, an average value of 0.15 MPa

was adopted for all masonry materials. This value was estimated considering that the masonry tensile strength was approximately 5% of its compressive strength. The crack bandwith value was automatically calculated by the software as previously mentioned.

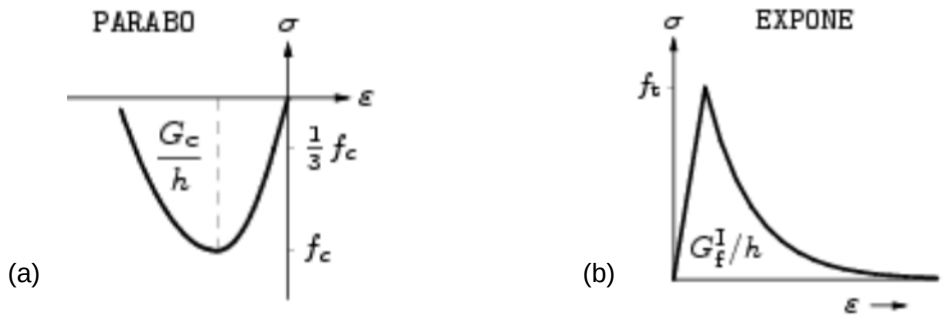

Figure 58. Non-linear behaviour for masonry: (a) parabolic curve for compressive behaviour; (b) exponential softening curve for tensile behaviour (TNO DIANA BV 2014)

In order to save computational effort, timber material was considered to behave within its linear-elastic range. Later verifications were done to control that indeed the stresses in the fibres of the linear elements were always under the linear-elastic range. However, these elements are more prone to fail in the connections and not in the members. The material properties for timber elements were obtained from experimental tests and the probabilistic model code, as proposed by (Poletti 2013). The final values used for the wooden linear elements are shown in Table 18.

Table 18. Linear-elastic and non-linear properties of timber (Poletti 2013)

Pine wood

Material property	**Symbol**	**Value**	**Unit**
Density	ρ	600	kg/m^3
Modulus of elasticity (parallel to fibres)	E_0	13000	MPa
Poisson's ratio	ν	0.30	--
Timber tensile strength	$f_{t,0}$	15	MPa
Timber compressive strength	$f_{c,0}$	25	MPa

Finally, since limited damage is expected on the lintel elements, the granitic material defined for these parts is supposed to behave always within its linear-elastic range. The properties of the granitic stone are presented in Table 4 (see Chapter 4).

5.2 Modifications in the non-linear model

Besides the new material definition, other changes were introduced in the numerical model in order to prepare it for the non-linear analyses:

(1) The integration scheme of the two-dimensional curved shell elements were modified to have 5 integration points along their thickness.

(2) A continuous interface was applied at the base of the walls so as to simulate the soil behaviour under the foundations of the building. For this purpose, T18IF elements were introduced in the model. T18IF is an interface element between two planes in a three-dimensional configuration. The element is based on linear interpolation and by default it has a 3-point integration scheme.

5.3 Soil and foundation assumptions

The diagnosis (see Chapter 3) allowed concluding that, in general, the church presents low to moderate damage, in which the cracks at the top of the south façade, transept walls and south walls of the chancel are highlighted. The most relevant damage is located at the connection between the south tower and the main façade (see Appx. A.2.2 and Figure 19). The floors of the chancel and Chapel of the Blessed Sacrament present high deformations, which is associated to the soil consolidation. The church presents also other minor deformations, mainly at the arches of the dome. On the whole, the structural damage present in the building can be associated to a possible foundation settlement.

Due to the high level of the water table it was not possible to determine the type or depth of the foundations under the base of the walls. However, based on the data collected from the geotechnical prospection, it was possible to implement different scenarios into the calibrated numerical model as to simulate the real condition of the soil and the soil-foundation interaction. For the different assumptions, the structural damage obtained for the self-weight of the structure (vertical load factor equal to 1) was compared to the actual damage pattern of the church, which was used as a guide to validate the accuracy of the proposal.

The main variables used to establish the different possible scenarios were the depth of the foundations, the integrity condition of the sustaining soil and the type of foundation under the walls.

5.3.1 Depth of the foundation

The results of the SPT carried out during the geotechnical survey (see Section 3.5) show a geologic profile characterized by a superficial layer of soft clay that extends until approximately 4.00 m deep. Below it, there is a gravelly sand transition layer and finally a modified and highly fractured rock layer. This rock starts at depths between 4.20 and 5.50 m. Regarding the mechanical characteristics, the superficial layer of clay is very little resistant and deformable, presenting SPT values lower than 10. The resistance gradually increases in depth until the altered and fractured rock.

Attending to the mechanical properties, two main hypotheses were proposed. First, a medium-depth foundation located at the gravelly sand level was proposed. The modulus of elasticity of the soil was estimated according to the SPT results and the value for the interface normal stiffness was calculated.

Subsequently, a deeper foundation based on the rock level was assumed. For this case, the interface normal stiffness was directly proposed. In both cases, the interface transversal stiffness was given a high value, doubling the normal stiffness, and consequently its influence in the results would be minimum.

a) Medium-depth foundation hypothesis

According to the SPT results (see Section 3.5.1), a foundation around 4.00 m deep would be standing on the gravelly sand level. In order to estimate the modulus of elasticity of that type of soil, the following relation was proposed by (Denver 1982):

$$E = 7 \cdot \sqrt{N} \quad [MPa] \tag{9}$$

The value for the interface normal stiffness is given by the relation:

$$k_n = E/L \quad [MPa/mm] \tag{10}$$

where N is the average value of $N_{SPT} = N_{15-30} + N_{30-45}$ and L is the thickness of the soil layer.

According to equations (9) and (1), the average modulus of elasticity (E), as well as the average value for the interface normal stiffness (k_n) were calculated as shown in Table 19. Note that the contribution of the foundation under the walls to the interface normal stiffness was neglected.

Table 19. Modulus of elasticity and interface normal stiffness of the gravelly sand soil layer

SPT1

Depth [m]	[15]	[30]	[45]	N_{SPT}	E_1 [MPa]
3.00	8	23	18	41	44.82

LAYER

From [m]	to [m]	Thickness [m]	k_{n1} [kN/m³]
2.50	4.20	1.70	26,366

SPT2

Depth [m]	[15]	[30]	[45]	N_{SPT}	E_2 [MPa]
4.50	11	12	11	23	33.57

LAYER

From [m]	to [m]	Thickness [m]	k_{n2} [kN/m³]
4.00	5.50	1.50	22,381

SPT3

Depth [m]	[15]	[30]	[45]	N_{SPT}	E_3 [MPa]
4.50	9	6	4	10	22.14

LAYER

From [m]	to [m]	Thickness [m]	k_{n3} [kN/m³]
4.00	5.30	1.30	17,028

***E*avg [MPa] = 33.51** ***kn*,avg [kN/m³] = 21,924**

b) Deep foundation hypothesis

On the other hand, assuming a deep foundation, both the foundation under the walls and the deep soil interface were taken into account in order to estimate the supporting conditions. The foundation under

the walls was assumed to have the same breadth and similar characteristics as the supported walls. Thus, a value of $E = 1620$ MPa was adopted. The equivalent interface normal stiffness is given by the expression used for springs in series:

$$\frac{1}{k_{eq}} = \frac{1}{k_1} + \frac{1}{k_2} \tag{11}$$

where k_1 corresponds to the stiffness provided by the foundation with assumed depth L:

$$k_1 = E/L \quad [MPa/mm] \tag{12}$$

and k_2 is the deep soil interface with a value ranging between 1 and 100 N/mm^3 (Senthivel and Lourenço 2009) (Lourenço 1996).

For a foundation supported on the sediment rock level, about 6.00 m deep, $k_1 = 405{,}000$ kN/m^3. Note that the numerical model already includes 2.00 m of the walls under the level of the ground, so for equation (12), $L = 4.00$ m. For a value $k_2 = 100$ N/mm^3 the resulting equivalent normal stiffness would be $k_{eq} = 400{,}000$ kN/m^3. On the other hand, for the lowest value, $k_2^* = 1$ N/mm^3, the final equivalent stiffness would be $k_{eq}^* = 290{,}000$ kN/m^3.

5.3.2 Condition of the soil

The structural damage observed in the church may be associated to a differential settlement, since the damage pattern seems to be especially related to some parts of the building. For instance, the high level of the water and the presence of the stream nearby could have caused part of the soil and even small masonry stones or mortar to be washed away under the foundations, which would have caused this phenomenon.

The possible loss of integrity of the soil was introduced as a variable in the soil-structure interaction. In order to simulate this situation, a reduction of the normal stiffness was considered: $k_{red} = 10\%\ k_{eq}$.

5.3.3 Type of foundation

Another possible reason to explain the differential settlements or the located distribution of damages could be related to the process of construction and the type of walls and foundations. Considering the history of the building, it could be theorised that some parts were added later, and in that case the type of foundation under the more modern walls could be different. Attending to the morphology of the church, a comparison between major and minor walls, according to their structural role and dimensions, could also be established. The same differentiation could be extended to the foundations under one or the other type of walls.

Since during the inspections the high water table prevented direct access to the foundations, it was not possible to clarify these aspects. However, several scenarios were hypothesised for the numerical analysis according to a possible scheme based on the location of the walls, their width and dimensions, and the presence of damage.

5.3.4 Interface models

Different combinations of the aforementioned parameters were prepared and implemented into the numerical model in order to study the influence of each variable and validate the accuracy of the results. The more representative interface proposals generated and analysed during this process are shown in the next plans. The colours of the walls represent the type and condition of the foundation associated with them, and therefore the value of the interface normal stiffness applied: (1) deep sound foundation, k_1 = 400,000 kN/m^3; (2) deep foundation with soil loss, k_2 = 40,000 kN/m^3; (3) mid-depth sound foundation, k_3 = 22,000 kN/m^3.

The first configuration (Figure 59) proposes deep foundations under the main thick walls that enclose the spaces of the church, i.e. towers, façade, nave, north and south transepts, and chancel. The annexed spaces surrounding these parts would have walls based on mid-depth foundations. Finally, the south tower, around which most of the damage appears, is considered to have poor soil / masonry conditions, due to the presence of the water stream.

Model A

Interface legend:

- Deep sound foundation
- Deep foundation with soil loss
- Mid-depth sound foundation

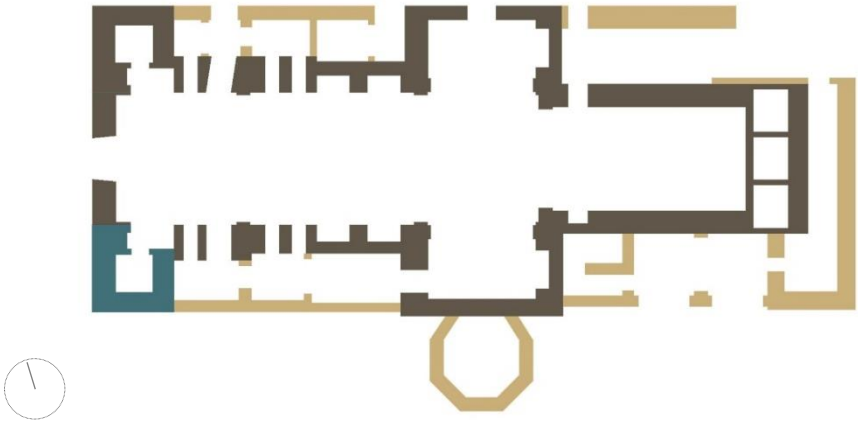

Figure 59. Interface Model A

The second proposal (Figure 60) follows an organisation similar to the previous case but with all the annexed parts connected directly to the monastery supported on deep sound foundations.

Model B

Interface legend:

- Deep sound foundation
- Deep foundation with soil loss
- Mid-depth sound foundation

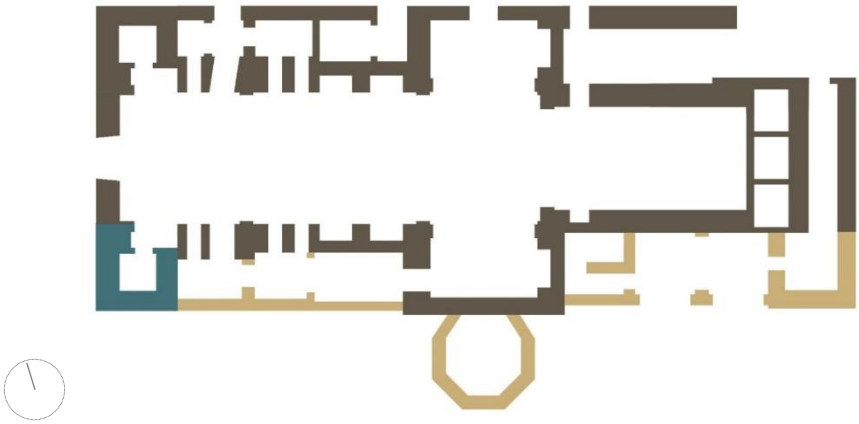

Figure 60. Interface model B

A third plan (Figure 61) was theorised with all the walls resting on deep foundations, but considering different soil conditions. Taking into account the location of the water course, the soil / masonry under the southern walls of the church was considered to be washed.

Model C

Interface legend:

- Deep sound foundation
- Deep foundation with soil loss

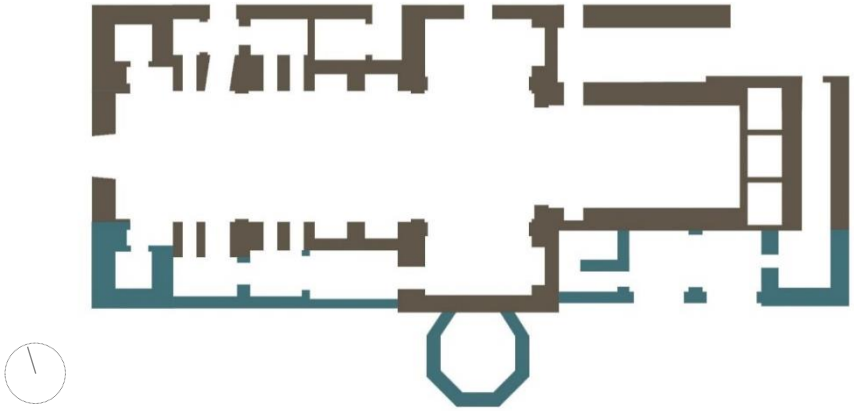

Figure 61. Interface model C

The last studied configuration (Figure 62) repeats the previous approach assuming poorer conditions of the soil only under the south tower and the southwest annexes of the church, where most of the actual structural damage is located.

Model D

Interface legend:

- Deep sound foundation
- Deep foundation with soil loss

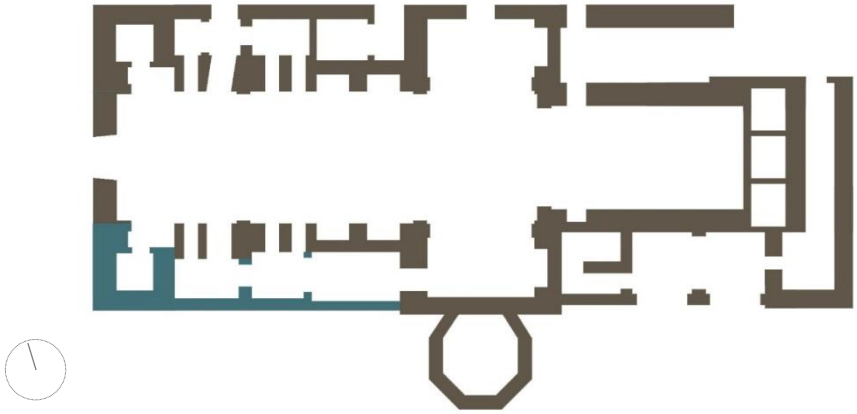

Figure 62. Interface model D

All the interface models were analysed using DIANA software and the results were collected and evaluated in order to find the proposal that better matches the existing damage when subject to the existing gravitational loading. Taking into account the results (Figure 63), the Model C showed the closest results to reality. The following section presents a detailed description of the analysis and results obtained for that proposal, denoted by “foundation updated model”.

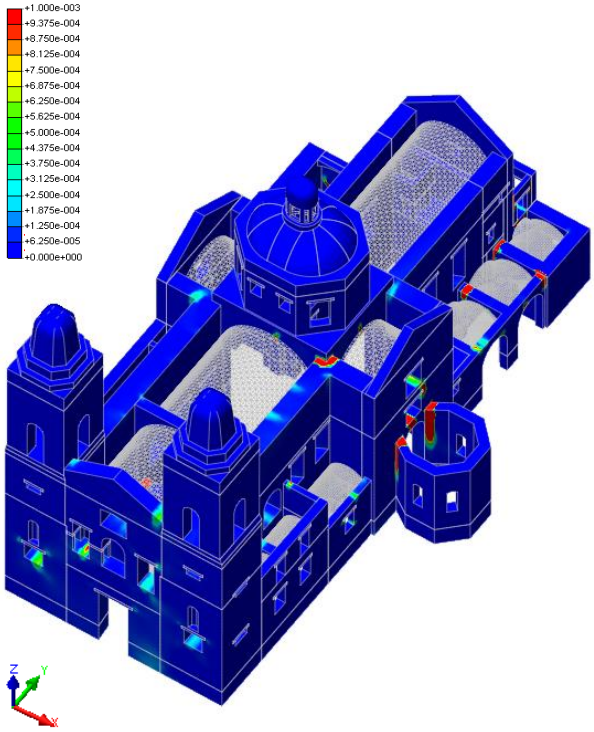

(a)

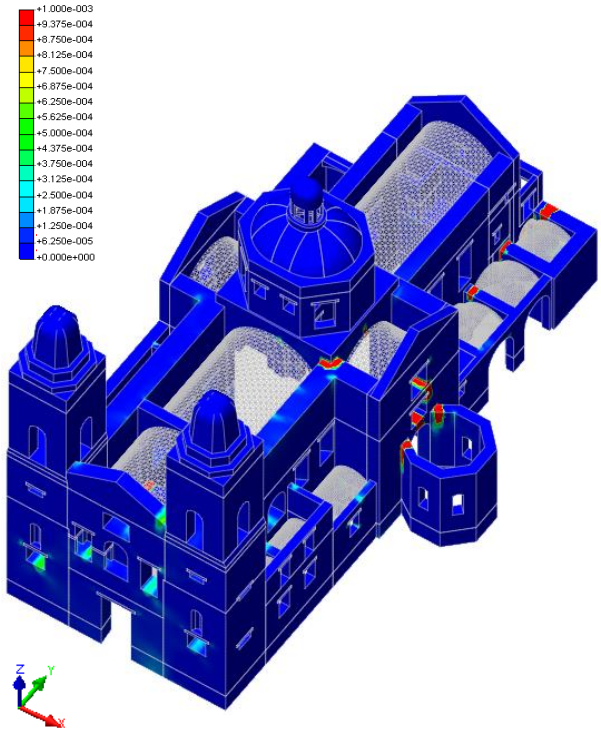

(b)

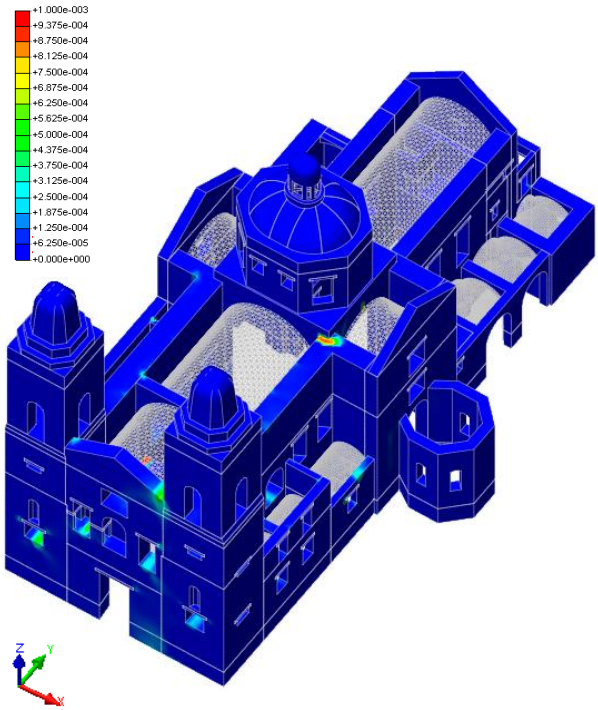

(c)

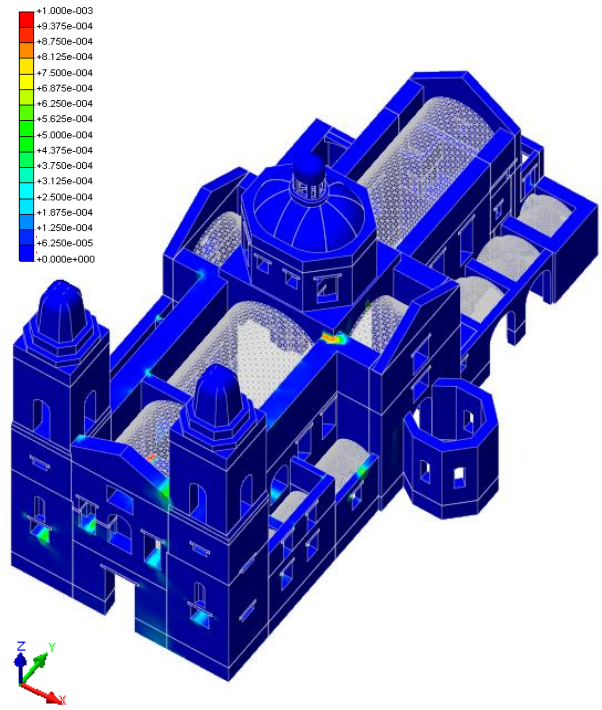

(d)

Figure 63. Non-linear static analysis for existing gravitational loads. Maximum principal strains due to self-weight for: (a) Model A; (b) Model B; (c) Model C; (d) Model D. (Units: m/m)

5.4 Analysis of the foundation updated model for gravitational loading

A non-linear analysis for increasing gravitational loading was performed in order to understand the damage condition of the church and evaluate the stability of the structure. In a first step, only the self-weight of the structure was considered. Subsequently, the vertical loading capacity of the building was analysed by gradually increasing the gravity loads until collapse.

The non-linear structural analyses were performed using the finite element software DIANA, taking into account the material properties defined in Section 5.1 and the assumptions and proposals developed in this chapter. The regular Newton-Raphson iterative method was adopted to obtain the solution of the non-linear response. In this method, a new tangent stiffness matrix is calculated within each iteration; thus, if compared with other methods, it has the advantage of converging with a less number of iterations, but each of those iterations is more time consuming. The analysis convergence was based on energy control with a tolerance equal to 10^{-3}. Furthermore, considering the strong non-linear behaviour of this kind of structure, the line-search algorithm and arc-length method were adopted in the non-linear analyses in order to stabilise the convergence in the iteration process.

The highest node on the south tower is chosen as a representative point in order to control and evaluate the displacements throughout the analyses. Similarly, a representative point of the nave vault is picked to follow the deformation of the shell elements. The point is located at the haunch of the vault since this part shows greater deformations and is directly associated with the local failure mode. Both control points are shown in Figure 64.

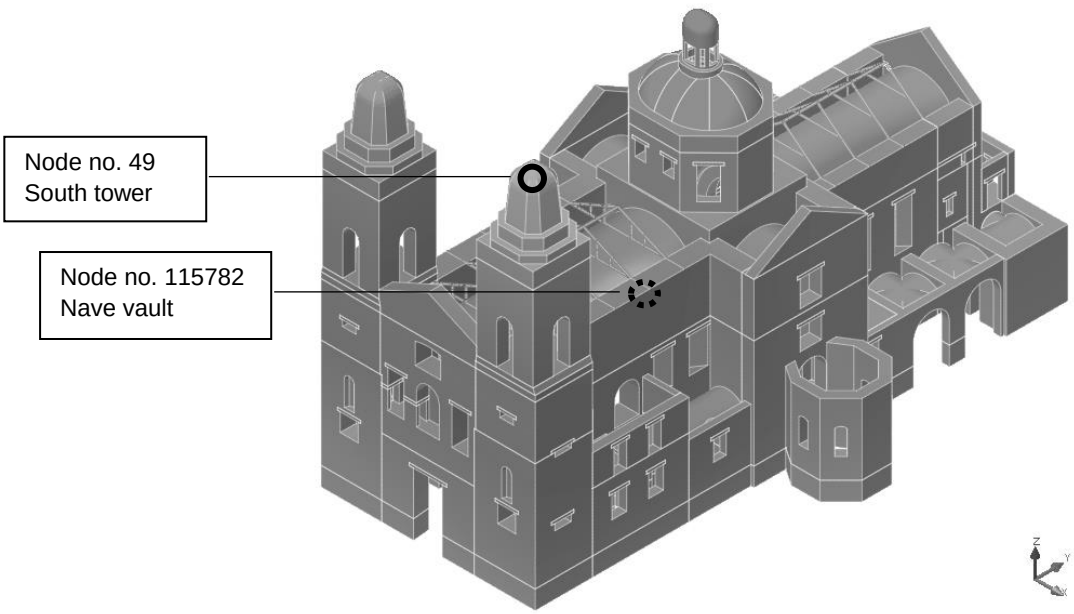

Figure 64. Location of the nodes to control and evaluate the displacements

Figure 65 presents the deformed shape and the vertical displacement of the structure due to its self-weight, i.e. with a vertical load factor equal to 1. The maximum total displacement was located at the

top of the south tower: u_x = 16 mm; u_y = -12 mm; u_z = -16 mm. The soil-structure interface (and the restrain introduced by the nave and side chapels) causes the towers and façade to lean outwards in +X and -Y directions.

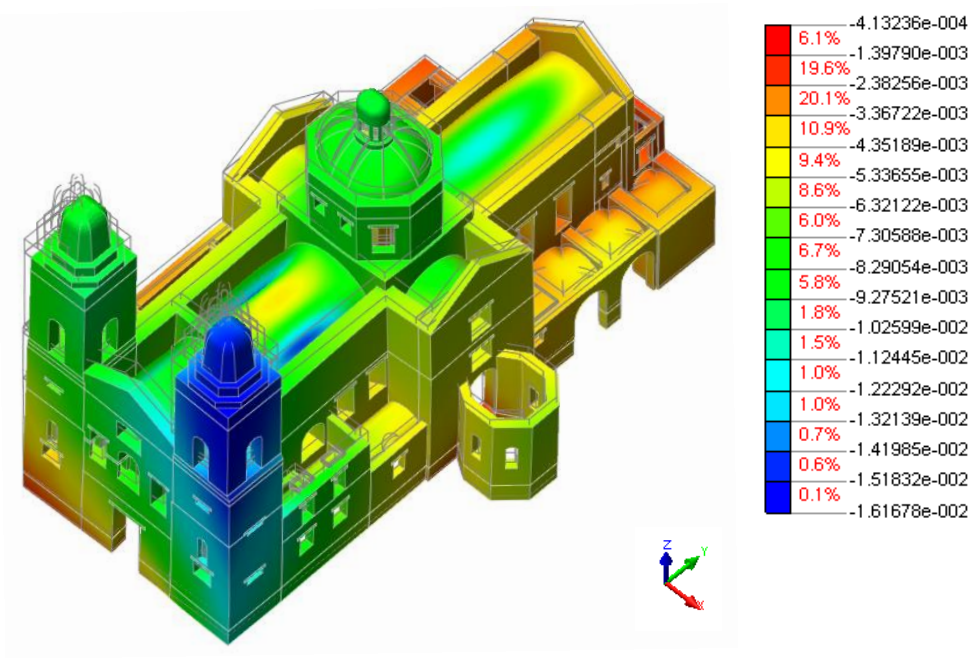

Figure 65. Non-linear static analysis for gravitational loads: Vertical displacement due to self-weight (Units: m)

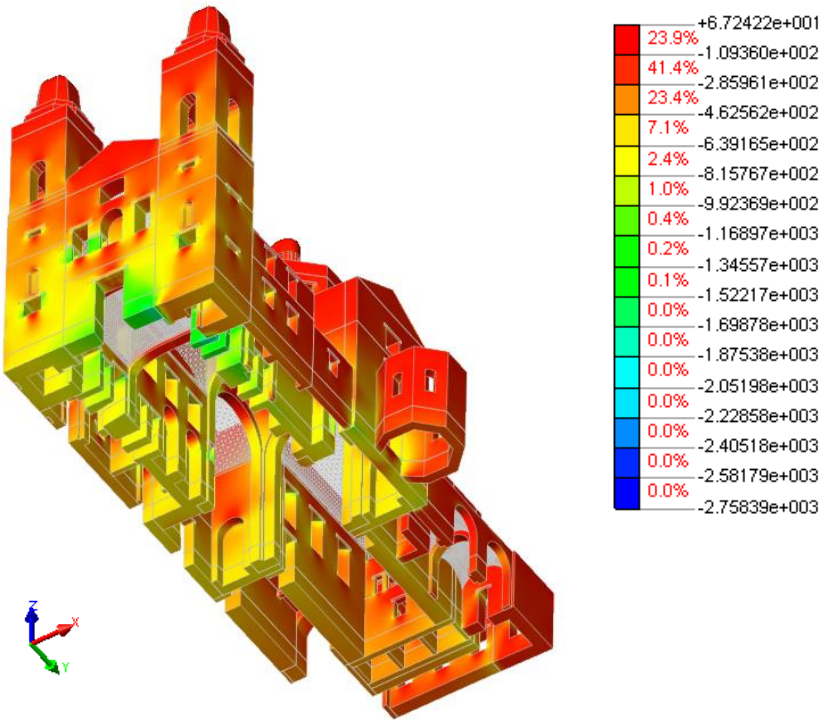

Figure 66. Non-linear static analysis: Minimum principal stress due to self-weight (Units: kPa)

Figure 66 shows the distribution of the maximum compressive stresses due to the self-weight of the structure. High values appear in slender parts of the structure or concentrated in lintel corners, always within a reasonable range. On the other hand, the highest values are located at the base of the structure, mostly in the zones of transition between the sound foundation and the deteriorated one. The stiffest interfaces receives the maximum compression.

The structural damage resulting from the gravitational loads of the building was measured by analysing the maximum principal strains ε_1, which is associated with cracking (strains caused by tensile stress). Figure 67 shows the crack configuration for the walls of the church. The damage is highly concentrated in specific parts of the structure and it reflects quite accurately the pattern described during the visual inspection (see Appendices A.2.1 to A.2.4): connection between the south tower and the façade, corner between the south tower and the wall of the nave, connection between orthogonal walls of the transept and the nave, damage linked to the openings of the façade, arches of the crossing and the choir loft, and minor cracking associated to openings of the south annexes.

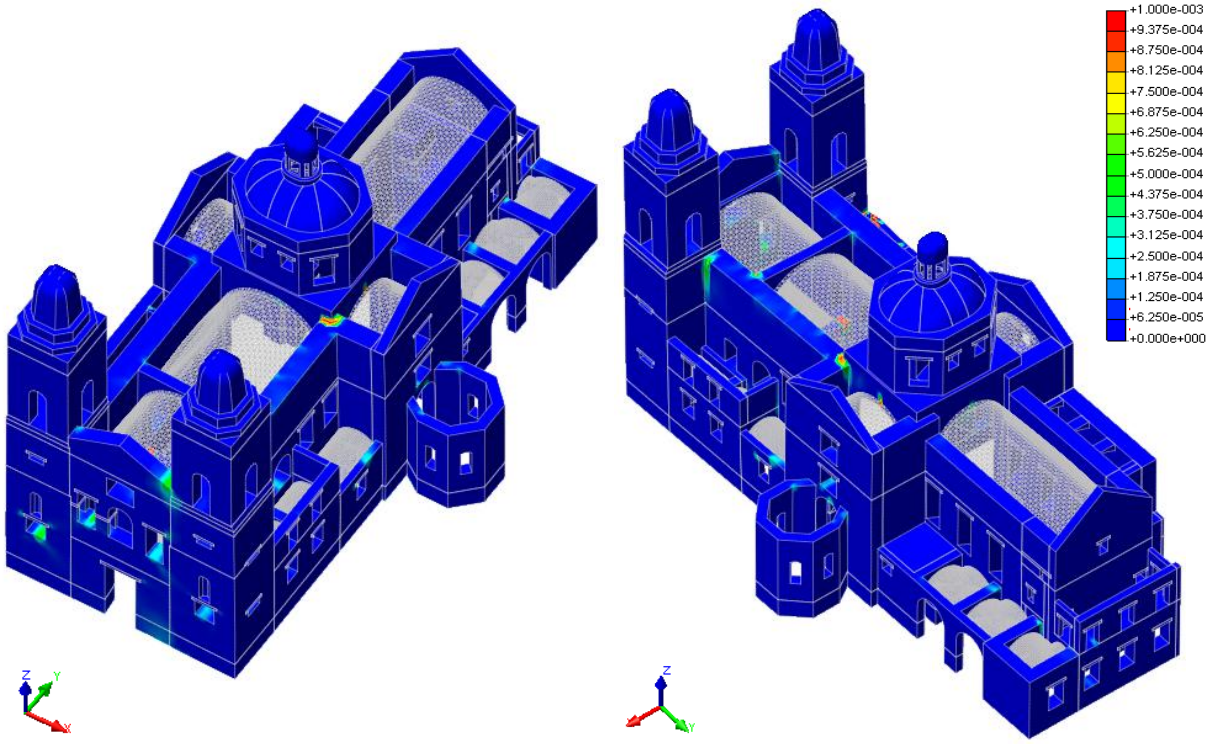

(a) (b)

Figure 67. Non-linear static analysis: Maximum principal strains due to self-weight (Units: m/m)

The damage on the vaults was evaluated separately and it is shown in Figure 68. In this case, the numerical damage pattern resulted to be more severe than the actual condition of the structure. However, some trends could be identified, as the diagonalization of the cracking affecting the nave vaults or the damage associated with the openings and lunettes of the annexes.

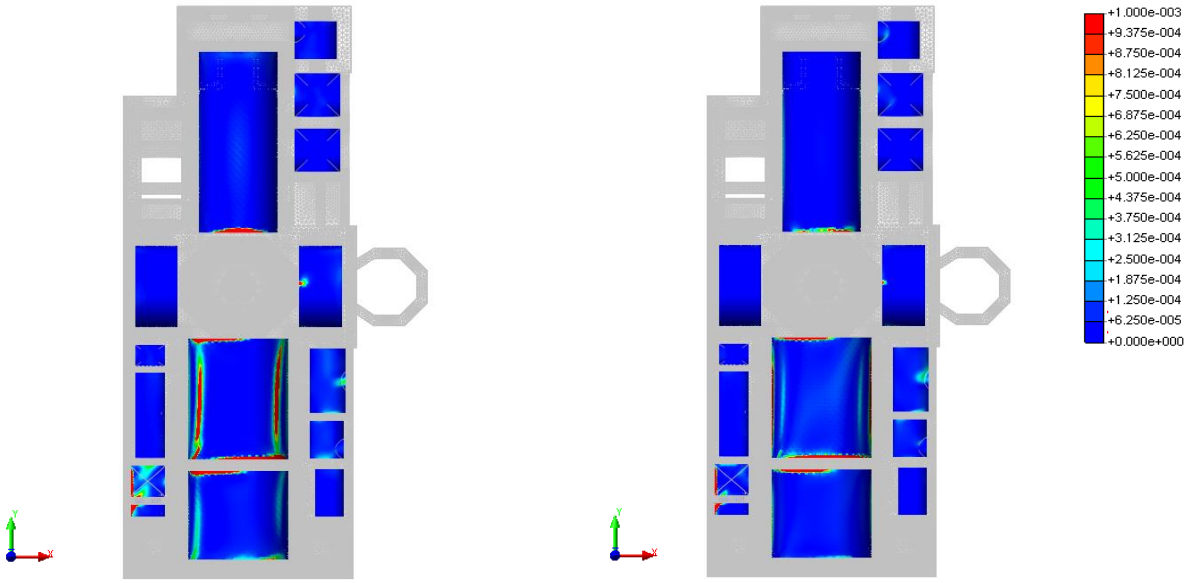

(a) (b)

Figure 68. Maximum principal strains in shell elements due to self-weight: (a) layer 1 corresponding to the vaults intrados; (b) layer 5 corresponding to vaults extrados. (Units: m/m)

Once the model was studied under its self-weight condition, the vertical capacity of the structure was analysed by progressively increasing the gravity loads until causing collapse. It must be noted that for the present study, the final loading state was not associated to a global failure of the building. Instead, the limit condition of the analysis turned out to be the concentration of damage in some parts of the structure, causing local mechanisms.

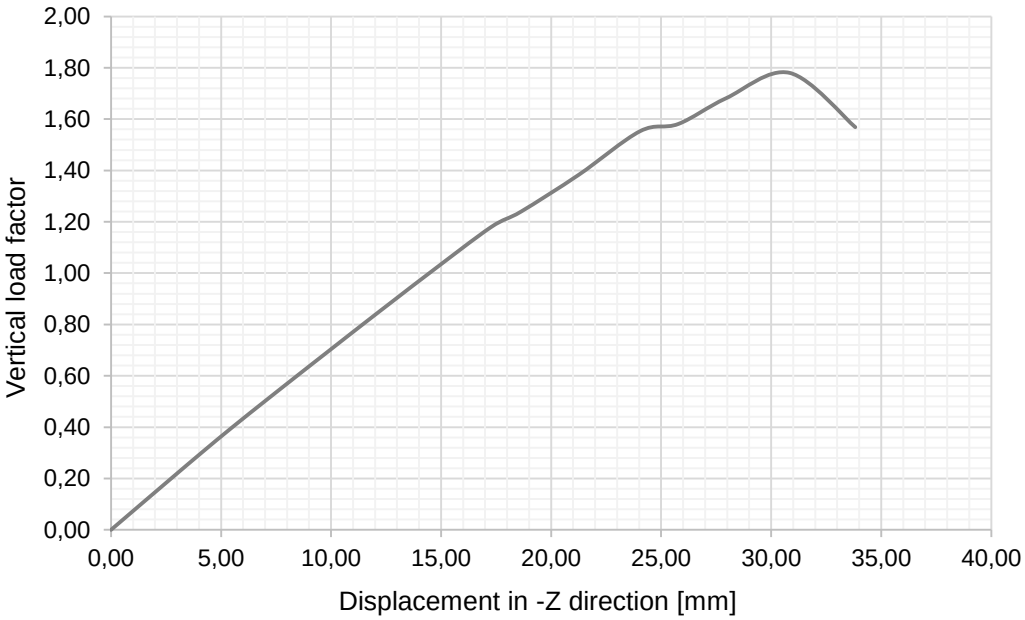

Figure 69. Capacity curve for the vertical loading analysis: Node 49 (South tower)

Figure 69 shows the capacity curve using the top of the south tower as control point for the vertical movement. The load factor is defined by the relation between the applied load and the self-weight of the structure. According to the results, the structure maintains a predominantly linear behaviour until a load factor of 1.55, where some damage appears causing a sudden variation on the response. However, the structure is still stable after this point and it is able to withstand a higher vertical load of around 1.80 its self-weight. After this peak, the failure occurs.

Nevertheless, in a complex structure such as the church of São Miguel, the selection of a certain control point may be misleading, for one solely node cannot represent the behaviour of the whole. In order to check another delicate part of the structure, a point belonging to the nave vault was also analysed and the results are presented in Figure 70. The graph shows a capacity curve rather different from the previous case. The more flexible brick vault undergoes higher deformations and it suffers an earlier collapse when the load factor gets to 1.55. Here, it must be noted that failure of the vaults is rather sensitive to the presence of backing and/or a cohesive infill, so it is possible that this local failure load, and associated mechanism, are significantly under-estimated.

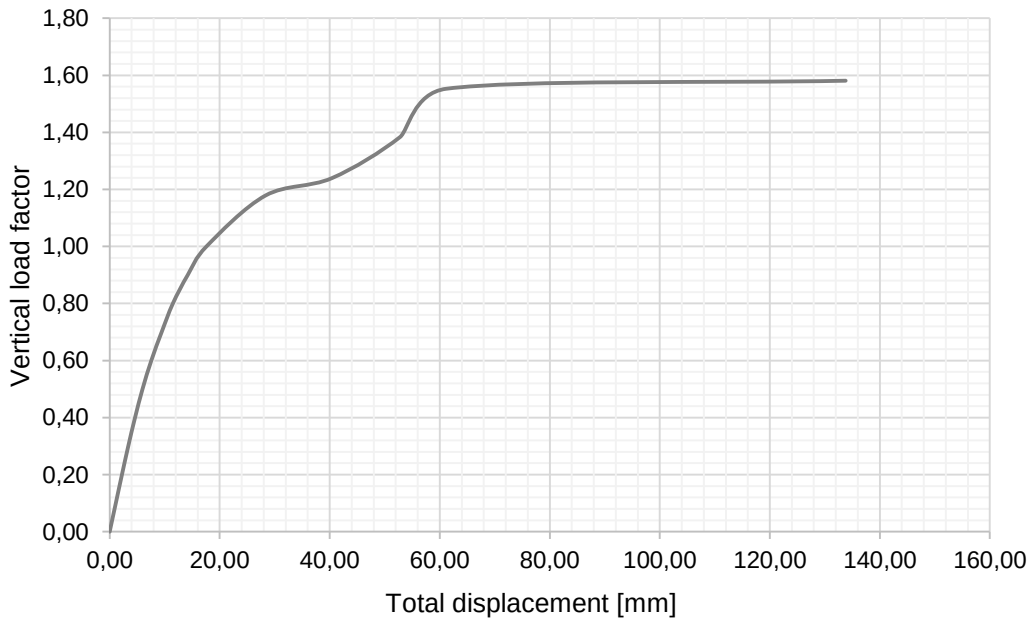

Figure 70. Capacity curve for the vertical loading analysis: Node 115782 (Nave vault)

The main aspects of the response of structure were analysed in detail, namely the peak and failure related to the nave vault, and the peak and end of the capacity curve obtained for the south tower.

Figure 71 show the damage located at the vaults and how the cracking pattern spreads from the last stable step (Figure 71a and b) and the subsequent collapse state (Figure 71c and d). In general, the damage is associated with the overloading caused by the infill and the settlement of the southwest corner of the church, which explains the propagation of the diagonal cracking.

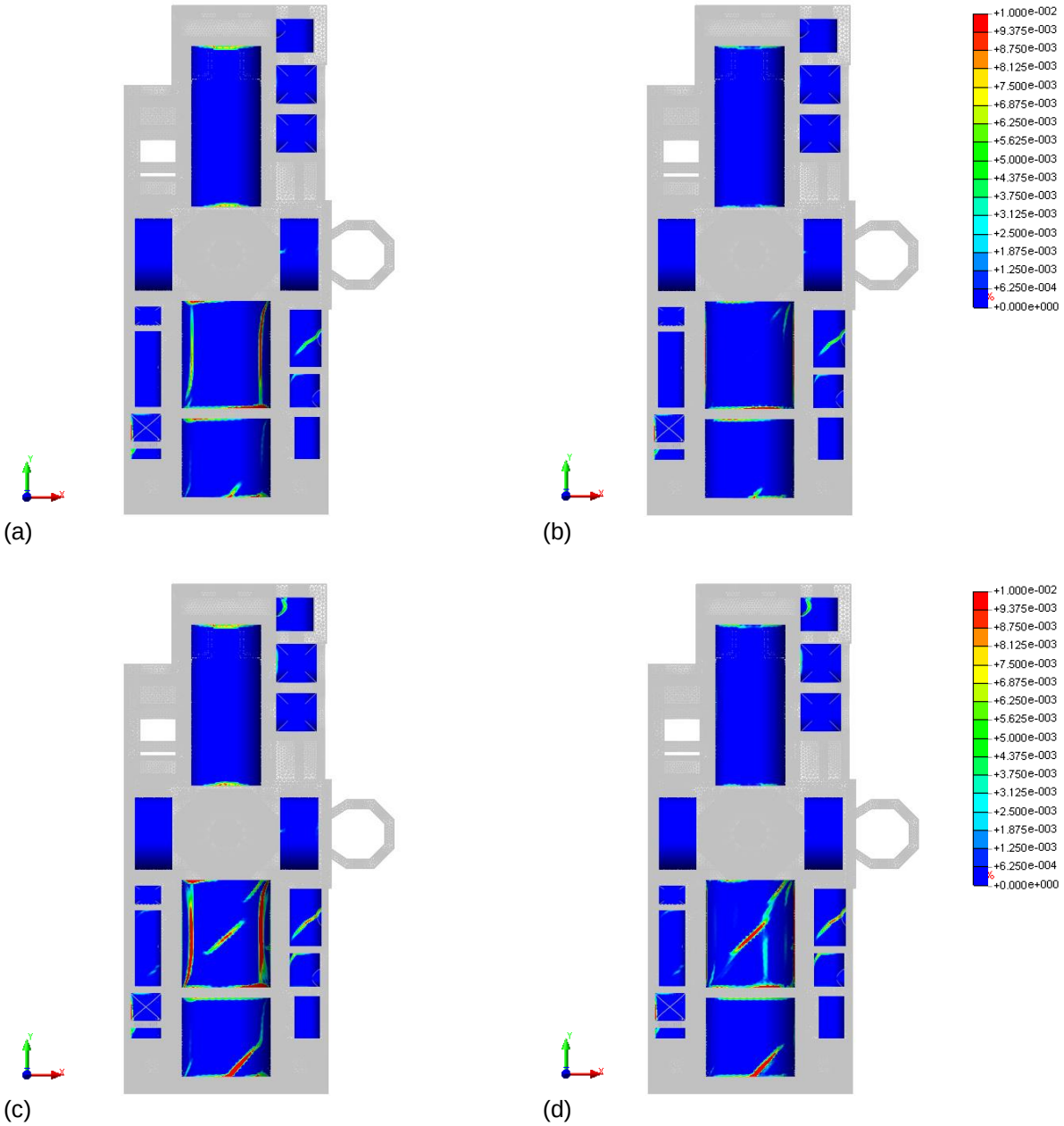

Figure 71. Maximum principal strains for the shell elements due to vertical loading. (Units: m/m)
Load factor 1.55: (a) and (b), layer 1 (intrados) and layer 5 (extrados), respectively
Load factor 1.58: (c) and (d), layer 1 (intrados) and layer 5 (extrados), respectively

Figure 72a and Figure 72b represent the damage presented by the structure at the peak of the capacity curve. The cracking pattern reveals a relevant concentration of damage in some parts of the building: following the openings of the façade, in the connection between the façade and the south tower and the angle between the south tower and the nave wall, south and north walls of the nave, arch of the choir loft, and moderate damages generally associated to other openings and orthogonal wall connections. Figure 72c and Figure 72d show the damage of the building at the last point of the diagram. The collapse mechanism corresponds to the concentration of damage around the south tower and a localised failure

that appears at the base of the wall. Figure 73 presents the displacement contour in which it is observed how the cracks detach the body of the tower and part of the façade so they may develop a mechanism. The foundation role in this mechanism is obvious, and a stiffer foundation would increase the capacity.

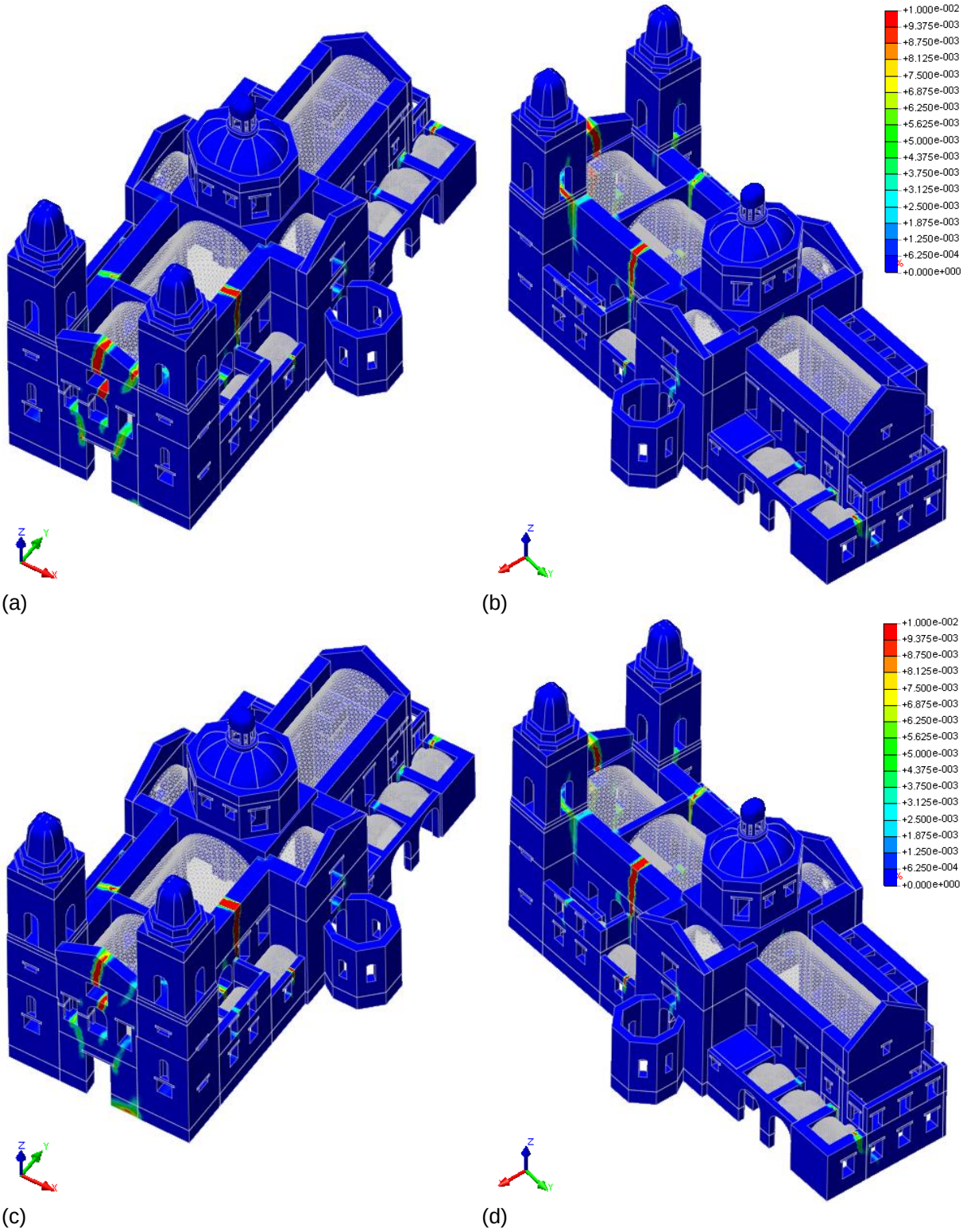

Figure 72. Maximum principal strains due to vertical loading: damage pattern at the peak (a and b) and at the end (c and d) of the capacity curve. (Units: m/m)

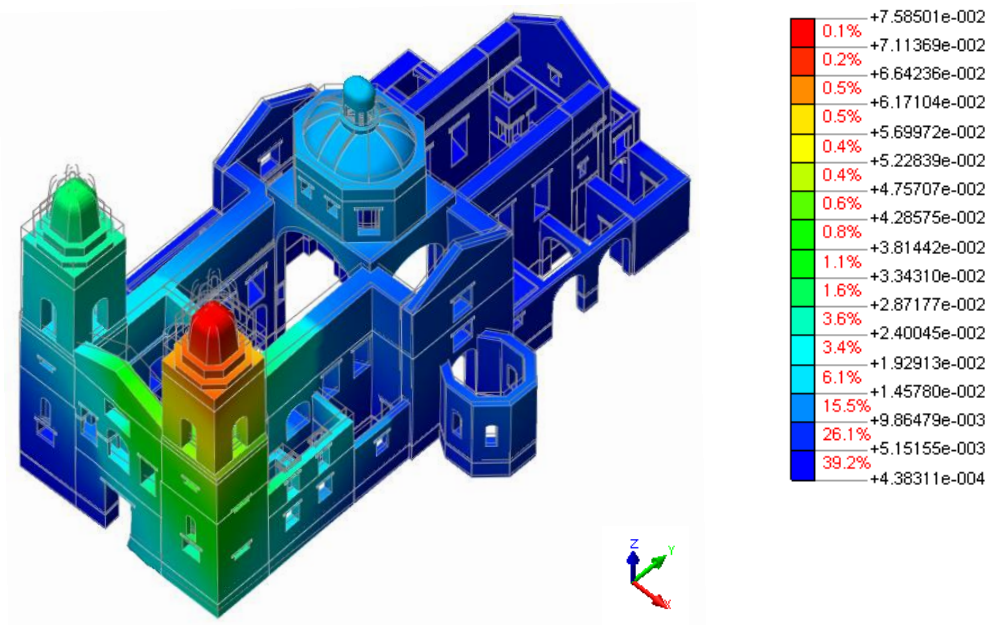

Figure 73. Total displacement due to vertical loading at the end of the capacity curve (Units: m)

Finally, the damage pattern is plotted attending to the crack width at the moment of failure (Figure 74). Most of the cracks range from 1 to 5 mm, but the most severe damages correspond to the cracks along the middle of the façade and in the lateral walls of the nave, with more than 10 mm width.

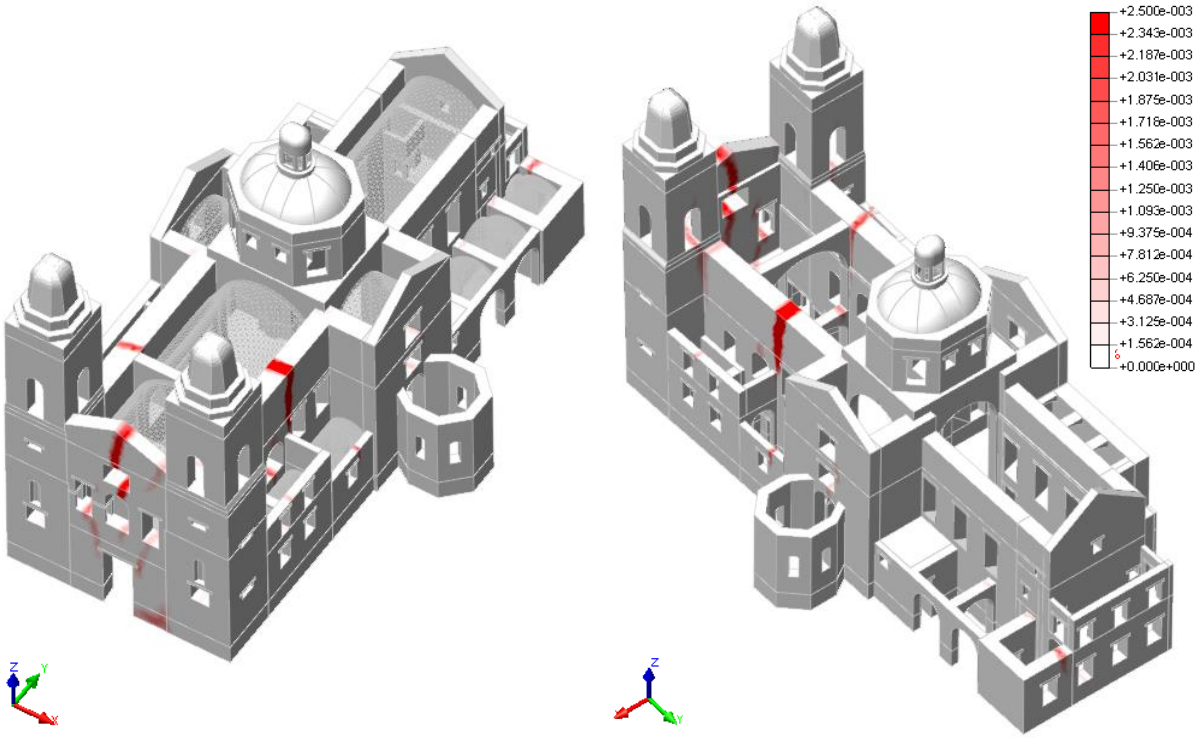

(a) (b)

Figure 74. Crack width associated to the maximum principal strain due to vertical loading at the end of the load-displacement diagram. (Units: m)

6. SEISMIC ANALYSIS

The foundation updated model introduced in the previous chapter to study the vertical loading capacity of the structure was also used to assess the seismic performance of the church by means of pushover analysis. The main objective of this new set of analyses is to identify the most vulnerable elements of the structure and to assess the safety of the building with respect to seismic actions.

6.1 Seismic performance of masonry constructions

Ancient masonry buildings were mainly designed to resist vertical static loads. Their structures were planned to take advantage of the good compressive behaviour of the material, but scarcely taking into consideration the possible horizontal actions caused by earthquakes. In general, masonry buildings are composed by load-bearing walls, which are characterised by a considerable in-plane stiffness and a rather poor out-of-plane behaviour. Therefore, the seismic performance of a masonry building depends primarily on two aspects: the direction in which the horizontal actions are applied and the capacity of the structure to redistribute the horizontal loads among the different elements in order to prevent out-of-plane mechanisms. Hence, the connection between orthogonal walls, as well as the existence of horizontal diaphragms and their connection to the walls greatly influence the seismic response of the building (Lourenço, et al. 2011).

From a material point of view, the seismic response of masonry constructions is equally complex to characterise as well. Masonry is a heterogeneous material, in which the properties may vary considerably depending on the type and material of the units, joints, and the overall arrangement of the ensemble. Nevertheless, some common properties can be identified to describe the mechanical behaviour of masonry: high specific mass, good compressive behaviour, low tensile and shear strengths, and low ductility (quasi-brittle behaviour).

Ancient masonry structures normally show a distinct non-linear behaviour, especially when affected by strong inertial loads caused by earthquakes. Considering a seismic scenario, the non-linear behaviour of the material may be triggered at early stages of the loading (Lourenço 2013). Consequently, linear-elastic analysis is not an adequate option and a non-linear analysis should be adopted.

6.2 Pushover analysis

Pushover analysis consists in a non-linear static analysis in which horizontal forces represent seismic actions. The method uses an incremental-iterative procedure assuming conditions of constant gravity loads and monotonically increasing the horizontal loads. This method can be used to estimate the failure mechanisms of a structure, to analyse the distribution of damage, to assess the structural performance of existing buildings and to predict the capacity curve of a structure, i.e. the base shear vs. a given control displacement response (EN 1998-1 2004).

In the first step of the pushover analysis, the structure is vertically loaded until reaching its self-weight state. Afterwards, the analysis continues with the horizontal loading that simulates the seismic load effect. In this second step, different loading patterns may be adopted. For the present work, the pushover analysis was carried out using a unidirectional mass-proportional pattern defined according to Eurocode 8 (EN 1998-1 2004): one-directional uniform loading pattern based on lateral forces proportional to mass regardless of elevation. This pattern is recommended for the analysis of masonry structures without box behaviour (Lourenço, et al. 2011).

The base shear factor is given by the seismic load coefficient α:

$$\alpha = \frac{\sum F_H}{\sum F_v} \tag{13}$$

where $\sum F_H$ is the sum of the acting horizontal forces and $\sum F_v$ is the sum of the acting vertical forces, calculated for each incremental loading step.

The seismic performance of the building was evaluated according to the global horizontal axes, X and Y, corresponding to the transversal and longitudinal directions of the church, respectively. The horizontal loading was applied in both positive and negative orientations of the longitudinal axis, +Y and -Y, and in the positive transversal direction, +X. The negative transversal direction was neglected due to the presence of the adjacent cloister and annexed buildings, introduced in the model as springs, which provide larger capacity in the direction.

The node at the top of the south bell tower (Figure 64) was used as control point for measuring the horizontal displacements and for developing the capacity curve of the structure in each analysed direction.

For the non-linear pushover analysis, the constitutive material law and material properties introduced in Chapter 5 were used. Finally, the same numerical tools used in the non-linear analyses for vertical loading were employed, i.e. regular Newton-Raphson method for the iteration process, energy convergence control with tolerance 10^{-3}, line-search algorithm and arc-length method. The non-linear pushover analyses were performed with the finite element software DIANA (TNO DIANA BV 2014).

6.2.1 Pushover analysis in the transversal direction of the church

The seismic response of the structure is first analysed in its positive transversal direction, +X. The capacity curve obtained is shown in Figure 75. The maximum load factor is 2.08 which represents the percentage of the weight of the building applied horizontally, or similarly, the proportional base shear force. According to these results, the building can bear a horizontal action of 2.08 *g* if the load is applied in the transversal positive direction. Note that at the beginning of the loading process, the node already has an initial displacement due to the self-weight of the structure (u_x = 16 mm).

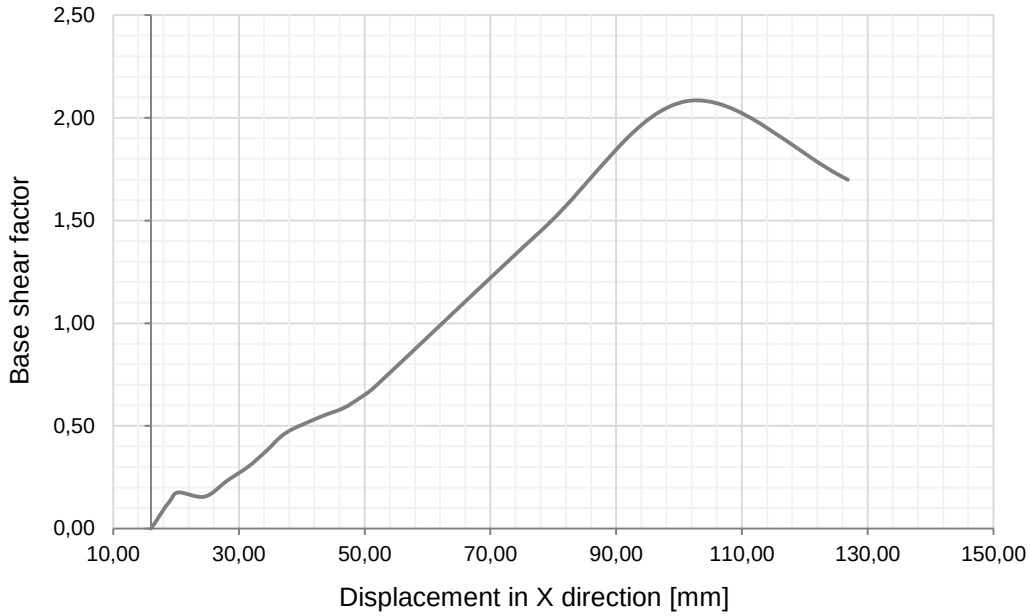

Figure 75. Capacity curve for pushover analysis +X: Node 49 (South tower)

According to the curve, the structure presents a considerable stiff behaviour. The first stiffness variation in the response corresponds to an important concentration of damage in the façade. This aspect might be associated to its in-plane vulnerability to horizontal loads, since it presents several openings. As it happened for the non-linear analysis with increasing gravitational loading (see Section 5.4), the vaults suffer higher deformations and fail at earlier stages of the loading process.

Figure 67 shows the damage pattern obtained for the pushover analysis +X corresponding to the stage of the maximum load factor. The damage is concentrated in the connection between the façade and the south tower and the angle between the south tower and the nave wall, south and north walls of the nave associated with the presence of orthogonal members, connection between the north tower and the nave wall, and following the openings of the façade.

Figure 77 shows the damage at the last point of the capacity curve obtained for the transversal pushover analysis. At the moment of failure, the extension of damage is considerable, which is consistent with the high capacity by the curve. The failure mode corresponds to the collapse of the south tower and part of the façade, and it is also associated with the concentration of damage at the foundation level.

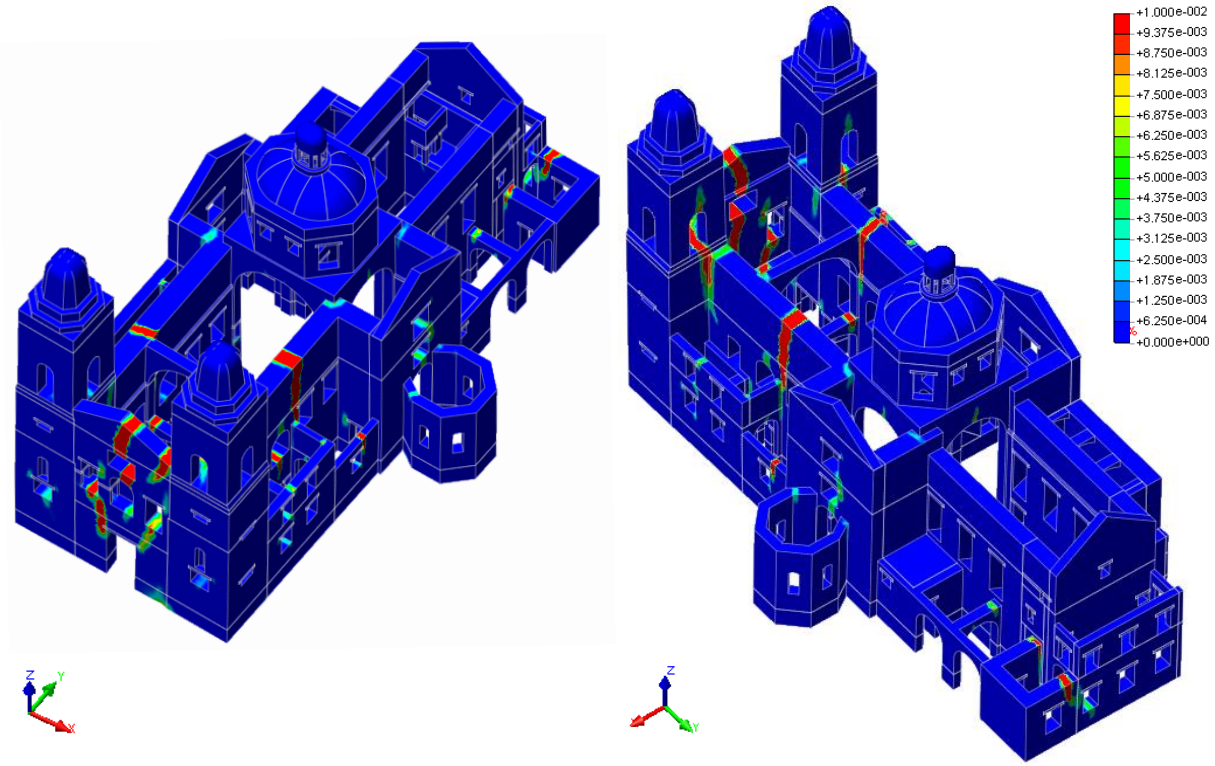

(a) (b)

Figure 76. Pushover analysis +X: Maximum principal strains at peak of the capacity curve (Units: m/m)

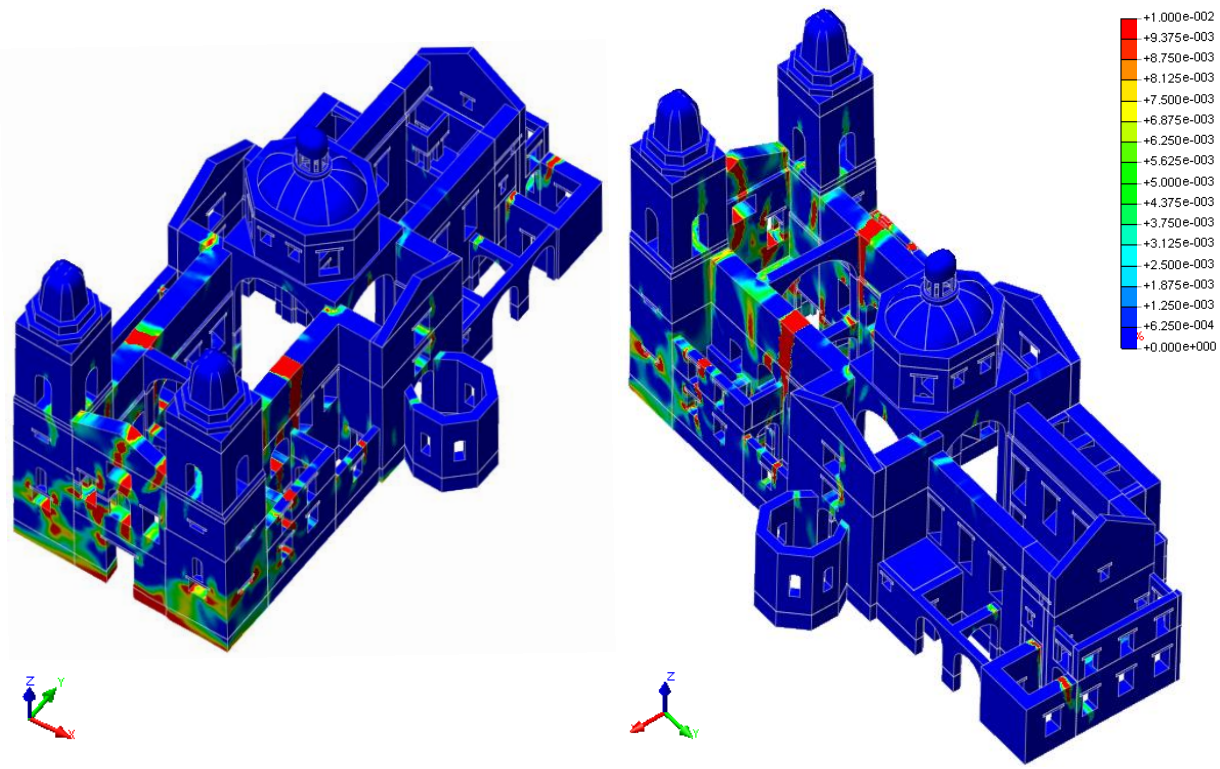

(a) (b)

Figure 77. Pushover analysis +X: Maximum principal strains at the end of capacity curve (Units: m/m)

6.2.2 Pushover analysis in the longitudinal direction of the church

As previously mentioned, two pushover analyses were done in the longitudinal direction of the building, one in the positive and the other in the negative orientation of the global axis Y, i.e. +Y and -Y.

a) Positive longitudinal direction

The capacity curve resulting from the pushover analysis +Y is shown in Figure 78. The maximum base shear factor for the positive longitudinal direction is equal to 0.89. Similar to the results obtained for the transversal direction, the curve shows an initial stiffness variation associated with an important development of cracks in the façade. A local failure of the nave vault is also detected at early steps of the pushover. After the first concentration of damage, the structure presents a rather linear behaviour (with lower stiffness) until reaching the maximum capacity, and subsequently a sudden failure occurs. It is worth noticing that, although the load is acting in the positive longitudinal orientation, the displacement registered at the top of the tower is negative, i.e. it leans in the opposite direction to the loading.

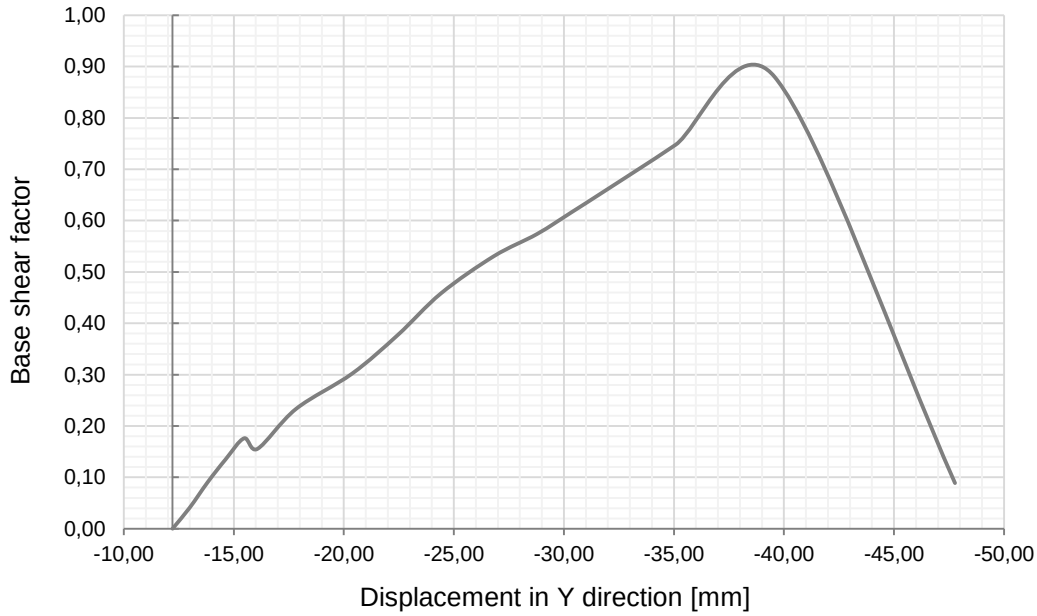

Figure 78. Capacity curve for pushover analysis +Y: Node 49 (South tower)

Figure 79 shows the damage obtained for the pushover analysis +Y corresponding to the peak of the capacity curve. The pattern is consistent with the vertical loading capacity and the pushover in the transversal direction, indicating the existence of weak points of the structure. Main damage is concentrated in the façade, and in the connection between orthogonal walls, such as the south tower and the façade, nave walls and towers, and nave walls and transversal elements.

On the other hand, Figure 80 shows the damage pattern corresponding to the last point of the capacity curve for the pushover analysis +Y. It is noticeable that the failure is mainly related to the foundation interface.

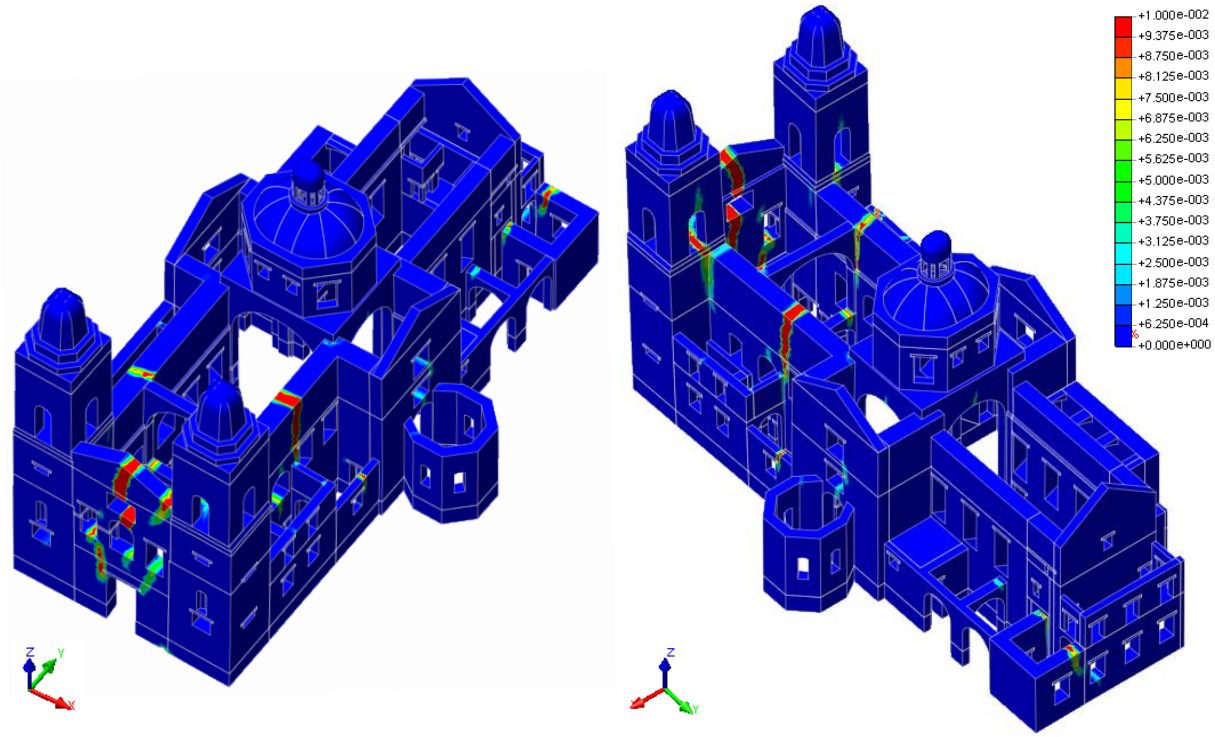

(a) (b)

Figure 79. Pushover analysis +Y: Maximum principal strains at peak of the capacity curve (Units: m/m)

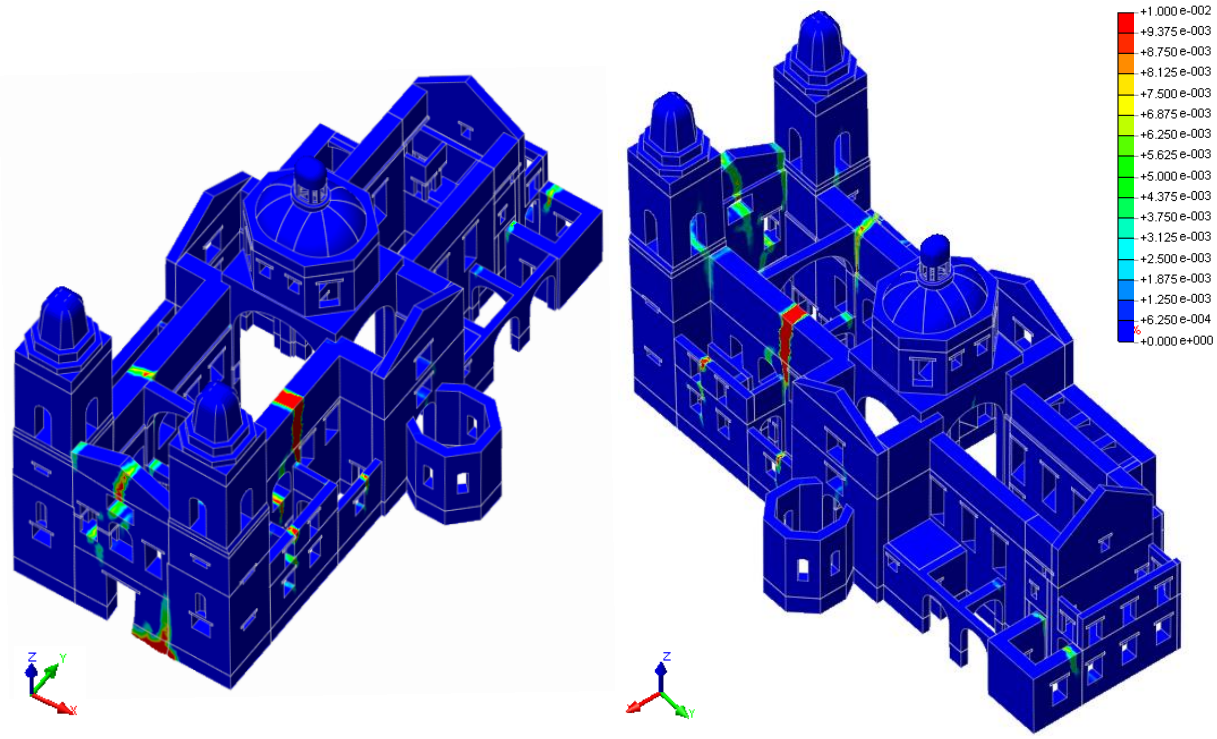

(a) (b)

Figure 80. Pushover analysis +Y: Maximum principal strains at the end of capacity curve (Units: m/m)

b) Negative longitudinal direction

The capacity curve obtained for the pushover analysis in the negative longitudinal direction, -Y, is shown in Figure 81. In this case, the maximum base shear factor obtained is 1.70, showing that the structure has a stiffer behaviour in this longitudinal orientation. As in the previous analysis, the development of cracks in the façade is reflected in the curve and a local collapse of the nave vault is detected at early stages of the pushover process. The relation shear-displacement is rather linear until the peak and a more ductile failure is detected.

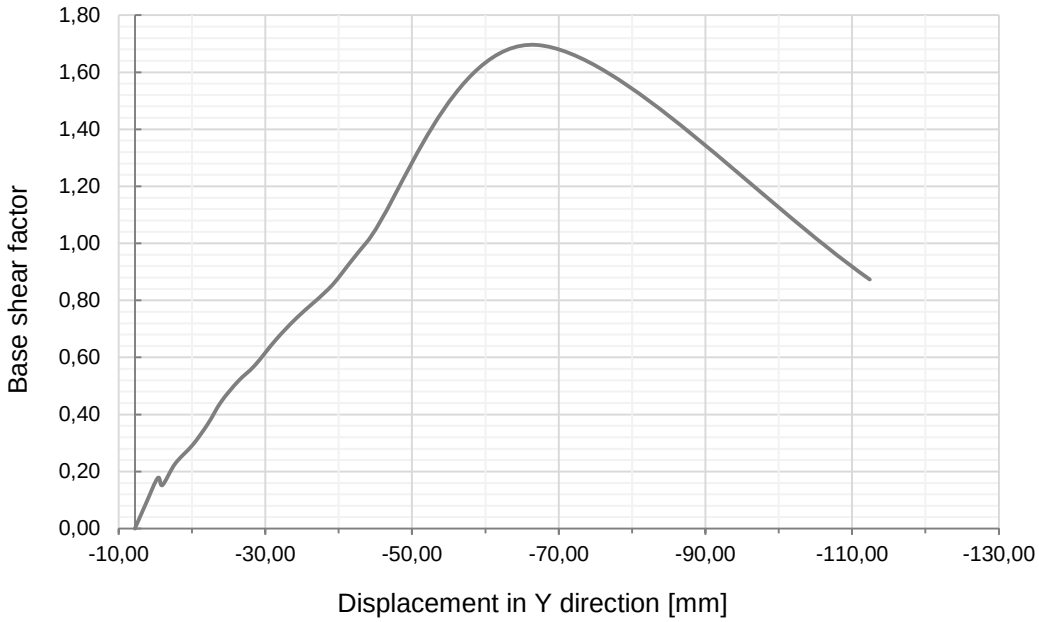

Figure 81. Capacity curve for pushover analysis -Y: Node 49 (South tower)

The damage pattern obtained for the pushover analysis -Y for the maximum load factor is shown in Figure 82. The distribution of damage is similar to the pattern obtained for the positive longitudinal direction, even if the damage in the main façade is different: connections between the south tower and the façade, and between the south tower and the nave wall, south and north walls of the nave in the joining with orthogonal members, and openings of the façade. However, the pattern shows higher strains in general, and cracking also appears around the north transept and the north tower.

Finally, the damage pattern associated to the failure at the end of the capacity curve -Y is presented in Figure 83. Once more, the foundation is directly related to the collapse and a more extended and severe state of damage is detected in the structure with respect to the pushover +Y, which may be related to the more ductile failure. Note that the capacity is higher in this direction (1.70), with respect to the pushover +Y (0.89), because the transverse walls act in compression with respect to the seismic loading, which is beneficial for the response.

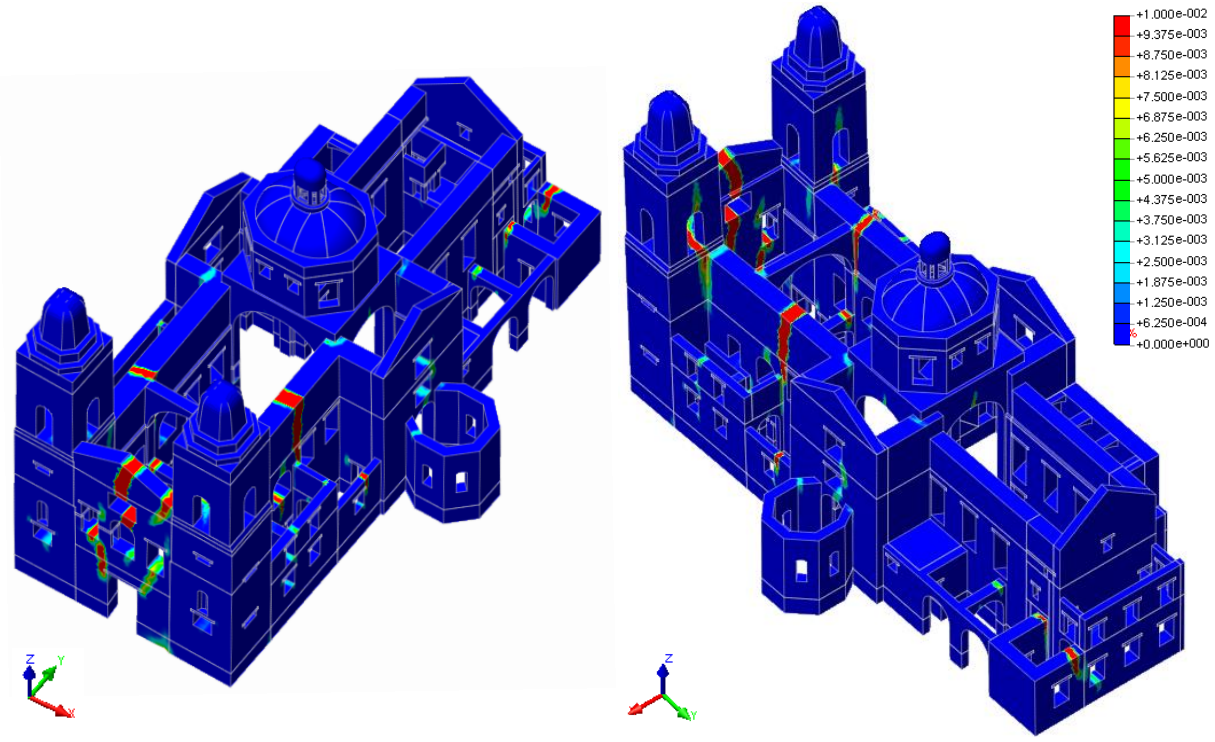

(a) (b)

Figure 82. Pushover analysis -Y: Maximum principal strains at peak of the capacity curve (Units: m/m)

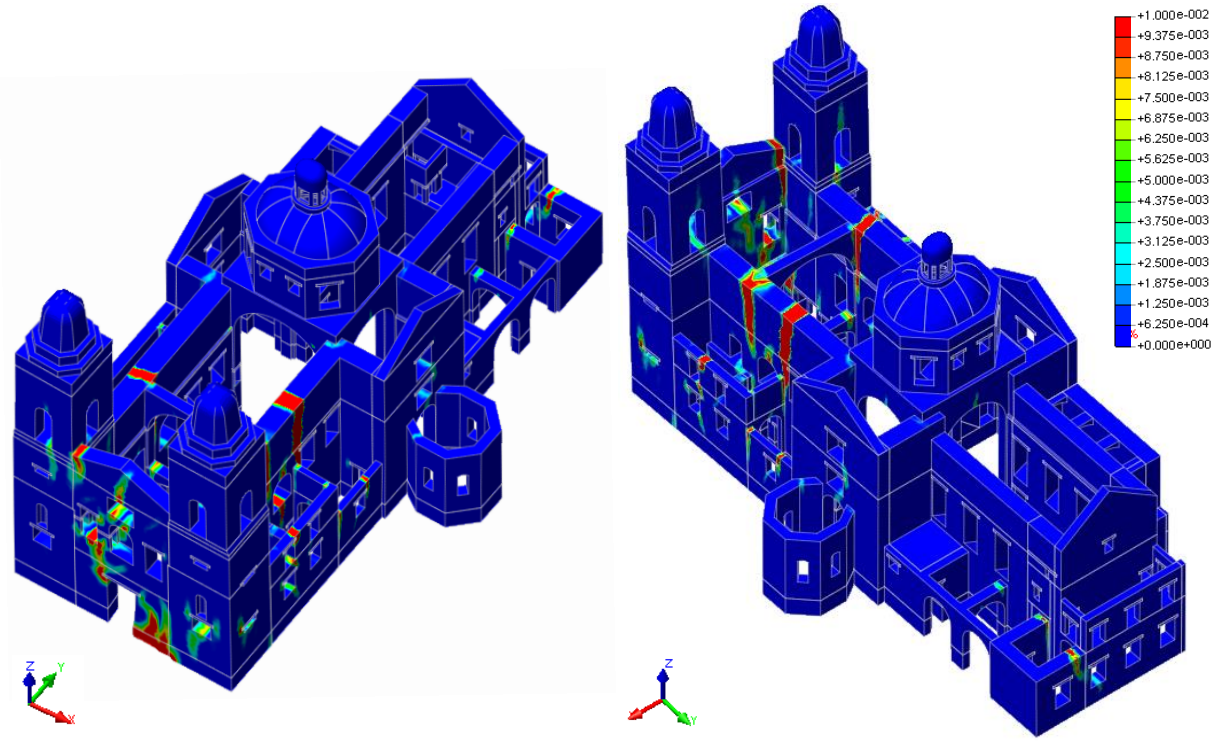

(a) (b)

Figure 83. Pushover analysis -Y: Maximum principal strains at the end of capacity curve (Units: m/m)

6.3 Seismic assessment of the church

The results obtained from the previous analyses can be used to assess the safety condition of the structure with respect to an actual seismic event. The peak values of the capacity curves represent the maximum static horizontal load that the building can withstand prior to develop a major collapse mechanism. Thus, those values can be compared with the reference peak ground acceleration considered for the region by the national codes and therefore determine the actual vulnerability of the structure.

The seismic zonation of the continental lands of Portugal is presented in Figure 84 and the respective values for the reference peak ground acceleration of each zone are shown in Table 5. Type 1 and Type 2 correspond to far field and near field seismic events, respectively.

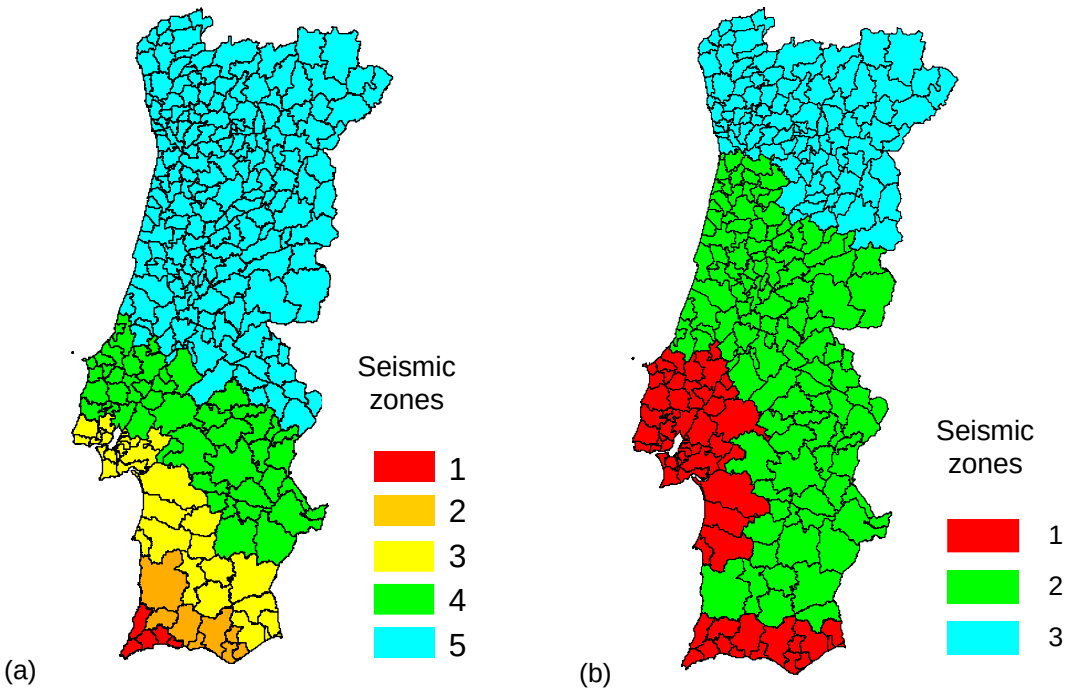

Figure 84. Mainland Portugal seismic zonation for Portuguese National Annex (EN 1998-1 2004): (a) Seismic action Type 1; (b) Seismic action Type 2

Table 20. Reference peak ground acceleration, $a_{g.R}$ (EN 1998-1 2004)

Type 1	Seismic zone	1	2	3	4	5
	$a_{g.R}$ [m/s^2]	2.50	2.00	1.50	1.00	0.50
Type 2	Seismic zone	1	2	3		
	$a_{g.R}$ [m/s^2]	1.70	1.10	0.80		

The church of São Miguel de Refojos is located in the north of Portugal, which is the area of lowest seismic risk: Zone 5 for Type 1 with $a_{g.R}$ = 0.50 m/s^2; Zone 3 for Type 2 with $a_{g.R}$ = 0.80 m/s^2.

According to the results of the pushover analyses, the most vulnerable direction of the structure is the longitudinal one, in its positive orientation. The capacity curve +Y presents the minimum peak among the responses, with a maximum base shear factor of 0.89. However, this value is higher than the reference peak ground acceleration considered for the region, both for far and near field seismic events, and therefore the structure is safe in terms of seismic phenomena. The safety factor for the seismic action is given by the relation between the maximum base shear factor in the most vulnerable direction, and the peak ground acceleration determined for the zone. In the case of São Miguel de Refojos, the safety factor is equal to 17.45 for Type 1, and 10.90 for Type 2.

7. CONCLUSIONS AND RECOMMENDATIONS

During the development of this thesis, different aspects related to the church of the Monastery of São Miguel de Refojos were studied in detail. Within the research process, three main phases were completed. The first step regarded the state-of-the-art, aimed at collecting all available data necessary for the generation of the numerical model. Concerning this part, the condition of the structure was assessed in light of the inspection works and the main structural parameters were estimated according to the experimental tests. The following step involved the preparation and validation of the numerical model. According to the data previously collected, a three-dimensional finite element model of the church was prepared. Subsequently, an eigenvalue analysis was performed and the model was calibrated by comparing the numerical results with the experimental data obtained from the dynamic identification tests. The last phase involved several non-linear analyses conducted to evaluate the observed damage and present condition of the structure, as well as to assess its safety. The soil-structure interaction was first studied and then two set of analyses were performed, namely the non-linear static analysis for vertical loading, aiming at evaluating the existing damage and assessing the stability of the structure under this loading condition, and the pushover analysis to study the seismic performance of the church. As a result of the previous works, the following conclusions and recommendations for further studies were proposed:

- In general, the current structural condition and the overall state of conservation of the church are good. However, an adequate intervention plan, including maintenance and monitoring, should be put into practice in order to prevent the building from suffering more damage. The main activities to be carried out should include: general repair of the roof and protection against infiltration of rain water, creation of a drainage system for the towers, protection of the openings against environmental elements and birds, measures to reduce the humidity and presence of water in the walls and floors, and repairing of cracks. The monitoring plan should entail the regular control of temperature and relative humidity, water table level, and the measurement of cracks and deformations.
- The inspection and diagnosis campaign allowed to identify and characterise the main aspects necessary to evaluate the structure and generate the numerical model. Nevertheless, further investigation is recommended in order to clear up some uncertainties and verify the assumptions made during the process, such as the boundary conditions of the vaults.
- A detailed inspection of the vaults and roof on top of the transepts and chancel needs to be carried out. The access to these areas could take place during the repairing works of the roof. The diagnosis

should encompass a complete geometric and material survey of the vaults, infill and timber trusses, as well as the evaluation of their state of conservation.

- In any case, a deeper study of the vaulted system is suggested. The thickness of the vaults should be measured in order to corroborate the results of the GPR tests. On the other hand, considering the mechanical behaviour of a vault, the presence of backing or a cohesive infill has a strong influence and it can affect to the global structural behaviour as well. Therefore, a thorough study of the infill material is advisable. Since no information was available, the present model disregards the effect of the infill (less favourable condition). The model should be updated with respect to the data collected in these future studies.
- The material properties for timber elements were estimated from literature. In situ minor-destructive testing to calculate the actual characteristics of the material is suggested, as well as a particular study to characterise the wood joints and the overall state of conservation.
- Masonry typologies were identified by means of GPR analyses and their mechanical characteristics were proposed according to literature and then calibrated with respect to the experimental dynamic results. Further investigation can be carried out for a better understanding of the masonry internal condition. Non-destructive tests are proposed to corroborate the numerical properties (indirect sonic tests) and analyse in detail the global quality of the masonry (direct sonic tests). Likewise, thermography may be of help to study the composition of the walls, reveal the presence of lintels and relieving arches, and determine the quality or grade of interlocking between elements. These aspects can have influence on the behaviour of the structure, therefore any major discovery should be taken into account and implemented into the numerical model.
- The initial eigenvalue analysis already proved a good quality of the model, with similar mode shapes and slightly lower frequencies. That fact may be considered as supporting of the initial material and geometric hypothesis. Afterwards, the calibration was performed attending to the three most representative modes obtained from the experimental tests and the results were verified with the MAC values, successfully validating the model.
- The damage pattern of the building was mainly associated with geotechnical causes and, accordingly, a non-linear model was prepared so as to take into account the real behaviour of the soil. Two main obstacles had to be faced: the impossibility to access, and therefore characterise, the foundations, and the shortage of experimental results. Based on past experiences and engineering judgment, the problem was partially overcome by proposing different cases combining several possible scenarios. Finally, one of the proposals was selected as the most representative in terms of parallelism between real and numerical damage. However, it should be noted that the existing damage can be associated to other causes, or at least be emphasised by other factors, such as thermal phenomena, poor interlocking between parts, etc. Furthermore, the geotechnical examination conducted during the inspection works does not provide sufficient information as to

validate the soil profile under the church, and therefore, more experimental tests should be performed in representative areas close to the building.

- The results of the non-linear analyses showed that the foundation interface plays an important role in the development of failure and collapsing mechanisms. As mentioned before, the interface was hypothesised and justified attending to the damage pattern, but more empirical proofs should be collected to ratify this assumption. A stiffer foundation or soil interface would considerably increase the capacity of the structure, and vice versa.
- The structure presents a considerable safety level in terms of gravitational loading. The non-linear analysis for vertical loading showed that the south tower is the most vulnerable part of the massive structure. Nonetheless, the first failures appear at earlier stages in the vaults. As it was mentioned before, the failure of the vaults is rather sensitive to the presence of backing or a cohesive infill, so it is also possible that this local mechanism is under-estimated.
- The pushover analysis demonstrated once more the vulnerability of the south bell tower and the significant influence of the soil interface in the results. Moreover, the longitudinal orientation of the church is the most vulnerable in terms of seismic action, especially for loadings acting in the positive direction, +Y, for which a maximum base shear factor of 0.89 was obtained.
- Regarding the seismic safety of the building, a good overall seismic performance of the structure is assessed. All the directions present base shear values higher than the peak ground acceleration considered for the zone. In this sense, the safety factor for the seismic action is equal to 10.90, which corresponds to a near field earthquake acting in the positive longitudinal direction. However, considering the aforementioned considerations, further analyses and verifications are required in order to reach an adequate judgment.

REFERENCES

Allemang, J.R. “The Modal Assurance Criterion - Twenty Years of Use and Abuse.” *Sound and Vibration*, 2003: 14-21.

CEB-FIB. *Model Code 1990: Design Code.* London: T. Telford, 1993.

Denver, H. *Modulus of Elasticity of Sand Determined by SPT and CPT.* Amsterdam: Proc. ESOPT 2, 1982.

DGPC. *Igreja e sacristia do Convento de Refóios, assim como o teto de uma das salas do antigo mosteiro de frades beneditinos.* Direção-Geral do Património Cultural, 2015. (in Portuguese)

Douglas, B. M., and W. H. Reid. “Dynamic tests and system identification of bridges.” *Journal Struct. Div.* (ASCE) 108 (1982): 2295-2312.

EN 1998-1. *Eurocode 8: Design of structures for earthquake resistance - Part 1: General rules, seismic actions and rules for buildings.* 2004.

Ewins, D. *Modal testing: theory, practice and application. 2nd Edition.* Baldock-Hertfordshire: Research Studies Press LTD, 2000.

Lemos, C., F. Queiroga, A. Vitorino, e L. Melo. *Remodelação dos Claustros do Mosteiro de S. Miguel de Refojos, Cabeceiras de Basto. Relatório Final de Trabalhos Arqueológicos.* Perennia Monumenta, 2013. (in Portuguese)

Lourenço, P. B. “Computational strategies for masonry structures: Multi-scale modelling, dynamics, engineering applications and other challenges.” *Congreso de Métodos Numéricos en Ingeniería, SEMNI-APMTAC 2013.* Bilbao, Spain, 2013.

Lourenço, P.B. *PhD Thesis. Computational Strategies for Masonry Constructions.* Delft: Delft University Press, 1996.

Lourenço, P. B. *Recent advances in masonry modelling: Micromodelling and Homogenisation.* Vol. 3: Multiscale Modelling in Solid Mechanics, in *Computational and Experimental Methods in Structures*, edited by Ugo Galvanetto and M. H. Ferri Aliabadi, 251-294. 2010.

Lourenço, P. B., N. Mendes, F. Fernandes, and T. Miranda. *Diagnóstico do estado de conservação da Igreja do Mosteiro de São Miguel de Refojos de Basto.* Universidade do Minho, 2016. (in Portuguese)

Lourenço, P. B., N. Mendes, L. F. Ramos, and D. V. Oliveira. “Analysis of masonry structures without box behaviour.” *International Journal of Architectural Heritage* 5, no. (4-5) (2011): 369-382.

Mendes, Nuno. *PhD Thesis. Seismic Assessment of Ancient Masonry Buildings: Shaking Table Tests and Numerical Analysis.* Portugal: University of Minho, 2012.

NTC. «Decreto Ministeriale 14 gennaio 2008: Nuove Norme Tecniche per le Costruzioni.» 04 de febbraio de 2008. (in Italian)

PAUTA. *Estudo do edificado da igreja e sacristia do convento de Refojos.* Câmara Municipal de Cabeceiras de Basto, 2000. (in Portuguese)

Pereira, José Fernandes. *Arquitectura Barroca em Portugal.* Lisboa: Instituto de Cultura e Língua Portuguesa (Ministério da Educação), 1992. (in Portuguese)

PIET-70. *Obras de fábrica. Prescripciones del Instituto Eduardo Torroja.* Madrid: CSIC, 1971. (in Spanish)

Poletti, E. *PhD Thesis. Characterization of the seismic behaviour of traditional timber frame walls.* Portugal: University of Minho, 2013.

Queiroga, F. *Sondagens arqueológicos no âmbito da "abertura de poços de observação" na Igreja do Mosteiro de São Miguel de Refojos, Cabeceiras de Basto. Relatório de Trabalhos Arqueológicos.* Perennia Monumenta, 2015. (in Portuguese)

RCCTE. “Regulamento das Características de Comportamento Térmico dos Edificios. Decreto-Lei n.º 80/2006.” Diário da República, 2006. (in Portuguese)

Roca, P., M. Cervera, G. Gariup, and L. Pela. “Structural analysis of masonry historical constructions. Classical and advanced approaches.” *Archives of Computational Methods in Engineering* 3, no. 17 (2010): 299-325.

RSECE. “Regulamento dos Sistemas Energéticos de Climatização em Edificios. Decreto-Lei n.º 79/2006.” Diário da República, 2006. (in Portuguese)

Senthivel, R., and P. B. Lourenço. “Finite element modelling of deformation characteristics of historical stone masonry shear walls.” *Engineering Structures* 31, no. 9 (2009): 1930-1943.

Sequeira, M. *A Igreja do Mosteiro de São Miguel de Refojos de Cabeceiras de Basto.* Vol. 2, em *Estudos em homenagem ao Professor Doutor José Amadeu Coelho Dias*, 223-32. 2006. (in Portuguese)

SVS. *ARTeMIS Modal.* Denmark: Structural Vibration Solutions A/S, 2009.

TNO DIANA BV. “DIANA Finite Element Analysis User’s Manual Release 9.6.” Delft, The Netherlands, 2014.

Tomazevic, M. *Earthquake-resistant and design of masonry buildings.* London: Imperial College Press, 1999.

Vasconcelos, Graça. *PhD Thesis. Experimental investigations on the mechanics of stone masonry: characterization of granites and behavior of ancient masonry shear walls.* Portugal: University of Minho, 2005.

APPENDICES

A.1 PAST INTERVENTIONS IN THE CHURCH AND CLOISTER

Year	Intervention
1829	Repair works on the south bell tower
1934	Replacing of the ground floor slabs in geometric stonework in the sacristy, stairs and several points of the ground floor.
1936 - 1938	Reconstruction of the staircase of the monastic dependencies. Construction of the staircase vault in reinforced concrete, including ribs. Repair works on the roof of the church. Repair of the lantern and sealing/waterproofing of the dome with lead panels. Placement of stained glass in the church windows.
1942	Replacement of the tiles of the church roof. Replacement of wood ceilings in chestnut lining.
1944	Placing of stone slabs in the galleries of the cloister.
1945	Repair of the solarium porch with replacement of the timber and a column.
1946	Reconstruction of the roof frame of the monastic dependencies. Repairing of timber floors in chestnut wood.
1949	Several arrangements in the church, including placement of stained glass, arrangement of the choir and annexes, general repair of plasters, arrangement and painting of window frames, general painting, exterior drainage, conclusion of the restoration of the porch balcony. Construction of a collector to drain the sacristy, cloister and other facilities. Propping of one of the walls of the cloister, which was showing severe overturning. Reconstruction of a portion of the cloister roof damaged due to a fire.
1953	Works in the sacristy, including waterproofing of the lateral walls, repointing of masonry joints and opening of vent channels. Repair of the floor and walls. Reconstruction of stained glass and profiles of the windows.
1954	Works inside the church, including painting, masonry cleaning and installation of stained glass.
1955	Works in ante-sacristy to provide moisture protection. Dismantling of the sacristy floor.
1965	Restoration work in the cloister, including landscaping.
1966	Repair of the south façade of the church.
1971	Conservation works of the dependencies in the north side of the chancel, including cleaning and arrangement of the roof.
1972	Reconstruction of stained glass windows and network protection. Small works in the sacristy, in particular furniture arrangement.

Year	Intervention
1973	Conservation works and plaster on the south façade of the church.
1974	Conservation and plaster works on the side south façade of the church
1975	Repair of the ground floor in the nave. Conservation works and reconstruction of the roof of the staircase body. Reconstruction of the stained glass windows of the chancel.
1976	Reconstruction of two stained glass windows of the chancel. Several works in the church, including arrangements in the nave altars.
1977	Conclusion of the repair works on the nave altars.
1979	Remodelling of roofs, including tile replacement and vegetation clearing.
1981	Interventions for the conservation of the church façades.
1982	Conclusion of the repair works in the main façade of the church.
1985 - 1990	Remodelling and improvement interventions in the church. Ground floor drainage in the zone of the transept.
1998	Cleaning, restoration and improvement of the monastery façade.
1999	Replacement and repair of the roofs of the church and the Town Hall. Conservation works on the dome, including treatment of openings, masonry cleaning, plaster repair and painting, removal of the ceramic coating and application of lead sheets in the dome and lantern.
2000	Major repair of the dome, with general improvement of the cover, cleaning of stone surfaces and sculptures and glass replacement. Conservation works on the main façade of the church and bell towers, including cleaning of granites, treatment of plaster and painted walls, repairing of windows, frames and stained glass, cleaning of the interior of the towers and restoration of the bells.
2001	Several interventions in the church, namely conservation works in the room next to the choir loft, including openings and exterior walls, stone cleaning, treatment of joints, application of plasters and paint on the walls, execution of new openings, treatment of stained glasses of the volume near the bell tower, repairing of ceilings, walls and floors, implementation of electricity wiring system, and conservation of the choir stalls. External painting of the City Hall rooms and the Church. Recovery of the choir and bellow room with extensive cleaning of the stalls, wood treatment and recovery of all the stained glass. Conservation works in the cloister with cleaning, painting and construction of false ceiling (2001 to 2006).
2002	Treatment of outer walls of the church. Conservation works in the roofs of the areas next to the north side of the chancel. Conservation of stained glass and lanterns.

Year	Intervention
2003	Restoration of the altarpiece in the sacristy. Conservation and improvement works in the old sacristy. Other improvements in the church. Rehabilitation of the old punishment cell in the southern side of the monastery, later reused and adapted to mortuary chapel.
2008	Intervention in the ante-sacristy and old sacristy for the creation of a Museum of Sacred Art.
2009	Restoration of the church pipe organ, including cleaning and painting also the decorative organ, and structural reinforcement of the rare arch of the organ.
2010	Rehabilitation and upgrading of the south side of the monastery. Cleaning of the façades, roofs and bell towers.
2012	Improvement works in the church, including treatment of roofs and outer walls of the Blessed Sacrament chapel, sacristy, choir loft and space where the bellows of the pipe organ are installed.
2013	Major refurbishment of the cloister.

A.2 GRAPHIC INFORMATION ANNEX

INDEX OF PLANS

Damage survey

Inspection trenches

Water level assessment

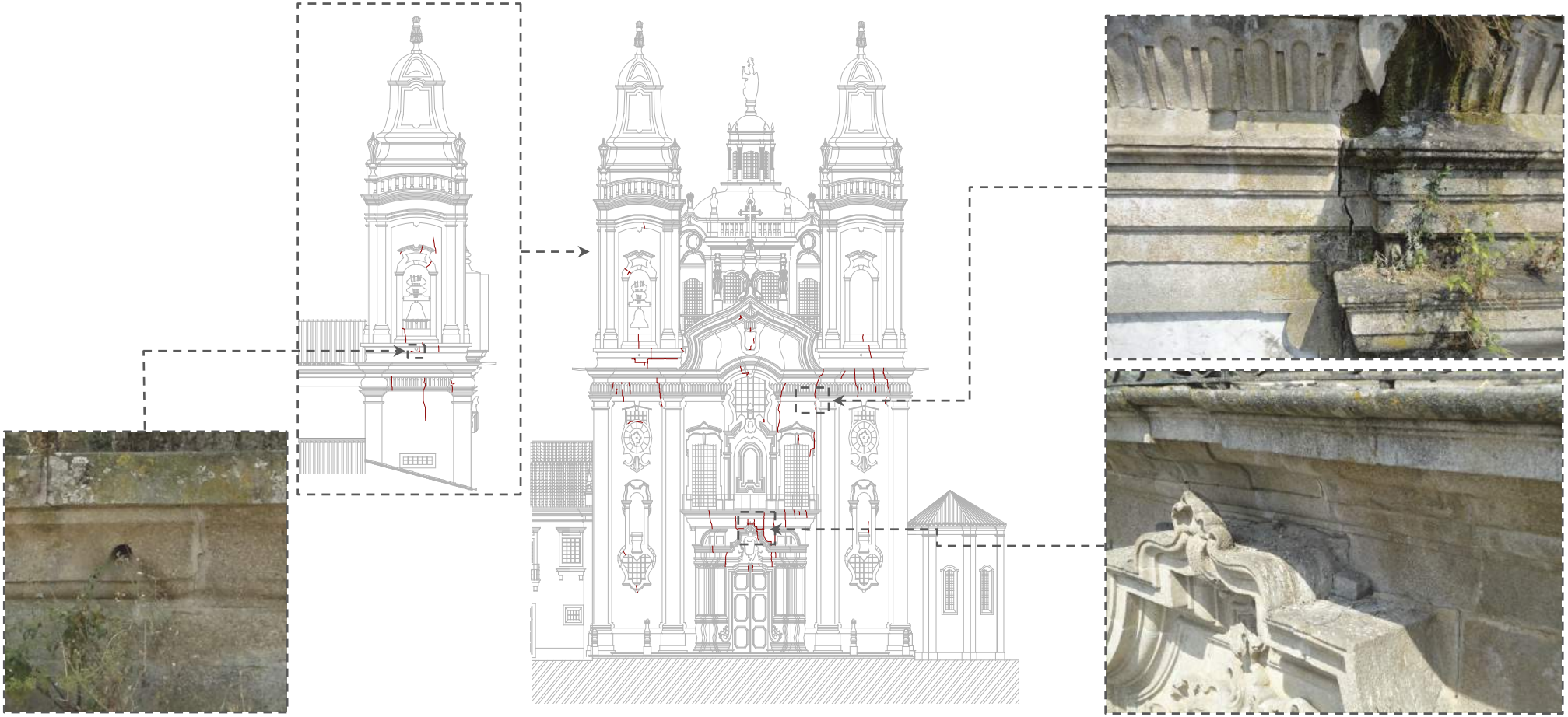

Crack pattern: main façade and north side of the north tower

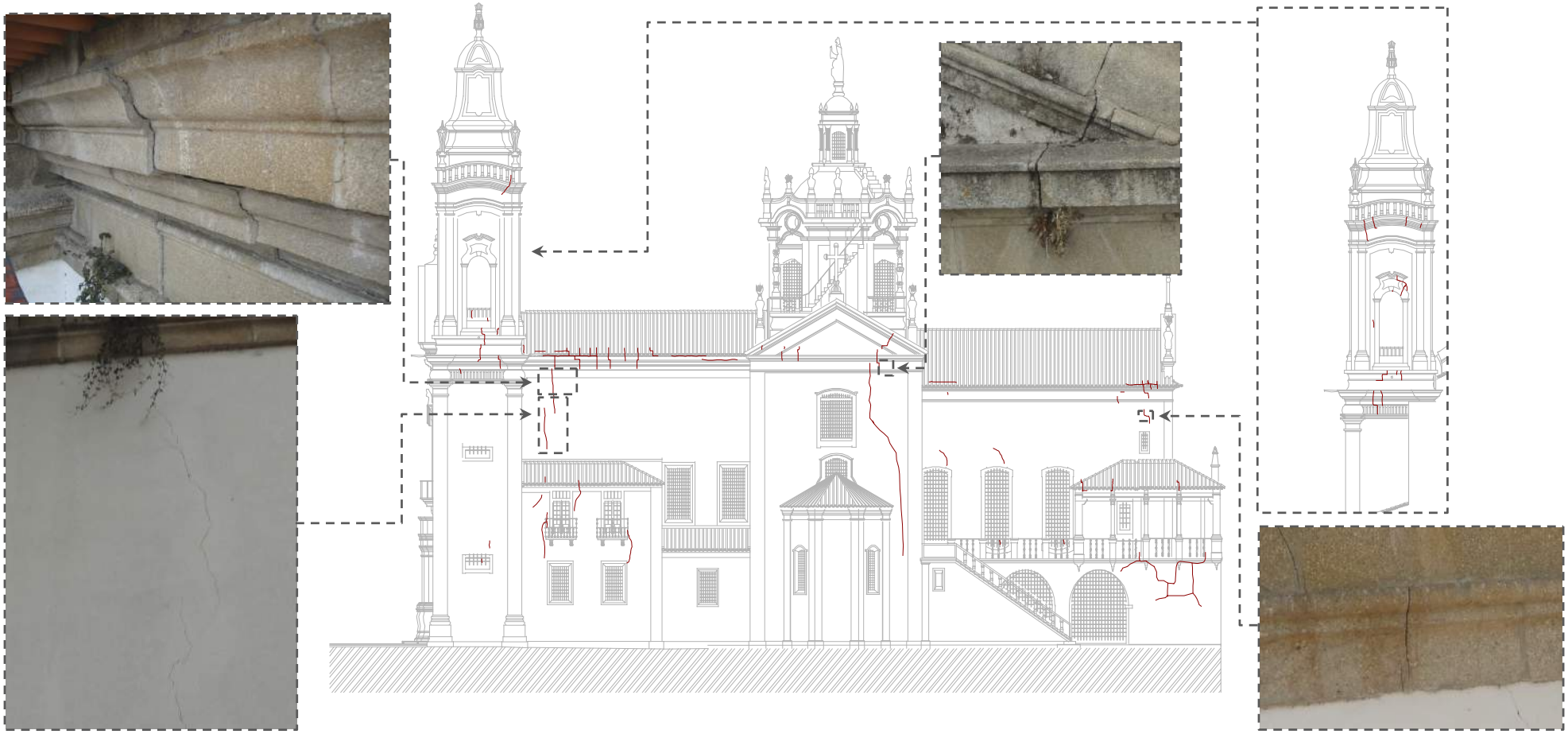

Crack pattern: south façade and east wall of the south tower

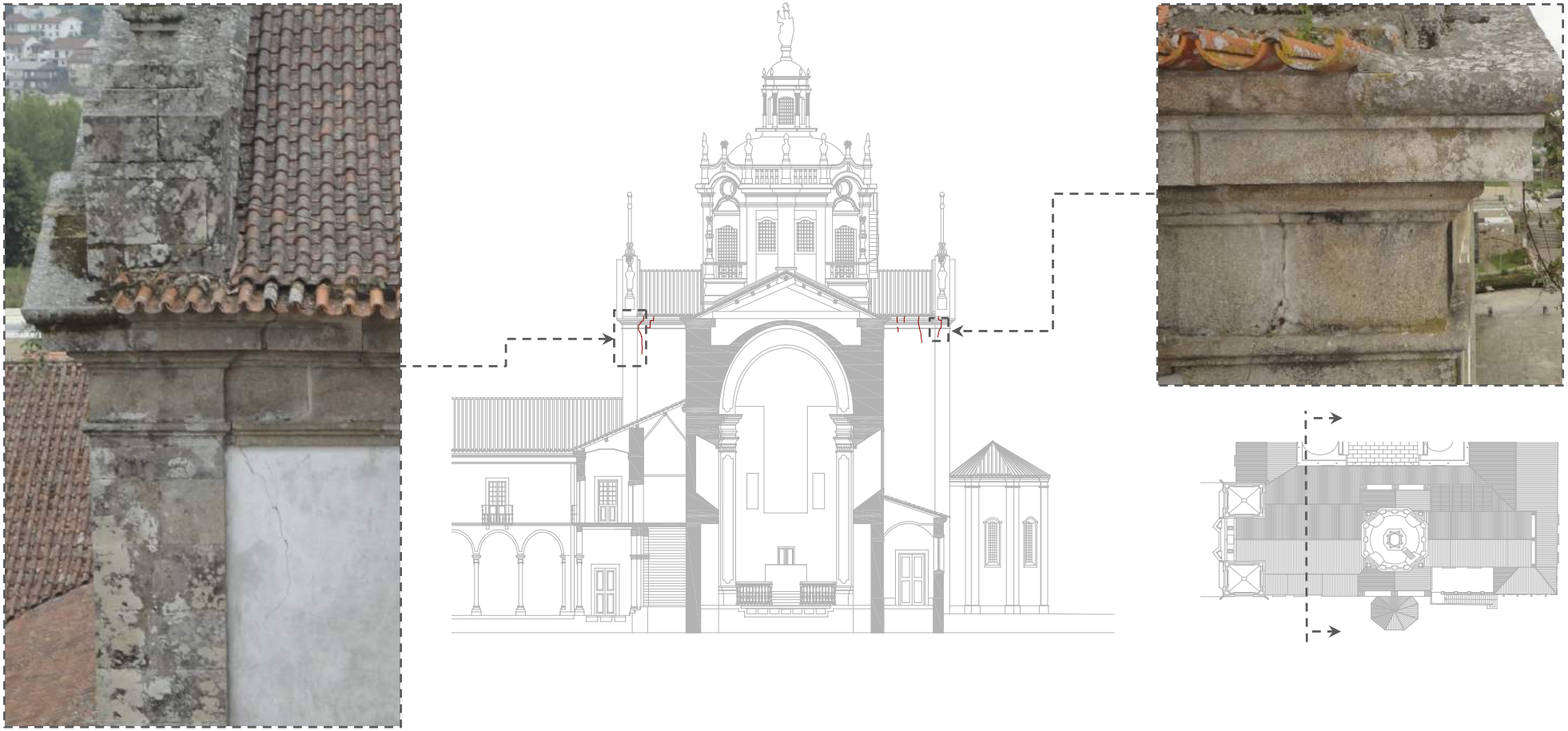

Crack pattern: west walls of the transept

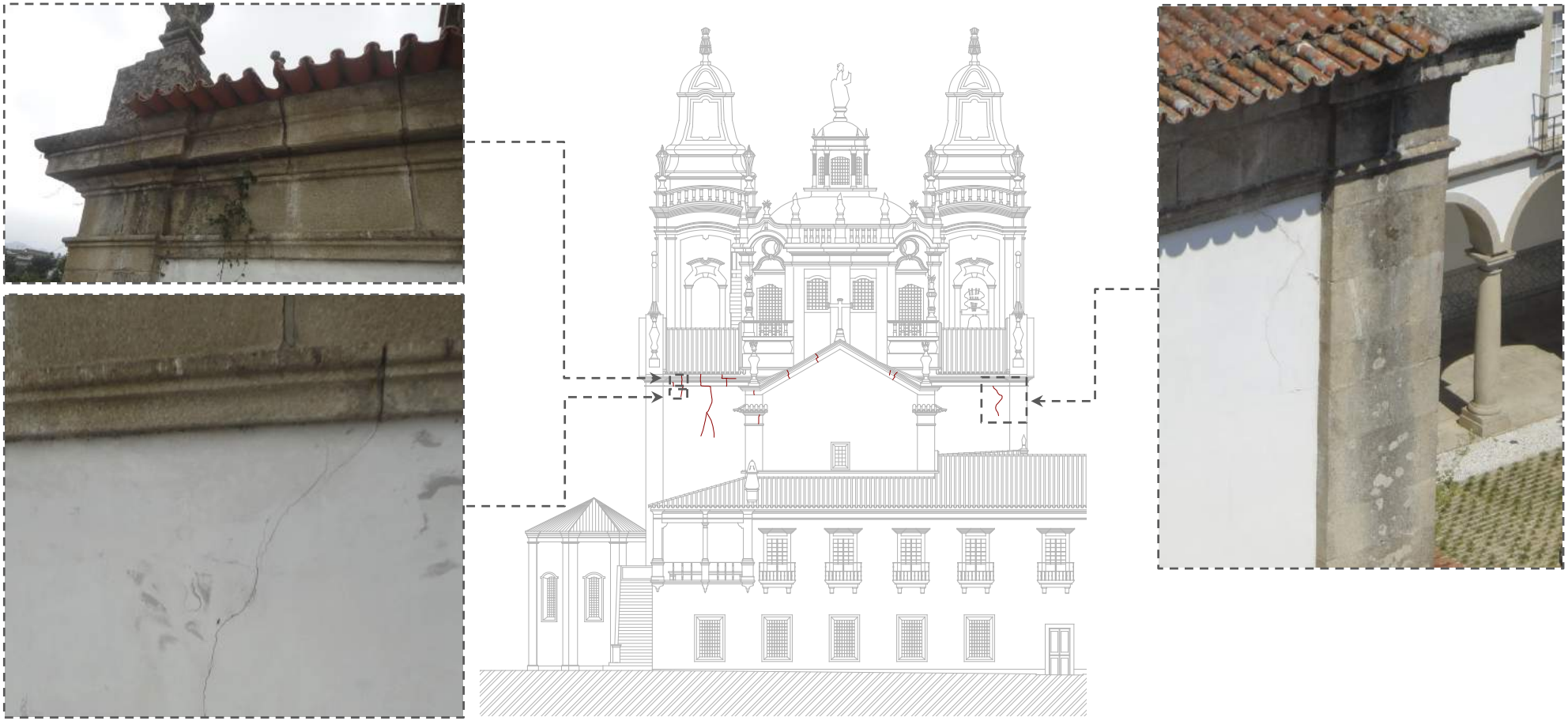

Crack pattern: east walls of the transept and east façade

Plan of Inspection trench 1

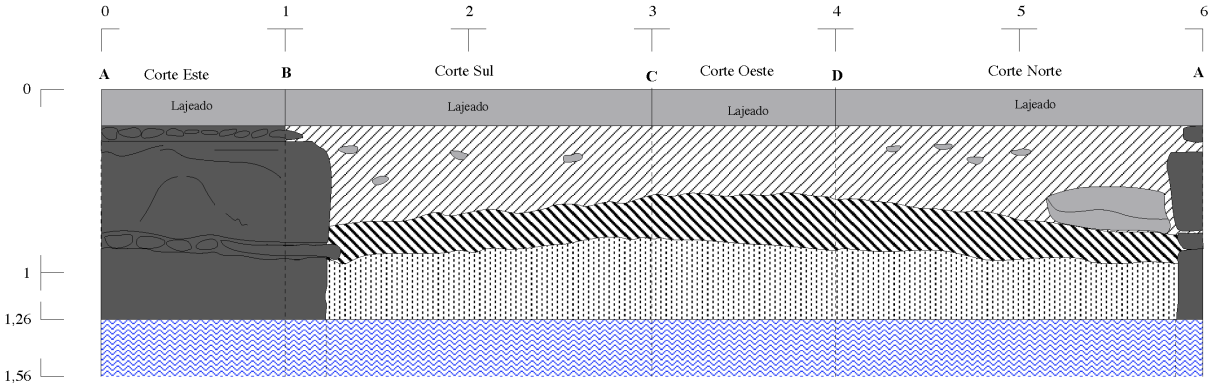

Cross-section of Inspection trench 1: East (A-B), South (B-C), West (C-D), and North (D-A)

0 1 m

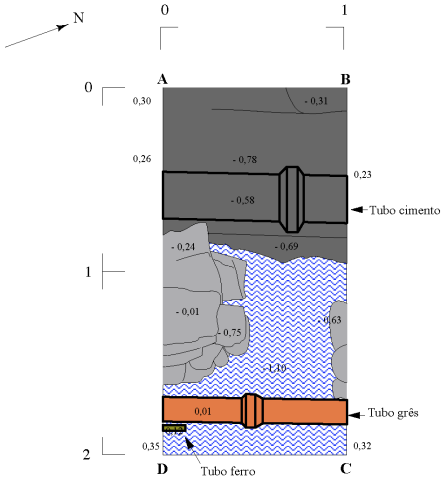

Plan of Inspection trench 2

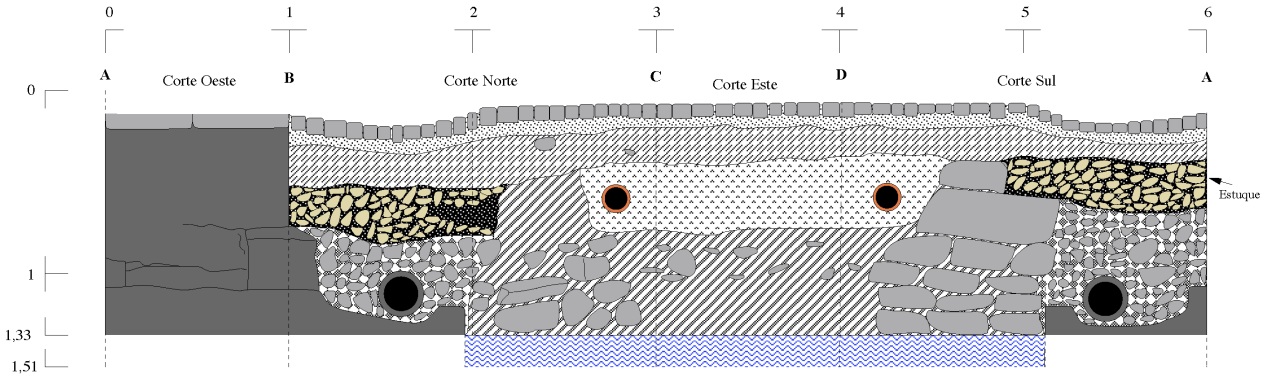

Cross-section of Inspection trench 2: West (A-B), North (B-C), East (C-D), and South (D-A)

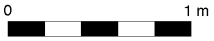

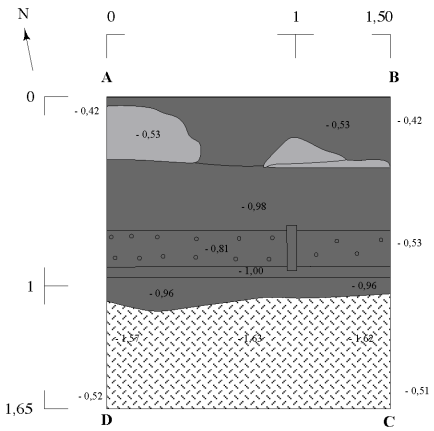

Plan of Inspection trench 3

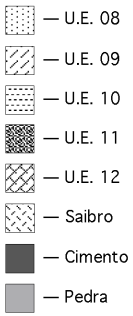

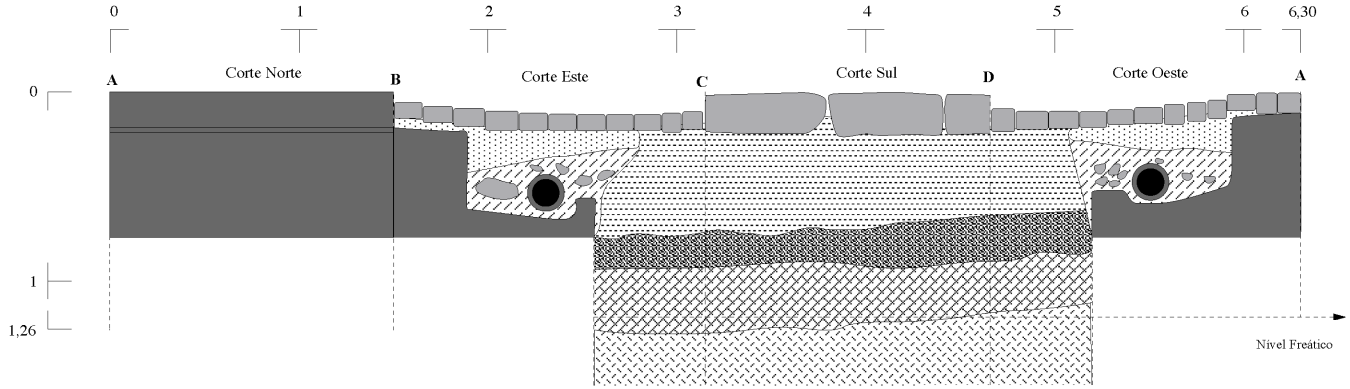

Cross-section of Inspection trench 3: North (A-B), East (B-C), South (C-D), and West (D-A)

0 1 m

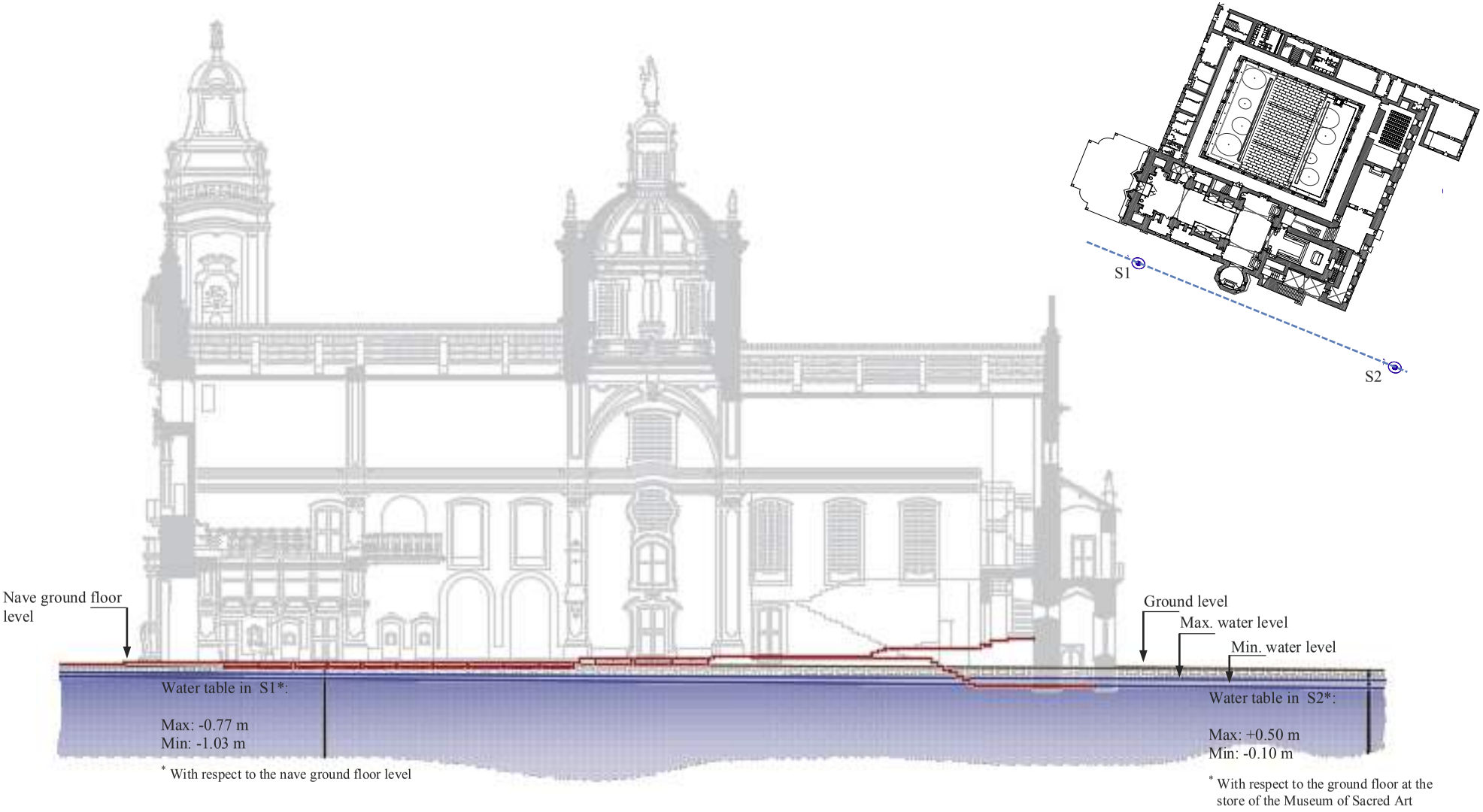
S1
S2
Nave ground floor level
Ground level
Max. water level
Min. water level
Water table in S1*:
Max: -0.77 m
Min: -1.03 m
* With respect to the nave ground floor level
Water table in S2*:
Max: +0.50 m
Min: -0.10 m
* With respect to the ground floor at the store of the Museum of Sacred Art

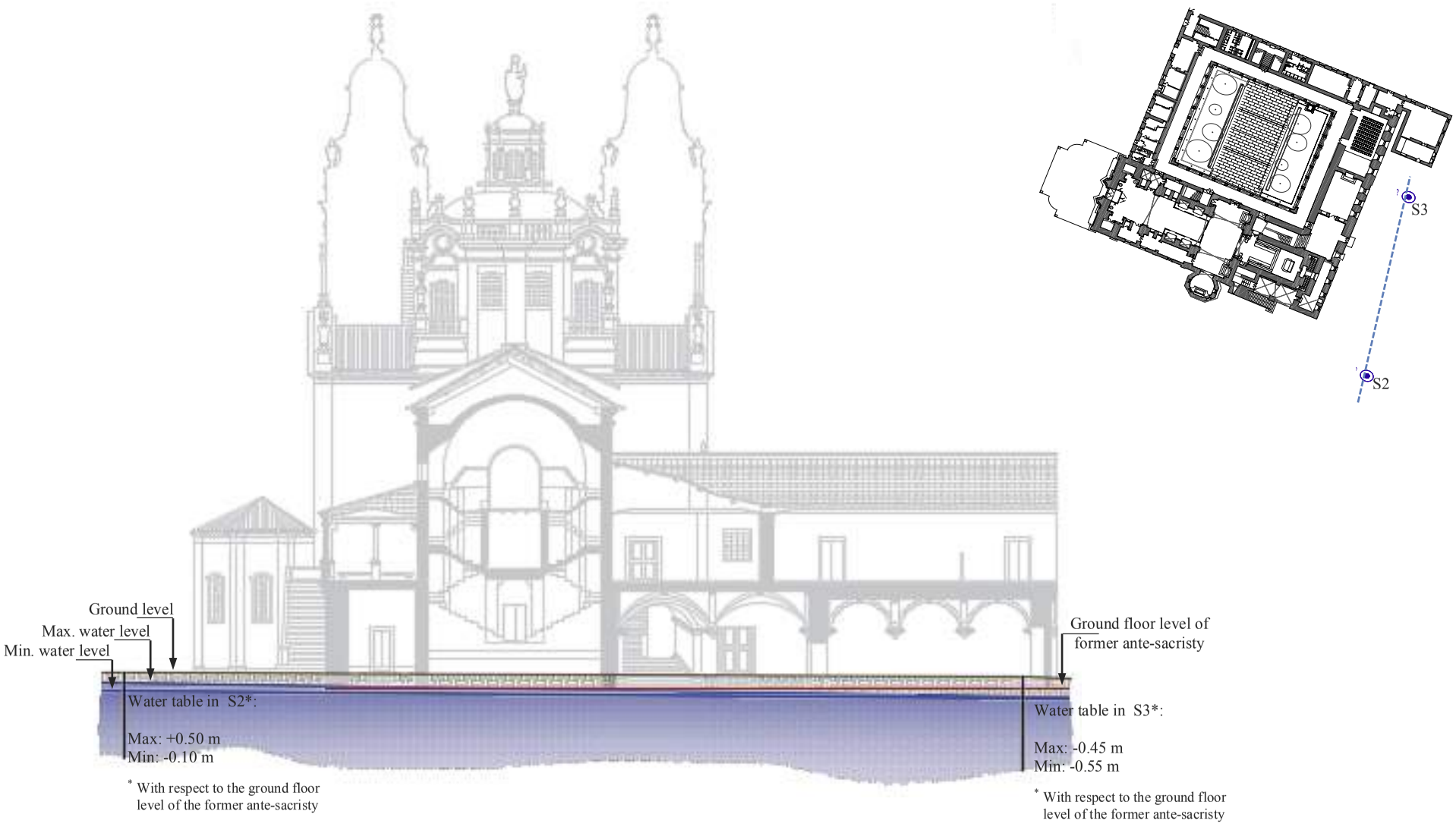
S3
S2
Ground level
Max. water level
Min. water level
Ground floor level of former ante-sacristy
Water table in S2*:
Max: +0.50 m
Min: -0.10 m
* With respect to the ground floor level of the former ante-sacristy
Water table in S3*:
Max: -0.45 m
Min: -0.55 m
* With respect to the ground floor level of the former ante-sacristy

A.3 TEMPERATURE AND RELATIVE HUMIDITY MONITORING

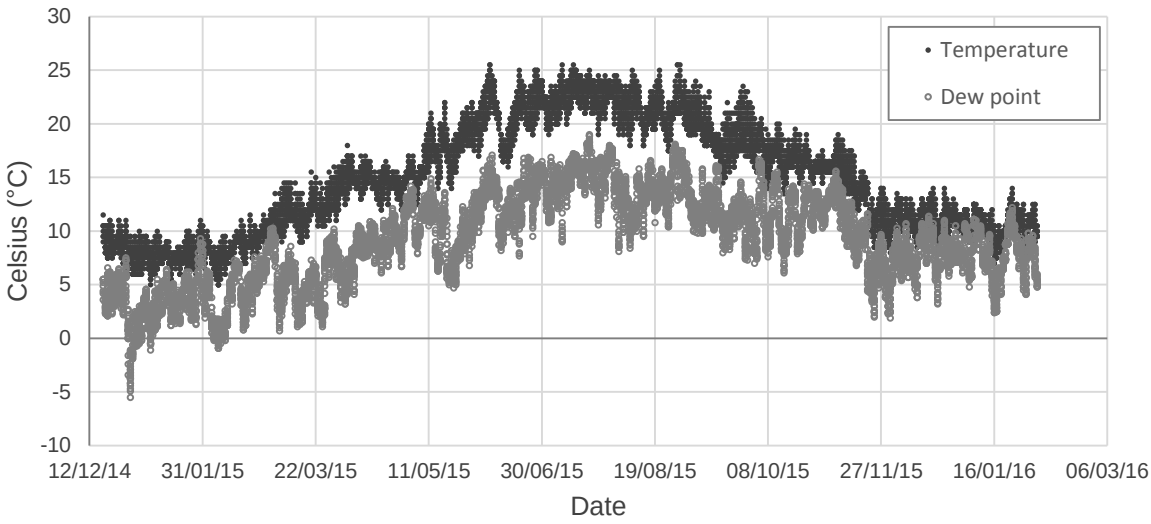

Figure A.3.1: Temperature and dew point measured in S1.

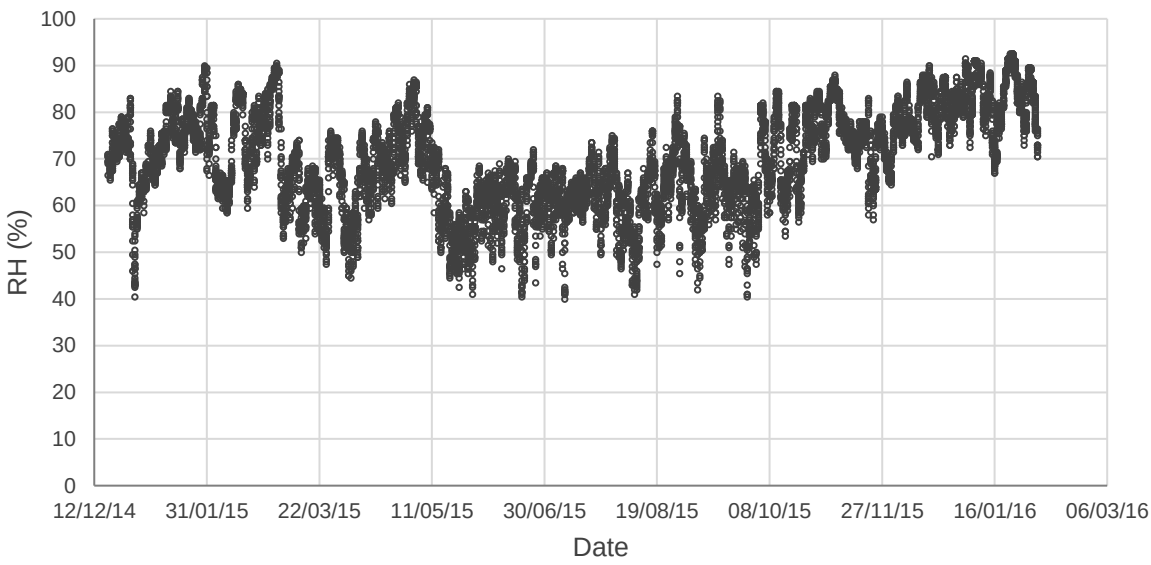

Figure A.3.2: Relative humidity measured in S1.

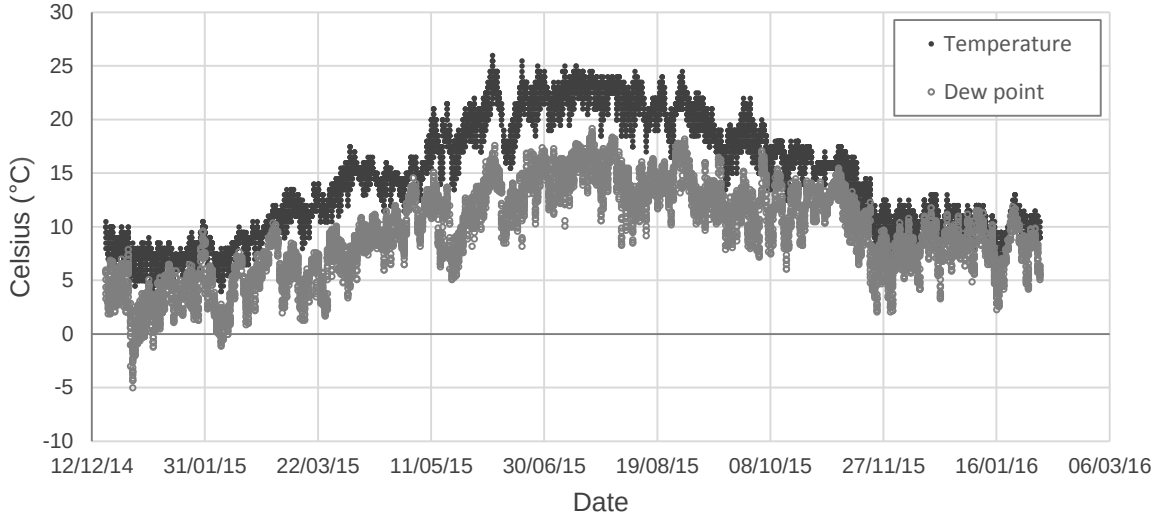

Figure A.3.3: Temperature and dew point measured in S2.

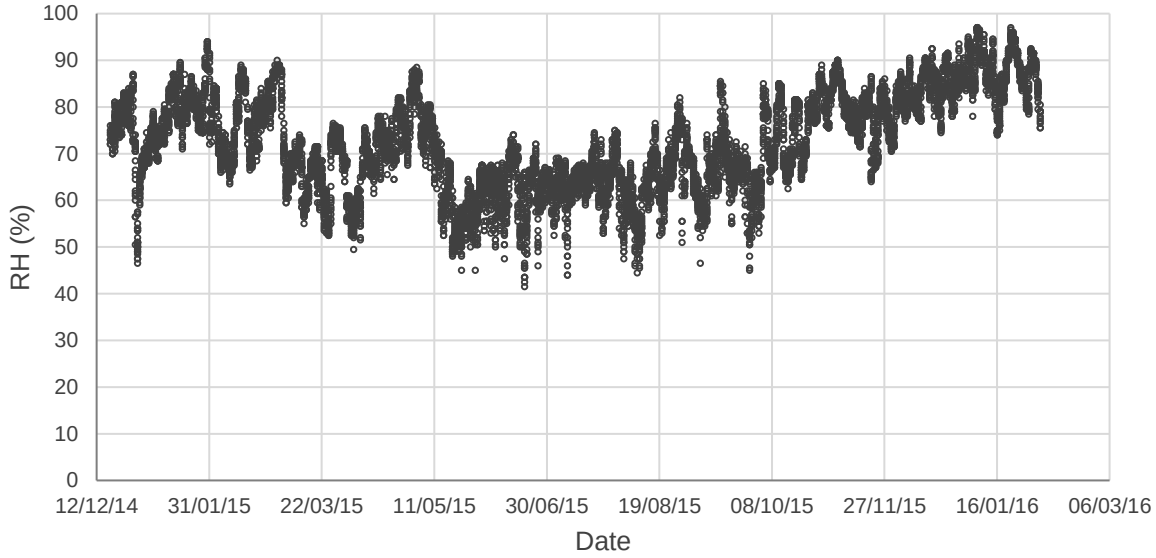

Figure A.3.4: Relative humidity measured in S2.

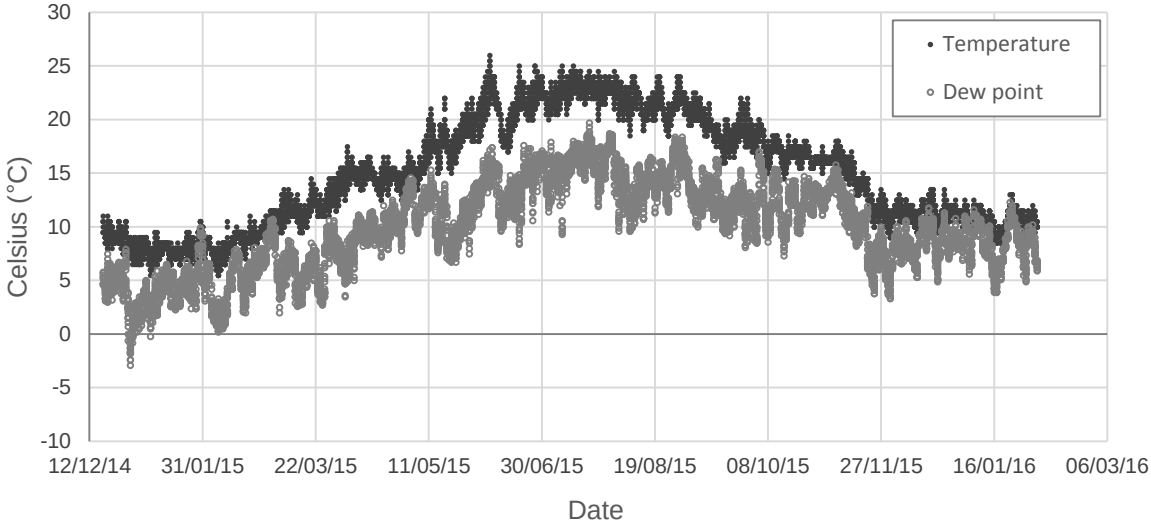

Figure A.3.5: Temperature and dew point measured in S3.

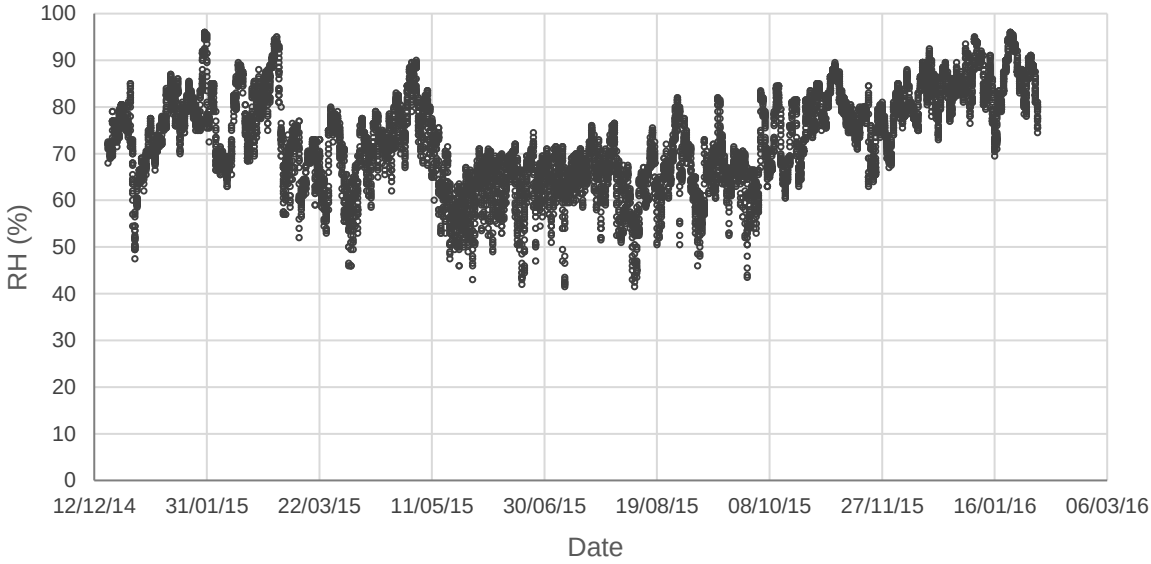

Figure A.3.6: Relative humidity measured in S3.

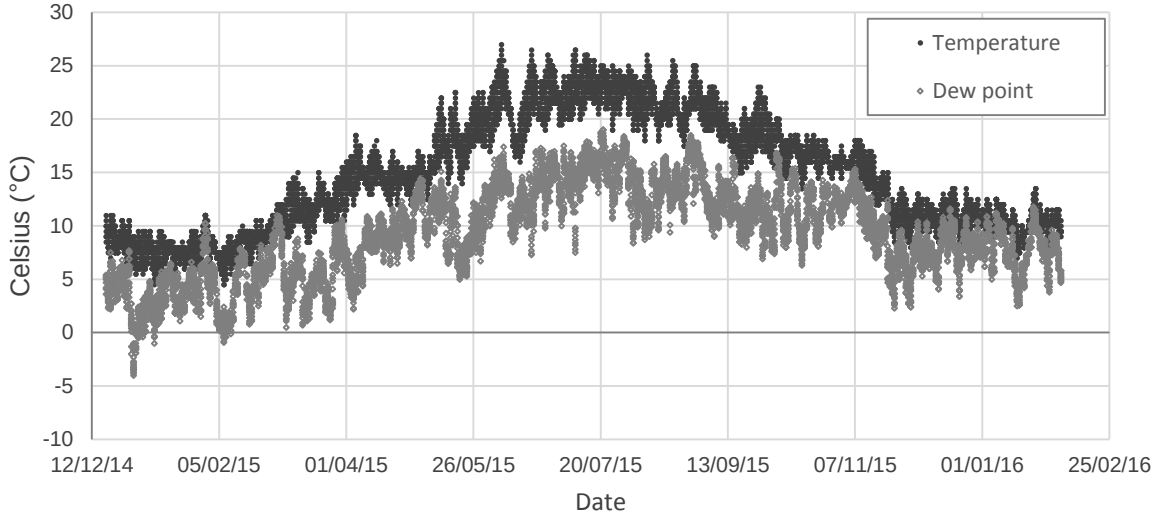

Figure A.3.7: Temperature and dew point measured in S4.

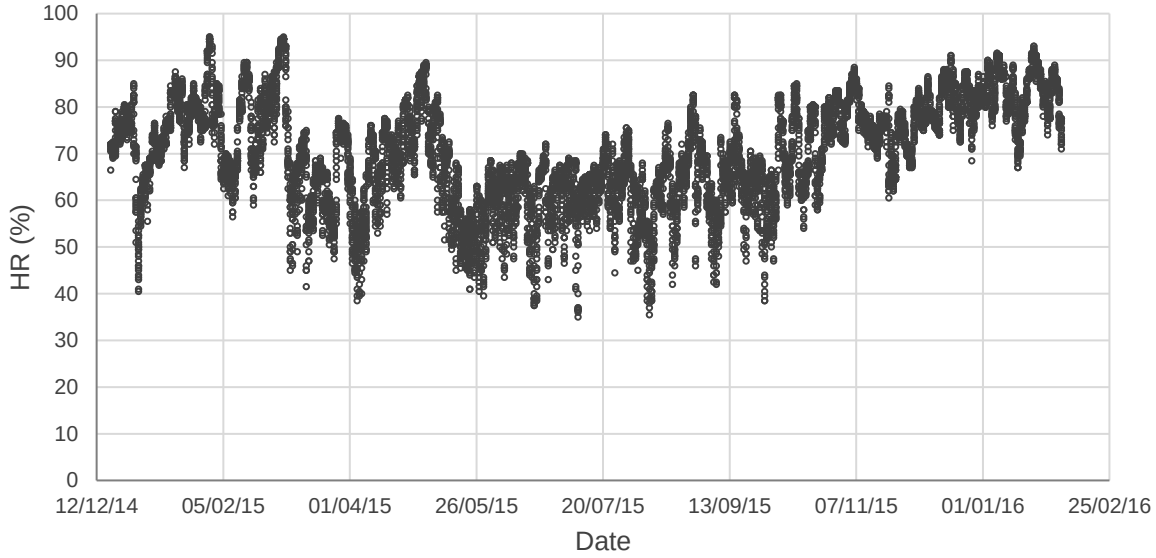

Figure A.3.8: Relative humidity measured in S4.